GEAP-3833

THE POST-IRRADIATION EXAMINATION OF A PuO_2–UO_2 FAST REACTOR FUEL

By
J. M. Gerhart

November 1961

Vallecitos Atomic Laboratory
General Electric Company
San Jose, California

UNITED STATES ATOMIC ENERGY COMMISSION · DIVISION OF TECHNICAL INFORMATION

DISCLAIMER

Printed in USA. Price $2.50. Available from the Office of Technical Services, Department of Commerce, Washington 25, D. C.

USAEC Division of Technical Information Extension, Oak Ridge, Tennessee

THE POST-IRRADIATION EXAMINATION OF A PuO_2 - UO_2 FAST REACTOR FUEL

Prepared for the

UNITED STATES ATOMIC ENERGY COMMISSION

Under

Contract AT(04-3)-189, P.A.#10
General Electric Requisition #474-30750

By

J. M. Gerhart

J. M. Gerhart

November 1961

APPROVED:

S. C. Furman

S. C. Furman, Manager
Radioactive Materials Laboratory

Karl Cohen

K. P. Cohen, Project Engineer
Fast Ceramic Reactor Program

TABLE OF CONTENTS

LIST OF ILLUSTRATIONS

LIST OF ILLUSTRATIONS (continued)

ABSTRACT

A program was carried out to determine the irradiation behavior of a PuO_2-UO_2 fast reactor fuel prototype. Forty (40) stainless steel clad fuel specimens were fabricated, encapsulated, and irradiated in the General Electric Test Reactor to burnups ranging from 5,000 to 99,000 MWD/T, and at heat fluxes ranging from 0.5×10^6 to 1.6×10^6 Btu/hr-ft^2. The cladding surface temperature ranged from 700 to 1200°F with most specimens in the 1000 to 1200°F range. All specimens were irradiated without rupture despite the high performance conditions imposed.

Following irradiation, the fuel specimens were examined in the Radioactive Materials Laboratory. The post-irradiation examination consisted of dimensional measurements, gamma scans, determination of fission gas release, visual examination of the fuel, measurement of central voids, and metallographic examination of selected samples.

Specimen and capsule fabrication is discussed, and the results of the post-irradiation examination are presented and discussed.

I. INTRODUCTION

The Atomic Power Equipment Department of the General Electric Company, under the sponsorship of the United States Atomic Energy Commission, has undertaken a program to develop an oxide fueled fast reactor. As part of this development program, plutonium-uranium oxide fuel specimens were prepared, encapsulated and irradiated in the General Electric Test Reactor (GETR). After irradiation, the fuel specimens were examined in the Radioactive Materials Laboratory (RML) to evaluate the performance of the fuel. The fuel fabrication, irradiation and examination portion of the fast oxide reactor program was performed at the General Electric Company's Vallecitos Atomic Laboratory.

The objectives of the experiment were threefold:

1. Study fuel fabrication techniques and compare two different fabrication methods.
2. Determine the behavior during irradiation of test specimens subjected to high power densities and burnups.
3. By post-irradiation examination, determine the irradiation characteristics of the fuel and evaluate its performance.

The entire experiment was designed, insofar as possible, to approximate the anticipated conditions in a fast reactor while subjecting the fuel to a range of power densities and burnups. For this experiment, the desired experimental parameters were as follows:

1. The capsules were designed and positioned in the reactor to achieve maximum heat fluxes ranging from 0.5 to 1.5 x 10^6 Btu/hr-ft^2. This corresponds to a range of fuel power densities which are both economically attractive and were calculated to produce central fuel temperatures above and below that necessary for central void formation.
2. The capsules were also designed so that the maximum outer clad temperature of the specimens would be about 1100°F in order to simulate temperatures expected in a prototype reactor.

3. The irradiation period for the various capsules was selected so that a range of burnups up to 100,000 MWD/T would be achieved. The demonstration of high burnups would lead to fuel cycle economies since the frequency and hence the cost of reprocessing and refabrication can be reduced accordingly.

Since the irradiation was carried out in the GETR, it was not possible to simulate the neutron velocity spectrum of a fast reactor. This substitution of a thermal neutron spectrum results in a flux depression in this highly enriched fuel and hence a fuel power density and associated burnup which is higher at the surface and lower at the center, for a given heat flux, than would be experienced in a fast neutron spectrum.

II. FUEL PREPARATION AND IRRADIATION CAPSULE FABRICATION

A. Fuel Preparation

Preliminary physics calculations showed that the appropriate fuel composition for this experiment would be a 1-4 mixture of plutonium-to-uranium. In order to achieve the desired high burnup while maintaining a relatively constant Pu-U ratio, ~ 50% of the uranium used in the fuel was the U-235 isotope. Thus the fuel composition selected for this experiment was a solid solution of plutonium and uranium oxide with the heavy element composition shown in Table I:

TABLE I

FUEL COMPOSITION

Isotope	Weight Percent
Pu-239	18.81
Pu-240	1.20
U-235	37.86
U-238	42.13

The fuel was prepared by coprecipitating the plutonium (IV) and uranium (VI) from a nitrate solution using ammonium hydroxide. The precipitate was dried and reduced to the oxide in a hydrogen-nitrogen atmosphere at 900°C. The oxide was then ground and separated into two size factions, -140 to +300 mesh and the -300 mesh material. The -140 +300 mesh material was sintered

in a hydrogen-helium atmosphere at 1400°C and then loaded into specimen tubes for swaging. The -300 mesh material was pressed into pellets (0.150" diameter x 0.250" long) and sintered at 1700°C in a hydrogen-helium atmosphere. The fuel fabrication procedure is shown on Figure 1, and described in detail in reference 1.

B. Irradiation Capsule Fabrication

The individual test specimens were placed in instrumented capsules for irradiation in the GETR. Fabrication details for both the test specimens and the irradiation capsules are described in reference 2. For reference, the two types of test specimens (swaged and pelleted) and the irradiation capsule components are shown on Figures 2 and 3.

A total of ten irradiation capsules were fabricated, each of which contained four fuel specimens. The capsules are identified with Roman numerals I through X, while the specimens in each capsule are numbered 1 through 4 starting from the bottom of the capsule. The specimens are further identified by a letter "S" for the swaged specimens and "P" for the pelleted specimens. Thus, specimen V-3-P is a specimen from capsule V, the third specimen up from the bottom, and contains pelleted fuel. This method of specimen identification is used throughout this report.

III. IRRADIATION HISTORY

The irradiation capsules were placed in the GETR, and irradiated for varying periods of time. A summary of the irradiation intervals is presented in Table II:

TABLE II

IRRADIATION HISTORY

GETR Operating Data															
Cycle No.	Started	Ended	Total MWD	Days @ 30 MW	Capsules in Reactor I	II	III	IV	V	VI	VII	VIII	IX	X
10	2/9/60	3/7/60	773	25.8	X	X								
13	5/26/60	6/19/60	546.9	18.2			X	X	X	X				
14	6/27/60	7/22/60	662.0	22.0			X	X	X	X	X	X		
15	8/15/60	8/27/60	375.9	12.5					X	X	X	X	X	X
16	9/3/60	10/2/60	849.2	28.3					X	X	X	X	X	X
17	10/6/60	11/5/60	824.1	27.4					X	X	X	X	X	X
18	11/13/60	12/12/60	609.9	20.2					X	X				
		Total days @ 30 MW			25.8		40.2		128.6			90.2		68.2

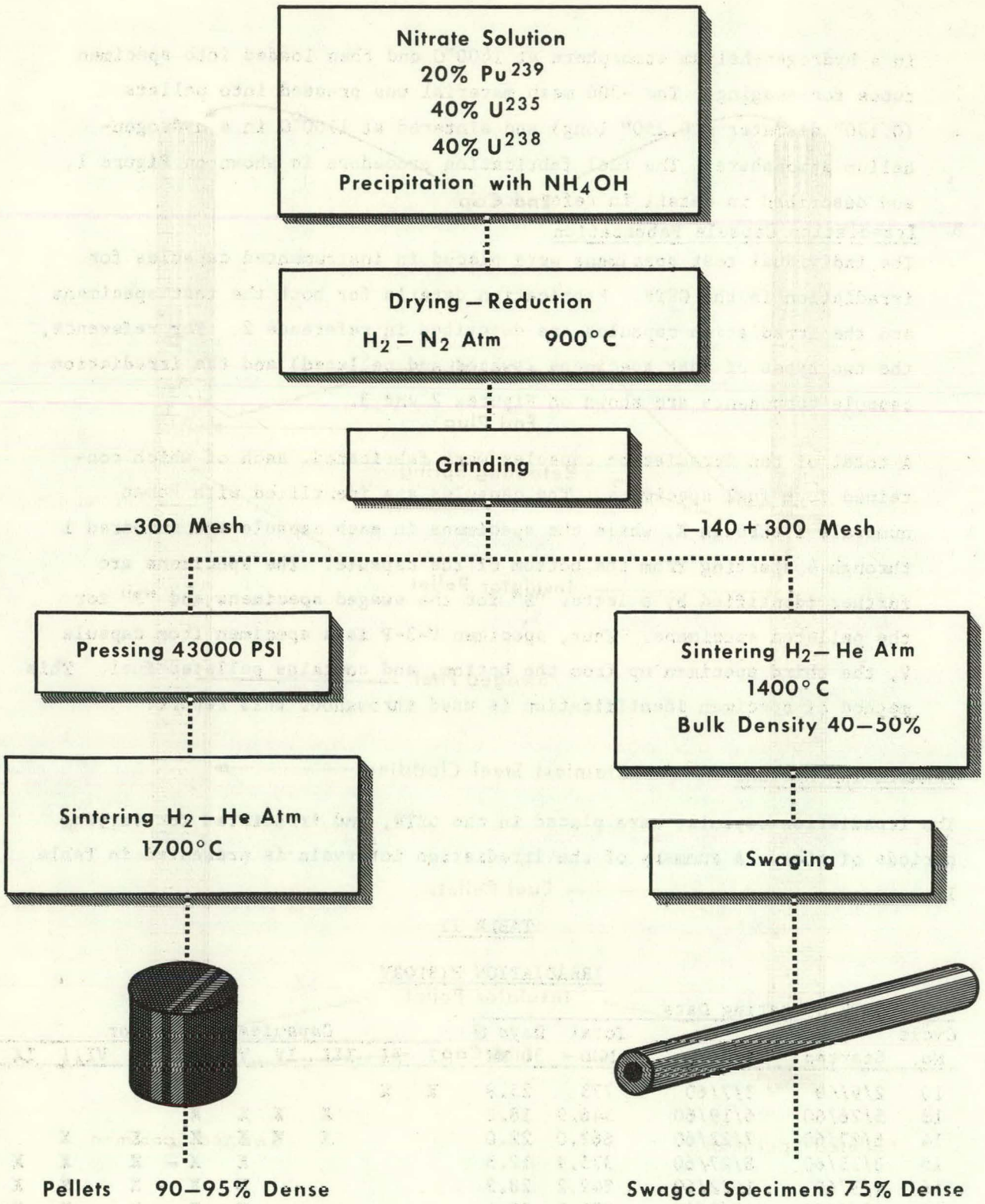

Figure 1. FUEL PREPARATION AND FABRICATION FLOW SHEET

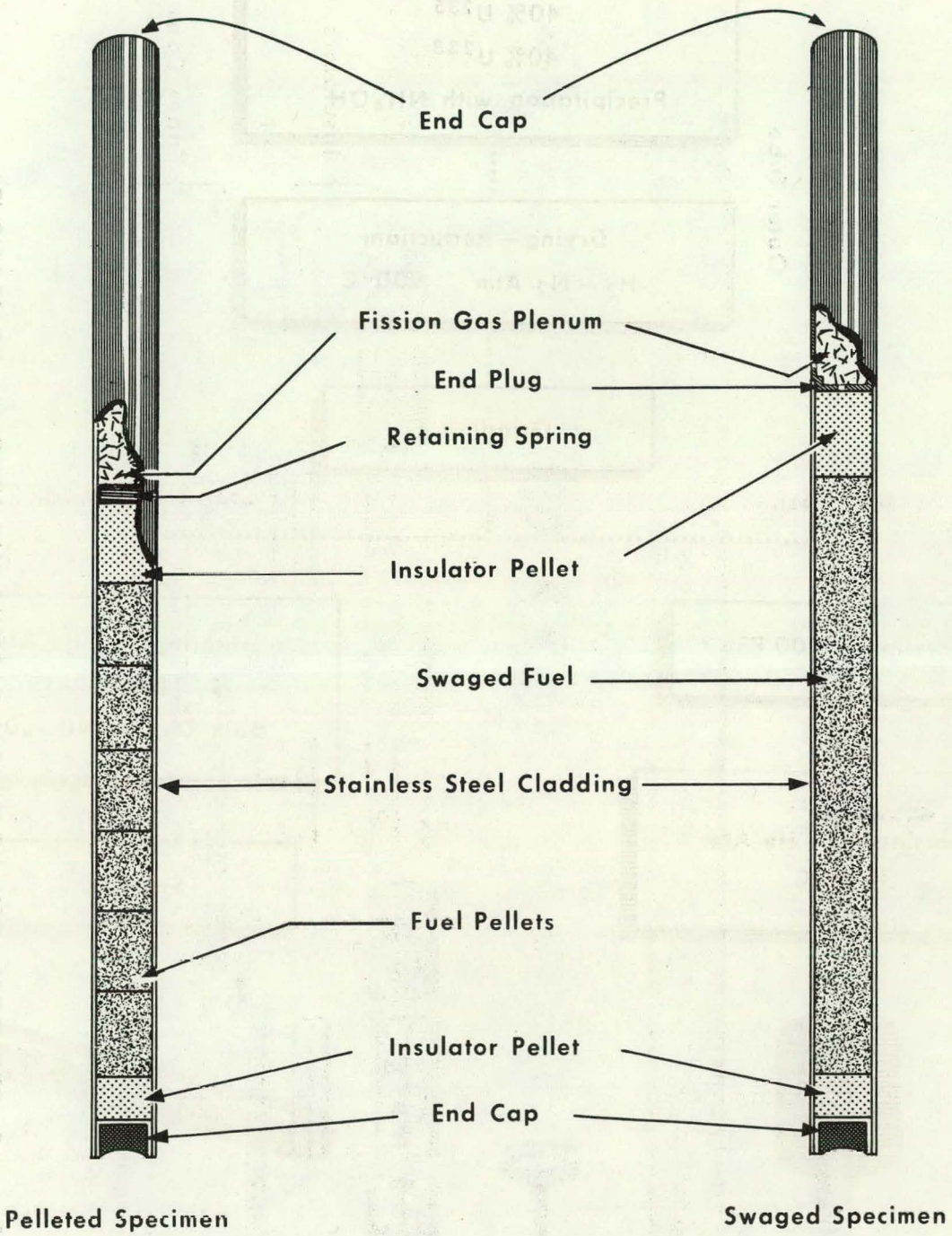

Figure 2. TYPICAL TEST SPECIMENS

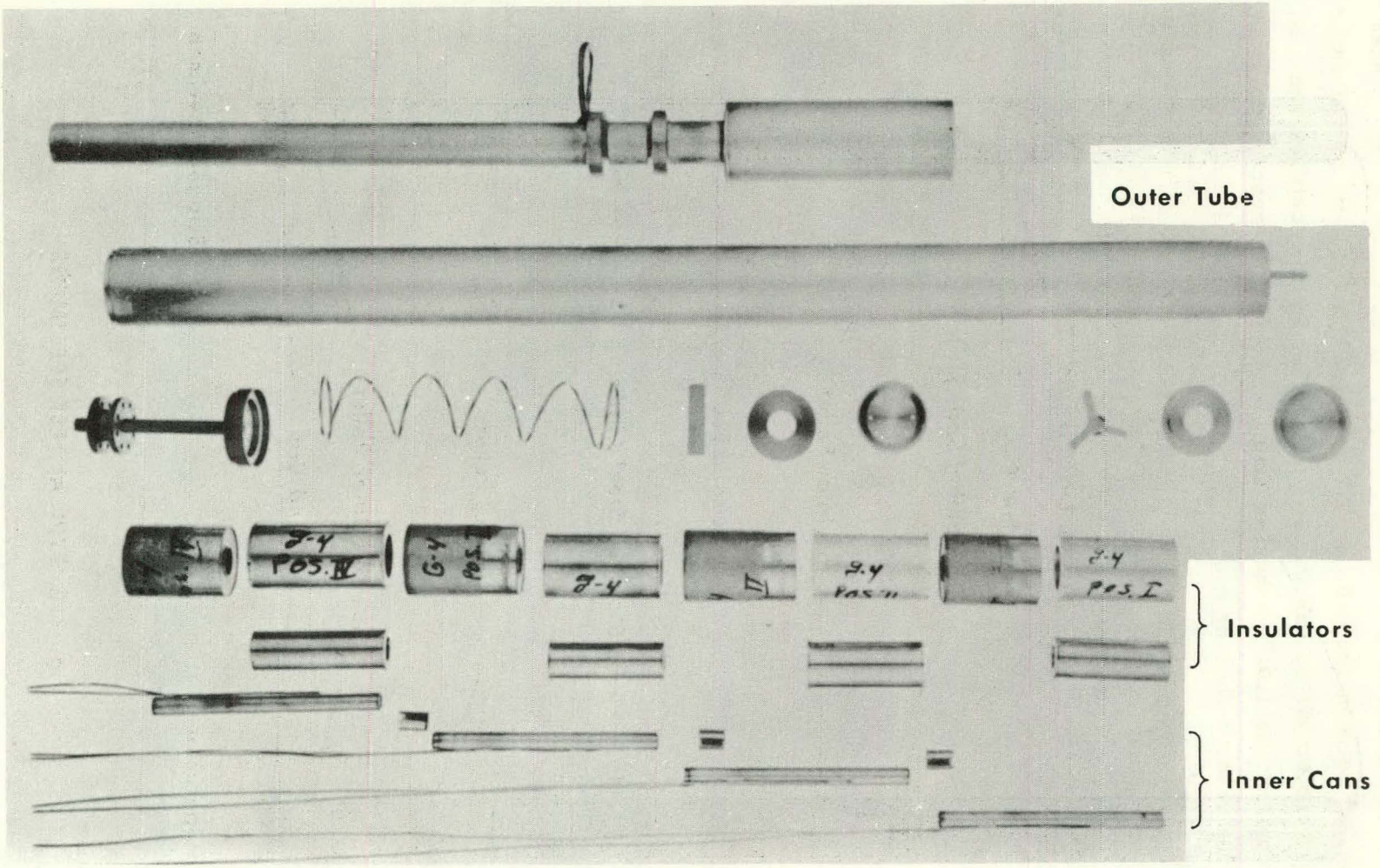

Figure 3. EXPLODED VIEW OF TYPICAL CAPSULE SHOWING ALL COMPONENTS

Temperatures were measured and recorded during the irradiation period for each specimen using the thermocouples shown on Figure 3. The performance of each specimen was monitored by two thermocouples. Thermocouple #1 was located in the NaK annulus between the O.D. of the specimen and the I.D. of the inner can, while thermocouple #2 was located in the NaK annulus between the O.D. of the inner can and the I.D. of the insulator. A third temperature reference point was the reactor cooling water which had a temperature of 100°F. Experimental parameters were calculated from the thermocouple data collected during the irradiation period. Briefly, the calculation method was as follows:[3]

Heat Flux

The heat flux was calculated from the conductance of the thermal path and the temperature difference across the path

$$Q/A = C' \Delta T$$

where Q/A = heat flux

C' = conductance of thermal path

ΔT = temperature difference

The entire thermal path consisted of zircaloy-2, aluminum, stainless steel, NaK, and water. In the computations of the conductance of the path, an estimate was included for the effects of convective heat transfer on conduction across the thin liquid metal annuli. Gamma heating within the heat path was neglected. This amounted to less than 1% for most specimens and no greater than 3% for the remainder.

The temperature difference, ΔT, was determined by subtracting the reading of thermocouple #2 from the cooling water temperature, 100°F. The average temperature was obtained by adding the thermocouple reading for a given specimen and dividing by the number of readings. Readings were taken every 8 hours. In interpreting data, care was taken to avoid any readings taken during the shutdown period or the transient period while changing reactor power. The maximum heat flux was based on scanning the data for points of maximum temperature.

Burnup

The fuel exposure was obtained from a knowledge of the average heat flux, surface area, exposure time and fuel weight. The exposure time was obtained from the GETR Daily Power Summary by adding the number of hours that the reactor was critical. It was noted from the power summary that the reactor is not operated for significant periods of time in the critical condition at zero power.

$\int kd\theta$

The $\int kd\theta$ is related to the heat flux (Q/A) and fuel diameter (D) in the following manner:

$$\int kd\theta = \frac{(Q/A)\ D}{4}^{*}$$

Cladding Temperature

The cladding temperature was calculated by correcting the thermocouple #1 reading to account for the temperature drop in the NaK film and the cladding wall.

Accuracy

In evaluating the accuracy of the calculation method used, three main areas of uncertainty were considered:

1. Heat loss from the ends of the specimens.
2. Gamma heating in the cladding and capsule components.
3. Uncertainties associated with the thermal conductance of the heat path.

An evaluation of the effect of these areas of uncertainty led to the assignment of a 10-20% accuracy to the computations.[4]

---

*This relationship neglects the effect of flux depression in the fuel. While it is recognized that this effect cannot be neglected in this fuel, the flux depression is the same in all the specimens of a given type so that the value of the $\int kd\theta$ is useful for comparative purposes.

The calculated experimental parameters for the individual specimens are presented in Table III. A summary of the experimental parameters for all specimens is as follows:

1.	Burnup	4,700 to 99,000 MWD/T
2.	Heat Flux	0.5 to 1.68 x 10^6 (max.), 0.4 to 1.3 x 10^6 (ave.) Btu/hr-ft^2
3.	$\int kd\theta$	2000 to 6200 (max.), 1400 to 5200 (ave.) Btu/hr-ft
4.	Cladding Surface Temperature	790 to 1260 (max.), 590 to 1060 (ave.) ^oF

IV. POST-IRRADIATION EXAMINATION

A. Description of Equipment and Procedures

The post-irradiation examination of the test specimens was carried out in the Radioactive Materials Laboratory (RML) at Vallecitos Atomic Laboratory. Since the fuel to be examined contained a significant amount of plutonium, the disassembly procedures used were somewhat different than those used for the examination of uranium fuels. The capsules "as received" from the reactor had three barriers between the fuel and the cell atmosphere; viz., the capsule, the inner can and the fuel cladding, so that in the event of rupture of a test specimen the activity would still be confined to the inner can. This permitted the partial disassembly of the capsules in the cell proper using the same techniques that would be used for the disassembly of a UO_2 capsule. Thus the capsules were disassembled and the inner cans removed (intact) before transfer to the alpha enclosures.

The disassembly of the inner cans and the subsequent examination was performed in the alpha enclosures shown on Figures 4 and 5. The alpha enclosures were designed and built specifically for the examination of these plutonium bearing specimens. The alpha enclosures used were essentially glove boxes placed inside the hot cell and adapted for remote operation using manipulators. In this way, all the alpha contamination was contained within the enclosure leaving the cell proper free of alpha activity. Upon completion of the post-irradiation examination, the boxes were removed and discarded intact.

TABLE III

EXPERIMENTAL PARAMETERS

Specimen Number		Burnup $\left(\frac{MWD}{T}\right)$ (b)	Heat Flux (Btu/hr-ft^2)		$\int kd\theta$ (c) (Btu/hr-ft)		Surface Temp (°F) (d)	
			Maximum	Average	Maximum	Average	Maximum	Average
I	-1-P (a)	16,600	1.41×10^6	1.30×10^6	5600	5200	1040	970
	2-P	13,600	1.36 "	1.10 "	5400	4400	1010	830
	3-P	8,700	1.03 "	0.75 "	4100	3000	1040	750
	4-P	4,700	0.62 "	0.40 "	2500	1600	1010	650
II	-1-S	19,400	1.33 "	1.28 "	5300	5100	1080	1050
	2-S	16,100	1.34 "	1.09 "	5400	4400	1120	940
	3-S	10,700	1.06 "	0.73 "	4300	2900	1160	830
	4-S	6,600	0.72 "	0.45 "	2900	1800	1130	750
III	-1-S	26,000	1.14 "	1.06 "	4600	4200	810	760
	2-P	18,800	1.10 "	0.96 "	4300	3800	790	730
	3-P	15,100	1.02 "	0.77 "	4000	3000	820	670
	4-S	11,700	0.75 "	0.48 "	3000	1900	710	500
IV	-1-S	19,100	0.91 "	0.78 "	3600	3100	890	820
	2-P	14,100	0.82 "	0.71 "	3200	2800	1030	910
	3-P	10,900	0.69 "	0.55 "	2700	2100	990	820
	4-S	9,000	0.53 "	0.37 "	2100	1500	880	660
V	-1-S	99,000	1.52 "	1.27 "	6000	5100	1260	1060
	2-P	77,400	1.58 "	1.30 "	6200	5100	1180	1020
	3-P	54,400	1.28 "	0.92 "	5000	3600	1130	880
	4-S	42,700	0.86 "	0.55 "	3400	2200	930	650
VI	-1-S	69,100	1.00 "	0.89 "	4000	3500	1140	1030
	2-P	41,600	0.79 "	0.68 "	3100	2700	1060	950
	3-P	34,900	0.76 "	0.57 "	3000	2200	1210	950
	4-S	30,900	0.62 "	0.40 "	2400	1600	980	680
VII	-1-S	70,300	1.44 "	1.31 "	5700	5200	1220	990
	2-P	49,900	1.50 "	1.32 "	5900	5200	1170	950
	3-P	38,900	1.24 "	0.92 "	4800	3600	1080	790
	4-S	29,600	0.86 "	0.55 "	3400	2200	950	630

TABLE III (Continued)

Specimen Number	Burnup $\left(\frac{MWD}{T}\right)$ [b]	Heat Flux (Btu/hr-ft^2) Maximum	Heat Flux (Btu/hr-ft^2) Average	$\int kd\theta$ [c] (Btu/hr-ft) Maximum	$\int kd\theta$ [c] (Btu/hr-ft) Average	Surface Temp (^oF) [d] Maximum	Surface Temp (^oF) [d] Average
VIII -1-S	45,200	1.07×10^6	0.83×10^6	4200	3300	1180	930
2-P	28,300	0.85 "	0,66 "	3300	2600	1220	920
3-P	23,100	0.75 "	0.54 "	2900	2100	1150	840
4-S	19,300	0.50 "	0.36 "	2000	1400	820	590
IX -1-P	47,600	1.40 "	1.36 "	5460	5270	1060	930
2-P[e]	38,300	1.36 "	1.19 "	5300	4700	(f)	(f)
3-P	34,500	1.21 "	0.95 "	4850	3200	990	740
4-P[e]	17,600	0.86 "	0.56 "	3350	2160	(f)	(f)
X -1-S[g]	36,300	0.91 "	0.88 "	3600	3500	(f)	(f)
2-P	23,700	0.85 "	0.75 "	3400	3000	(f)	(f)
3-P	16,800	0.71 "	0.54 "	2800	2200	(f)	(f)
4-S	15,000	0.57 "	0.37 "	2300	1500	(f)	(f)

(a) P - Pelleted Specimen
S - Swaged Specimen

(b) T - Tons of Pu and U (2000#/ton)

(c) Linear power generation = $4\pi \int kd\theta$

(d) Temperature at inner surface of cladding

(e) These specimens had no gas plenum

(f) Cladding thermocouple failed

(g) Estimated data - Majority of thermocouples failed during irradiation

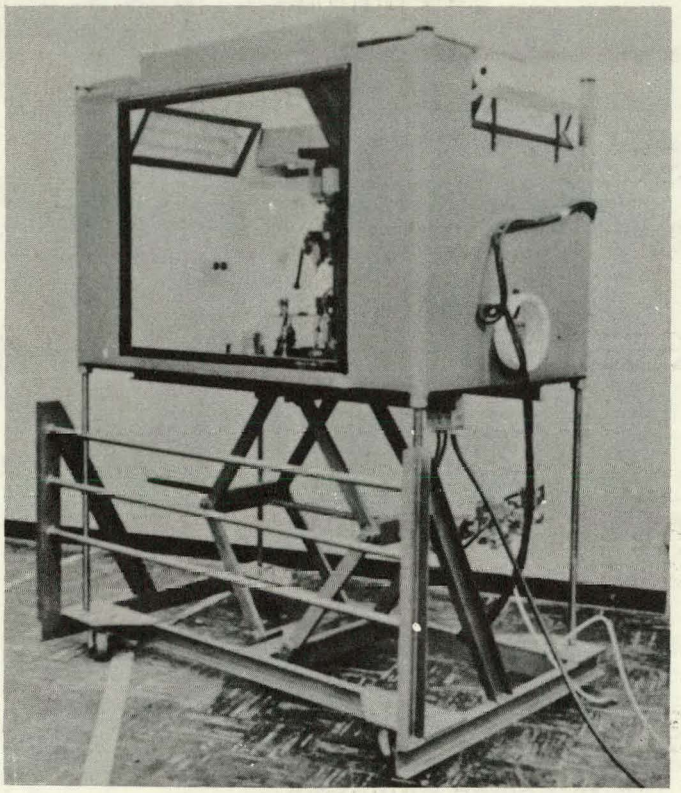

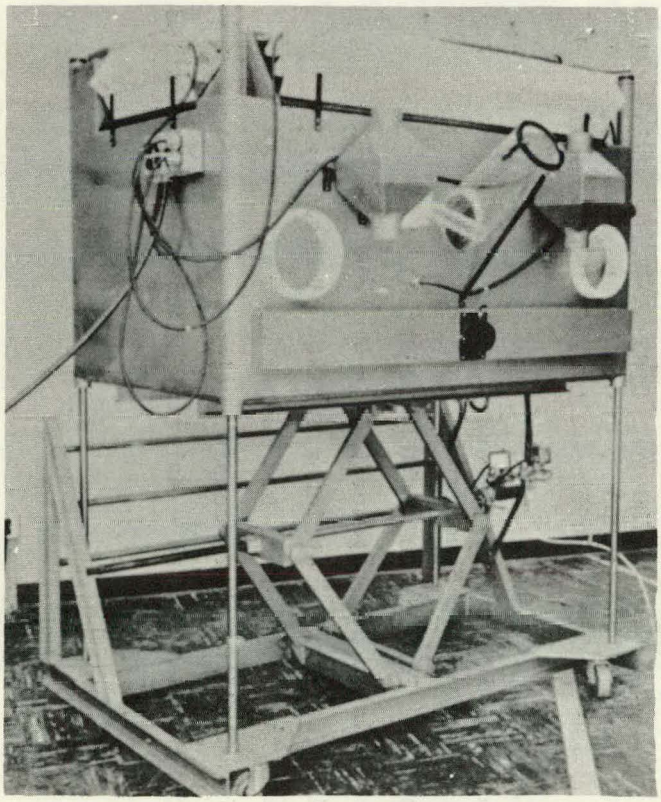

V 10639

Figure 4. EXTERIOR OF ALPHA ENCLOSURES

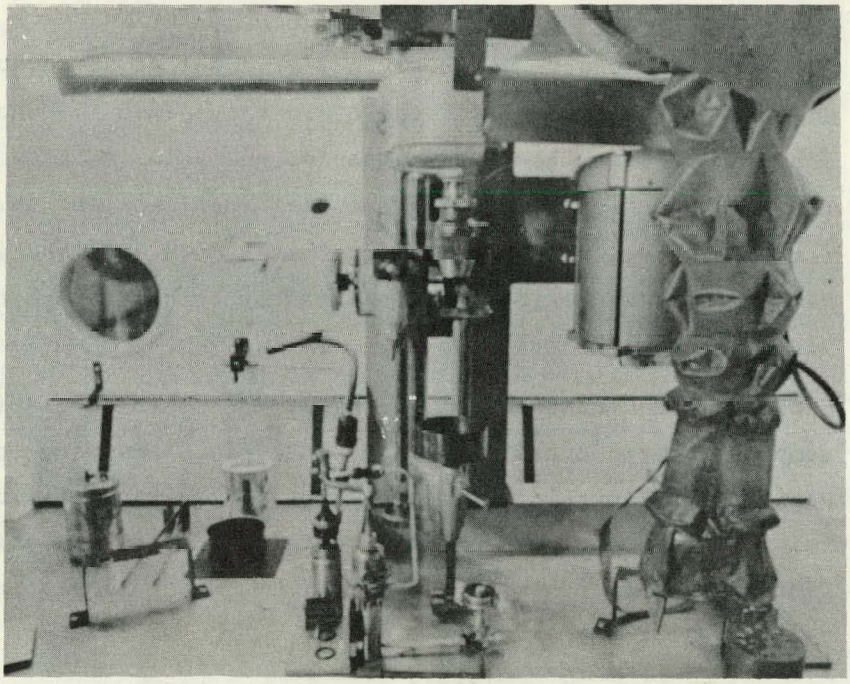

V10627

Alpha enclosure. Fission gas collection and sectioning equipment.

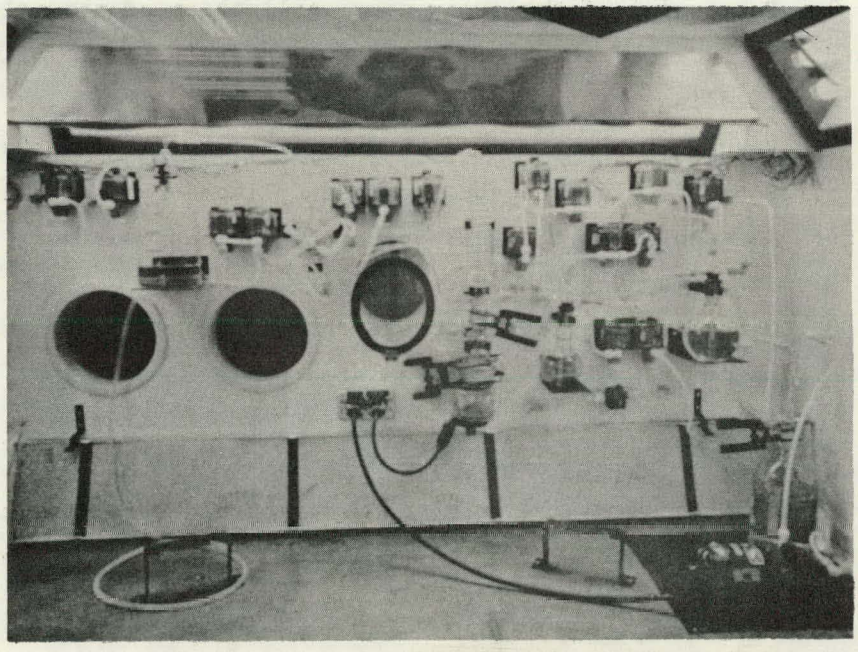

V10636

Alpha enclosure. Fuel dissolution and sampling equipment.

Figure 5. INTERIOR OF ALPHA ENCLOSURES

Two alpha enclosures were originally installed at adjacent cell stations. Enclosure #1 contained all the equipment needed to puncture the specimens and collect the fission gas for analysis, a lathe for cutting open the inner can and sectioning the fuel specimens, and the necessary lights, fixtures, etc. for photographing the exposed fuel sections. Dimensional measurements were also made in this box by photographing the specimens alongside a machinist's scale.

Enclosure #2 contained the equipment for dissolving specimens and taking samples for radiochemical burnup analysis. However, it was found that satisfactory correlation was obtained[2] between the burnup values obtained from thermocouple data and radiochemical analysis, and so dissolutions and radiochemical analysis were discontinued in favor of the already available thermocouple data.

The post-irradiation examination of the test specimens consisted of the following operations:

1. Visual examination of the capsule and disassembly of the capsule to remove the inner cans.
2. Gamma scanning of the fuel specimens.
3. Puncturing of the inner cans, collection of the released gas, and a check for the presence of fission gas; i.e., failure of the specimen cladding.
4. Visual examination and diameter measurements of the test specimens.
5. Puncturing of the specimen and collection of the fission gas.
6. Sectioning of the fuel specimen and measurement of the central void.
7. Photographing the exposed fuel sections.
8. Detailed metallographic examination of sections from eight test specimens plus one unirradiated pellet.

B. Visual Examination and Disassembly

The capsules were all received from the reactor in apparent good condition. Spot checks of the capsules O.D. revealed no change from the pre-irradiation O.D.

The capsules were disassembled by cutting through the capsule wall with an abrasive wheel (under an argon atmosphere to prevent ignition of the NaK). After the first circumferential cut had been completed, the entire

capsule was immersed in a tank of isobutyl alcohol to react the NaK, after which the capsule was disassembled by making further cuts as needed and withdrawing the internal components. Visual examination of the inner cans and other internal components showed no unusual discolorations or deformations.

C. Gamma Scanning

The gamma scans of the test specimens were made by loading the four specimens from a given capsule into a holder (in the same sequence and orientation as in the capsule) and then passing the fuel past a collimator slit (0.020" slit height) and recording the gross gamma activity (above 0.70 MEV) on a strip chart. The equipment used for gamma scanning is shown on Figure 6. The gamma scans (Figures 7, 8, 9, and 10) thus obtained yield several items of information:

1. The relative activities of the specimens provide a measure of the relative burnup of the specimens in a capsule.
2. The length of the scan, when compared with the scan of a calibration standard, shows the length of the active fuel zone.
3. The shape of the fuel scans gives an indication of the condition of the fuel, and shows whether or not any fuel or fission products have gotten past the upper insulator pellet.

1. Relative Burnup

The calculation of the relative burnup of the various specimens using the gamma scan data is complicated by several factors in this particular fuel system.

A gamma scan of the specimen gives only relative burnup values, but has the virtue of simplicity. This method is self-integrating but this is also a source of error. The observed gamma are predominantly from Zr-95 and other short half-life fission products. Accordingly, this method tends to weight the exposure at, or near the end, of the

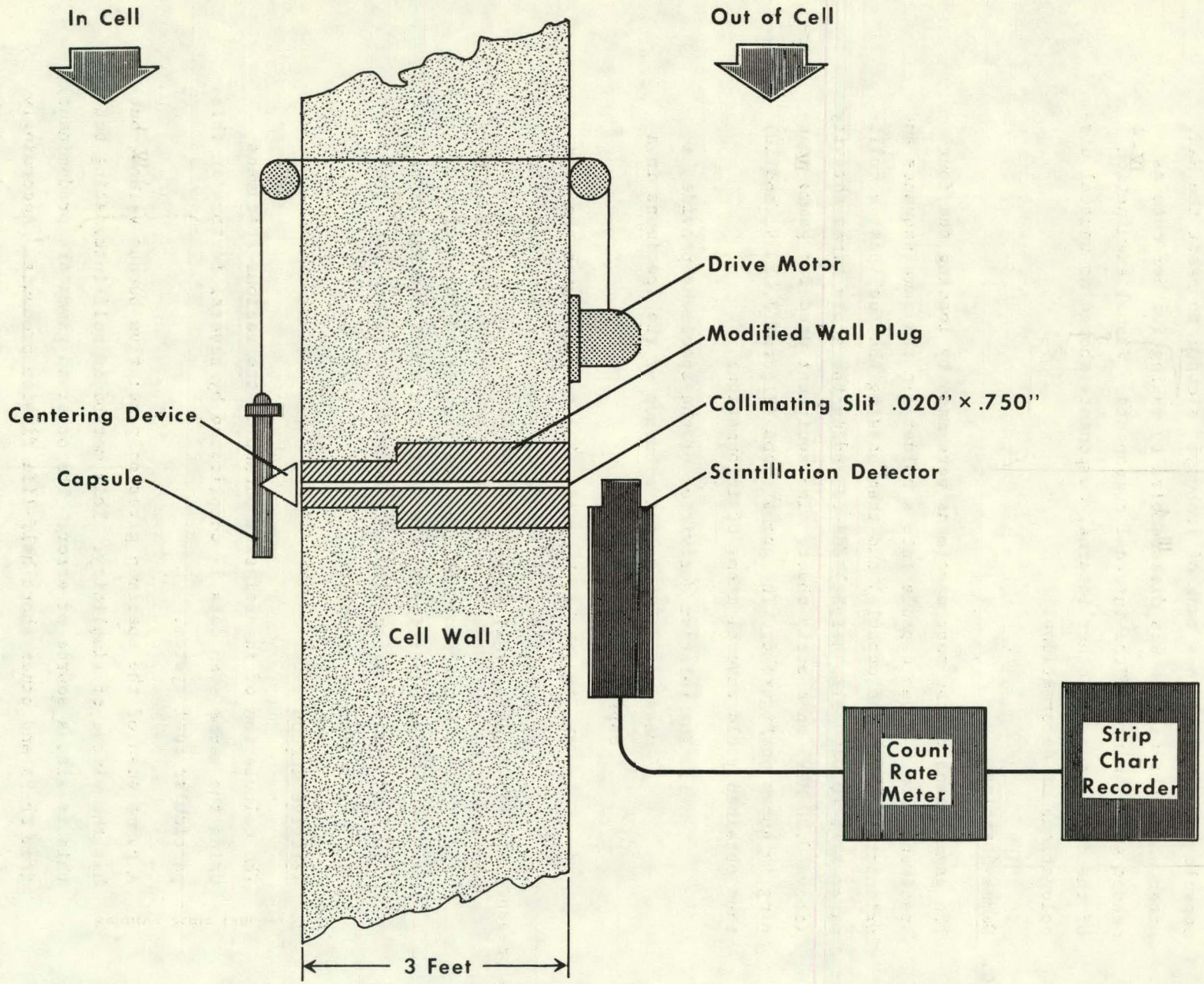

Figure 6. SCHEMATIC DIAGRAM OF GAMMA SCAN EQUIPMENT

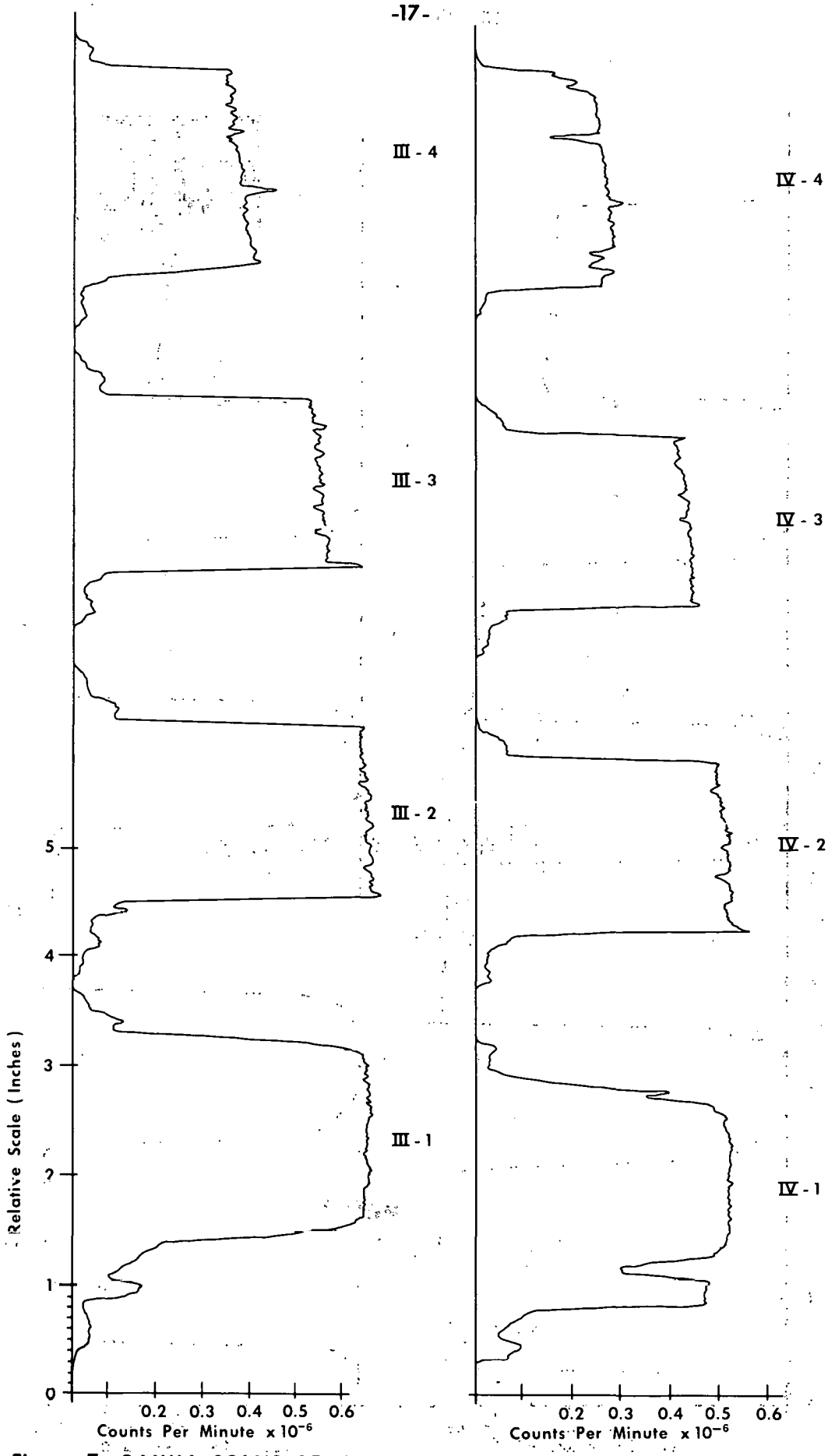

Figure 7. GAMMA SCANS OF FUEL SPECIMENS FROM CAPSULES III AND IV

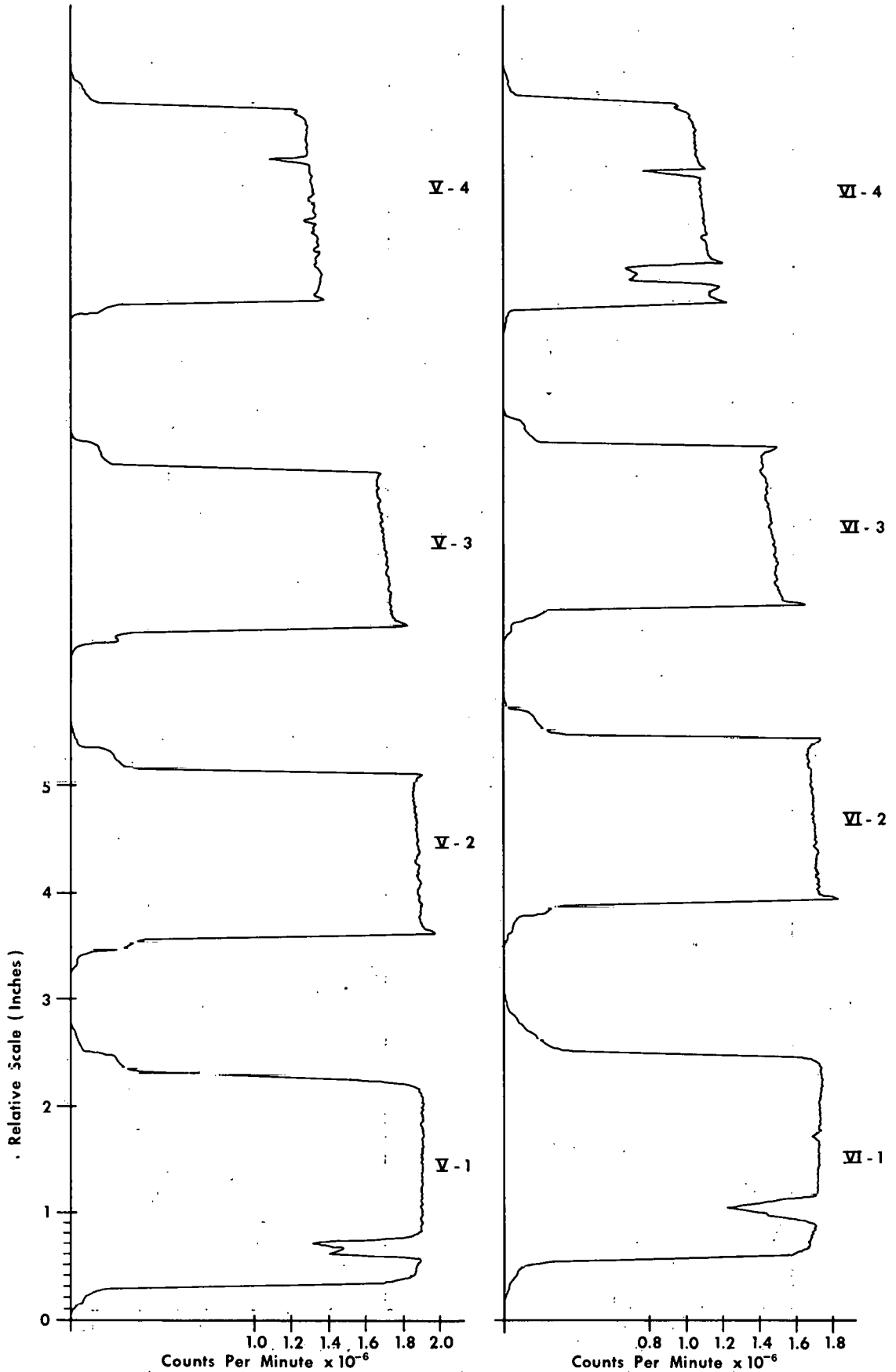

Figure 8. GAMMA SCANS OF FUEL SPECIMENS FROM CAPSULES V AND VI

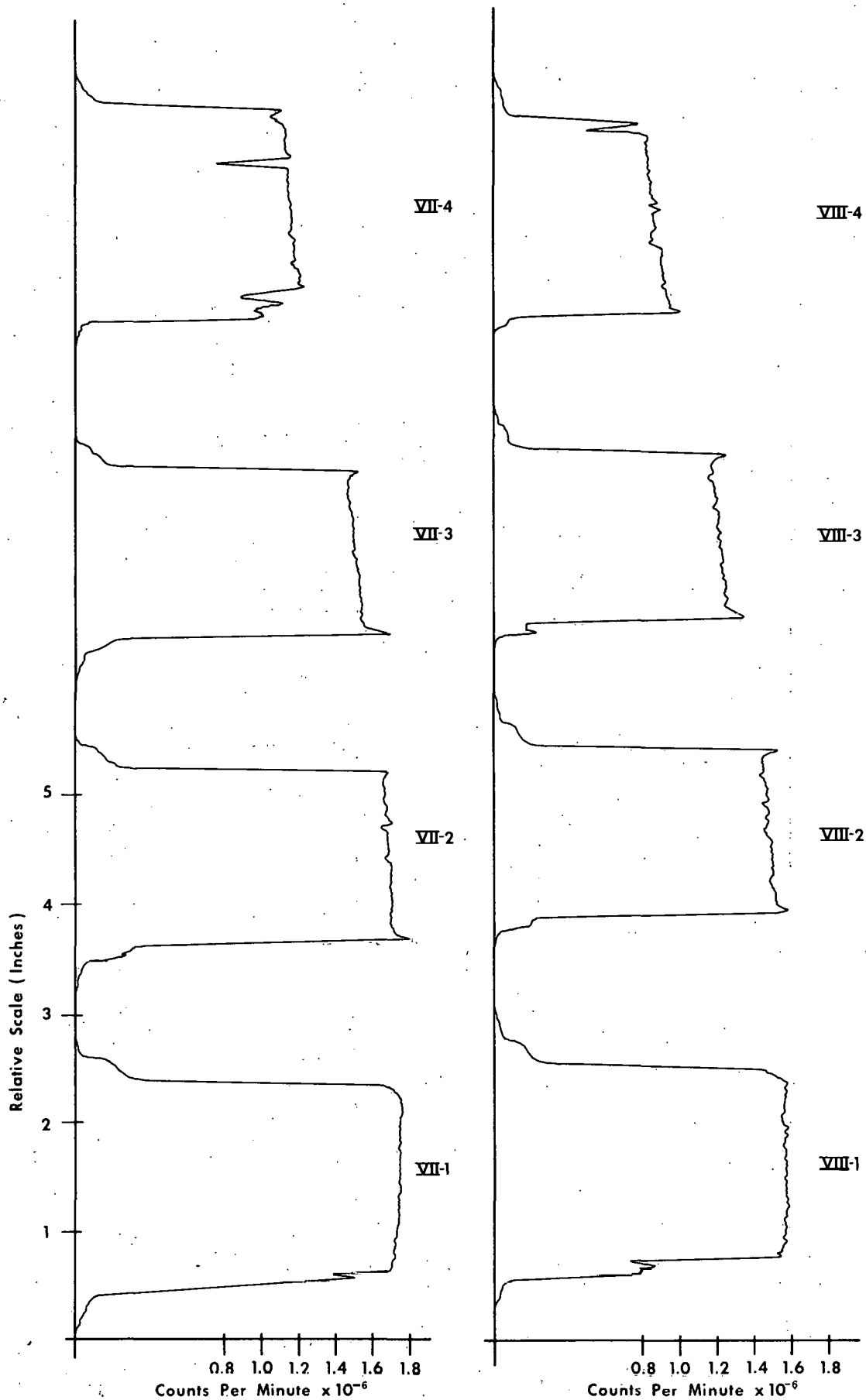

Figure 9. GAMMA SCANS OF FUEL SPECIMENS FROM CAPSULES VII AND VIII

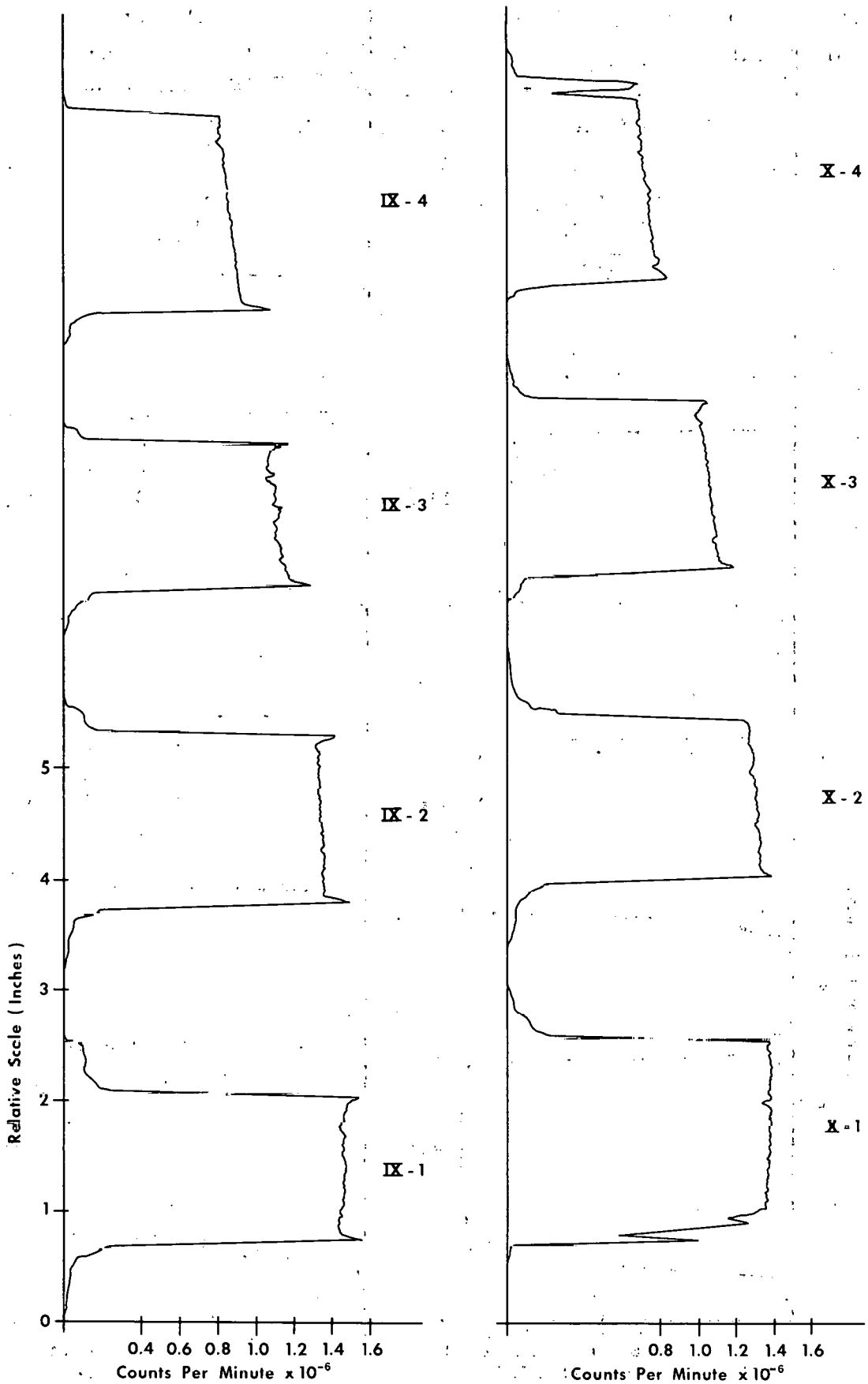

Figure 10: GAMMA SCANS OF FUEL SPECIMENS FROM CAPSULES IX AND X

irradiation period more heavily than the exposure in the early part of the irradiation period. The irradiation capsules were positioned with specimen #1 near the midplane of the reactor and specimens 2, 3, and 4 above the midplane. The flux profile in the GETR is such that as the control rods are withdrawn during the cycle, the peak flux moves upward with respect to the core. The net effect is that the neutron flux at the level of specimen #1 increases in the early portion of a cycle then remains fairly constant whereas the flux at the specimen 2, 3, and 4 level is constantly increasing during the cycle. Thus, the burnups, per the gamma scan data, for specimens 2, 3, and 4 relative to specimen 1 should appear to be higher than the true values.

The fact that the U-Pu fission ratio does not remain constant, as discussed in Section E-2-b (page 33), means that the total fission yield of the various isotopes is also changing during the course of the irradiation period. This effect is probably small since the predominant gamma activity is from Zr-95, and the fission yield from uranium and plutonium is nearly identical (6.2% and 5.9% respectively).

The high concentration of fissionable material in the fuel is also a source of some error. Ideally, since the scintillation counter "looks" at a constant volume of fuel (due to the collimator slit) the activity for two specimens at the same exposure (MWD/T) should differ only in proportion to the amount of fuel seen by the detector, i.e., the density. However, due to the severe flux depression in the fuel, the material in the center of a high density pellet is not contributing the same amount of activity as the same mass of fuel in a swaged specimen.

The gross gamma activity shown on Figures 7, 8, 9, and 10 are the observed count rates for the various specimens. Before this count rate can be used to compare relative burnups, it must first be corrected to account for the resolving time or dead time of the scintillation detector. For a detailed discussion of resolving time, the reader is referred to any of the standard texts on radiation measurement

techniques. Briefly, this correction is applied to account for the counts "missed" by the counter due to its insensitivity to additional pulses for a finite time after receiving an initial "pulse" or count. This relationship is given by the expression:

$$N = \frac{n}{(1 - nt)}$$

Where

N = true counting rate

n = observed counting rate

t = resolving time = 20 microseconds for the equipment used

The relative burnup of the specimens in each capsule is presented in Table IV. Since the estimated accuracy of the burnup values calculated from the thermocouple data is 10-20 percent, it can be seen that the relative burnups are in good agreement with the calculated values.

2. Length Measurement

The gamma scans of the individual fuel specimens also provided an accurate method for measuring the post-irradiation lengths of the active fuel zone in each specimen. By using a very narrow collimator slit and calibrating the cable speed, it was possible to obtain an accurate, reproducible correlation between the length of the active fuel zone, as shown on the strip chart recorder, and the actual fuel length. Previous measurements[5] of fuel lengths using this technique showed that the accuracy of this method is about $\pm$ 0.010" for this particular fuel length. This data is presented in Table V.

3. Fuel Condition

By observing the shape of the gross gamma activity scan it was possible to draw some conclusions as to the condition of the fuel within the specimens.

In the case of the pelleted specimens, the profile was fairly smooth in most cases, and followed the shape of the reactor flux profile indicating that the fuel was not severely fractured and had not experienced any gross longitudinal movement.

TABLE IV

RELATIVE BURNUP VALUES

Specimen	Density (Gms/in)	Observed Count Rate (CPM x 10^{-6})	Dead Time Corrected Count Rate (CPM x 10^{-6})	Count Rate Normalized to Density of 2 gms/in	Activity Ratio	Thermocouple Data	
						Burnup MWD/T	Burnup Ratio
III-1-S	2.26	0.61	0.76	0.67	1.00	26,000	1.00
2-P	2.74	0.60	0.74	0.54	0.81	18,800	0.72
3-P	2.78	0.50	0.60	0.43	0.64	15,100	0.57
4-S	2.26	0.30	0.32	0.28	0.42	11,700	0.45
IV-1-S	2.08	0.52	0.62	0.60	1.00	19,100	1.00
2-P	2.74	0.51	0.60	0.44	0.73	14,100	0.74
3-P	2.78	0.42	0.48	0.35	0.58	10,900	0.57
4-S	2.12	0.27	0.28	0.26	0.43	9,000	0.47
V-1-S	2.17	1.87	4.72	4.35	1.00	99,000	1.00
2-P	2.89	1.85	4.70	3.25	0.75	77,400	0.78
3-P	2.95	1.68	3.78	2.56	0.59	54,400	0.55
4-S	2.28	1.31	2.28	2.00	0.46	42,700	0.43
VI-1-S	2.20	1.73	4.04	3.68	1.00	69,100	1.00
2-P	2.87	1.70	3.88	2.69	0.74	41,600	0.60
3-P	2.89	1.48	2.88	1.99	0.55	34,900	0.51
4-S	2.20	1.04	1.58	1.44	0.39	30,900	0.45
VII-1-S	2.27	1.75	4.16	3.66	1.00	70,300	1.00
2-P	2.77	1.71	3.92	2.83	0.77	49,900	0.71
3-P	2.87	1.51	3.00	2.09	0.57	38,900	0.55
4-S	2.18	1.11	1.74	1.60	0.44	29,600	0.42
VIII-1-S	2.37	1.57	3.24	2.74	1.00	45,200	1.00
2-P	2.85	1.47	2.84	1.99	0.73	28,300	0.63
3-P	2.84	1.22	2.04	1.44	0.53	23,100	0.51
4-S	2.37	0.86	1.20	1.01	0.37	19,300	0.43
IX-1-P	2.66	1.46	2.80	2.10	1.00	47,600	1.00
2-P	2.85	1.35	2.40	1.68	0.80	38,300	0.80
3-P	2.76	1.11	1.74	1.26	0.60	34,500	0.68
4-P	2.88	0.87	1.22	0.85	0.40	17,600	0.37
X-1-S	2.34	1.37	2.48	2.12	1.00	36,300	1.00
2-P	2.99	1.31	2.28	1.53	0.72	23,700	0.65
3-P	2.89	1.06	1.62	1.12	0.53	16,800	0.46
4-S	2.35	0.73	0.96	0.81	0.38	15,000	0.41

TABLE V

POST-IRRADIATION FUEL MEASUREMENTS

Specimen Number	Burnup $\left(\frac{MWD}{T}\right)$[b]	Maximum Heat Flux $\left(\frac{Btu}{hr\text{-}ft^2}\right)$	Maximum $\int kd\theta$[c] $\left(\frac{Btu}{hr\text{-}ft}\right)$	Maximum Surface Temp. (°F)[d]	Pre-Irrad. Density (% of theoretical)	Active Fuel Length (inches)			Central Void Data			
									Diameter		Length	
						Pre	Post	Post / Pre	(inches)	% of Cross Sectional area	(in.)	% of Post-Irrad. length
I-1-P[a]	16,600	1.41×10^6	5600	1040	93.5	1.605	(c)		0.034-0.044	5.0-9.7	1.60	100
2-P	13,600	1.36 "	5400	1010	92.5	1.605	(c)		0.019-0.041	1.7-7.5	1.60	100
3-P	8,700	1.03 "	4100	1040	93.3	1.605	(c)		(c)		(c)	
4-P	4,700	0.62 "	2500	1010	92.7	1.600	(c)		No void			
II-1-S	19,400	1.33 "	5300	1080	75	1.825	(c)		0.051-0.071	11.7-21.3	1.67	90
2-S	16,100	1.34 "	5400	1120	75	1.825	(c)		(c)		(c)	
3-S	10,700	1.06 "	4300	1160	75	1.825	(c)		(c)		(c)	
4-S	6,600	0.72 "	2900	1130	75	1.825	(c)		0.017-0.021	1.4-2.0	1.18	63
III-1-S	26,000	1.14 "	4600	810	75	1.825	1.91	1.05	0.056-0.057	12.5	1.30	68
2-P	18,800	1.10 "	4300	790	93.3	1.544	1.65	1.07	0.014-0.018	1.0-1.1	0.50	30
3-P	15,100	1.02 "	4000	820	92.3	1.553	1.63	1.05	0.020-0.023	2.0-2.3	1.32	81
4-S	11,700	0.75 "	3000	710	75	1.825	1.91	1.05	0.014-0,050	1.0-11.0	1.33	70
IV-1-S	19,100	0.91 "	3600	890	75	1.825	2.07	1.13	0.036	5.7		
2-P	14,100	0.82 "	3200	1030	90.7	1.552	1.65	1.06	0.034-0.035	5.1-5.4	1.55	94
3-P	10,900	0.69 "	2700	990	89.0	1.564	1.63	1.04	0.031-0.035	4.0-5.4	0.70	43
4-S	9,000	0.53 "	2100	880	75	1.835	2.04	1.13	No void			
V-1-S	99,000	1.52 "	6000	1260	75	1.825	1.99	1.09	0.047-0.067	9.8-19.5	1.50	75
2-P	77,400	1.58 "	6200	1180	95.8	1.495	1.58	1.06	0.022-0.031	2.0-4.0	0.81	51
3-P	54,400	1.28 "	5000	1130	94.5	1.473	1.53	1.04	0.005-0.009	0.2-0.4	0.86	56
4-S	42,700	0.86 "	3400	930	75	1.825	1.89	1.03	0.031-0.045	4.0-9.1	1.78	94
VI-1-S	69,100	1.00 "	4000	1140	75	1.825	1.96	1.07	0.042-0.054	7.8-13.0	1.26	64
2-P	41,600	0.79 "	3100	1060	96	1.527	1.59	1.04	0.029-0.031	3.5-4.0	0.62	39
3-P	34,900	0.76 "	3000	1210	95.3	1.531	1.58	1.03	0.013-0.031	0.7-4.0	0.75	47
4-S	30,900	0.62 "	2400	980	75	1.825	1.96	1.07	0.026-0.034	3.0-5.1	0.75	38
VII-1-S	70,300	1.44 "	5700	1220	75	1.825	1.90	1.04	0.051-0.060	11.6-16.0	1.61	84
2-P	49,900	1.50 "	5900	1170	94.7	1.520	1.63	1.07	0.028-0.036	3.2-5.3	0.88	55
3-P	38,900	1.24 "	4800	1080	96	1.516	1.58	1.04	0.033-0.038	4.5-5.9	0.57	36
4-S	29,600	0.86 "	3400	950	75	1.825	1.98	1.08	0.022-0.036	2.2-5.8	1.32	67

TABLE V (Continued)

Specimen Number	Burnup $\left(\frac{MWD}{T}\right)$[b]	Maximum Heat Flux $\left(\frac{Btu}{hr\text{-}ft^2}\right)$	Maximum $\int kd\theta$[c] $\left(\frac{Btu}{hr\text{-}ft}\right)$	Maximum Surface Temp.[d] (°F)	Pre-Irrad. Density (% of theoretical)	Active Fuel Length (inches) Pre	Post	Post/Pre	Central Void Data: Diameter (inches)	Diameter: % of Cross Sectional area	Length (in.)	Length: % of Post-Irrad. length
VIII-1-S	45,200	1.07×10^6	4200	1180	75	1.825	1.82	1.00	0.040-0.049	7.1-10.8	1.44	79
2-P	28,300	0.85 "	3300	1220	94.2	1.530	1.57	1.03	0.013-0.013	0.7	1.17	74
3-P	23,100	0.75 "	2900	1150	94.3	1.529	1.59	1.04	No void			
4-S	19,300	0.50 "	2000	820	75	1.825	1.82	1.00	0.027-0.027	3.0	0.28	15
IX-1-P[e]	47,600	1.40 "	5460	1060	86.5	1.333	1.36	1.02	0.026-0.040	2.8-6.6	0.95	70
2-P[e]	38,300	1.36 "	5300	(f)	94.8	1.521	1.58	1.04	0.022-0.031	2.2-4.2	1.10	70
3-P[e]	34,500	1.24 "	4850	990	83.7	1.348	1.36	1.01	0.027-0.036	32.-5.7	1.36	100
4-P[e]	17,600	0.86 "	3350	(f)	95.8	1.774	1.83	1.03	No void			
X-1-S[g]	36,300	0.91 "	3600		75	1.825	1.85	1.01	0.040-0.054	7.1-13.0	1.72	93
2-P	23,700	0.85 "	3400		96	1.517	1.52	1.00	0.009-0.018	0.3-1.3	0.61	41
3-P	16,800	0.71 "	2800		96.5	1.514	1.57	1.04	0.013-0.027	0.7-3.0	0.42	27
4-S	15,000	0.57 "	2300		75	1.825	1.84	1.01	0.008	0.3		

(a) P - Pelleted Specimen
S - Swaged Specimen

(b) T = Tons of Pu & U (2000#/ton)

(c) No measurements taken

(d) Temperature at inner surface of cladding

(e) These specimens had no gas plenum

(f) Cladding thermocouple failed

(g) Estimated data - Majority of thermocouples failed during irradiation

The gamma scans of the swaged specimens did not show the same smooth profile as the pelleted specimens. In this case, over half of the gamma scans showed depressions at some place in the active fuel zone indicating a section with "missing" fuel. Upon sectioning these specimens, it was observed that the location of these depressions corresponded exactly to the location of an enlarged central void. An example of this enlargement is shown on Figure 27, surface E, and Figure 47, surface E (pages 52 and 72). This condition indicates that either a longitudinal movement of fuel took place during irradiation or the specimen was fabricated with a localized low density spot in the fuel. Since the remainder of the gamma scan does follow the shape of the flux curve with no indication of a local high activity spot, it appears more likely that this condition was caused by a low density section in the fuel.

The high activity at the ends of the specimen are caused by burnup peaking at the ends of the fuel due to the large surface area exposed to the unperturbed flux. It was noted that this peaking was more pronounced in the case of the pelleted specimens. This is probably due to the pellets retaining their shape during irradiation whereas the swaged specimens tended to form an irregular surface at the ends as shown on Figures 22, 35, and 39.

In addition to the active fuel zone, the location of the end insulator pellets can be clearly seen on the gamma scan. It is interesting to note that while these insulator pellets were fabricated from natural UO_2 there is a detectable activity associated with these pellets, and further that there is an activity variation in most of the pellets. The presence of activity is not unexpected, but the observed variation of activity could mean that there is some amount of fission product or fuel diffusion into the pellets.

D. Inner Can Punctures

The fuel specimens were removed from the inner can shown on Figure 3 by cutting through the can with the tubing cutter and reacting the NaK thermal bond with isobutyl alcohol. However, before this cut was made, it was desirable to determine whether or not the fuel specimen inside the can had ruptured during irradiation.

This was accomplished by placing the inner can, after removing the thermocouples, in the fission gas puncture equipment shown on Figure 5, and piercing the inner can. The puncture head was then evacuated, and the released gas was compressed into the short section of line adjacent to a GM Counter (see Figure 11 for a diagram of the fission gas collection system). Thus, by observing the count rate, it was possible to determine whether or not the puncture of the inner can had released any fission gas. Had fission gas been released, it could have been collected by merely opening the valve to the sample bottle. This technique provided a rapid, positive determination of cladding integrity since the count rate in this section of tubing would vary from 400-600 CPM with no fission gas in the line, (i.e., background radiation) to 20,000-80,000 CPM with fission gas in the line.

None of the specimens from Capsules III through X (this test was not used on Capsules I and II) gave any indication of a fission gas leak through the cladding. This fact was later verified, at least with respect to gross cladding ruptures, by a visual examination of each specimen.

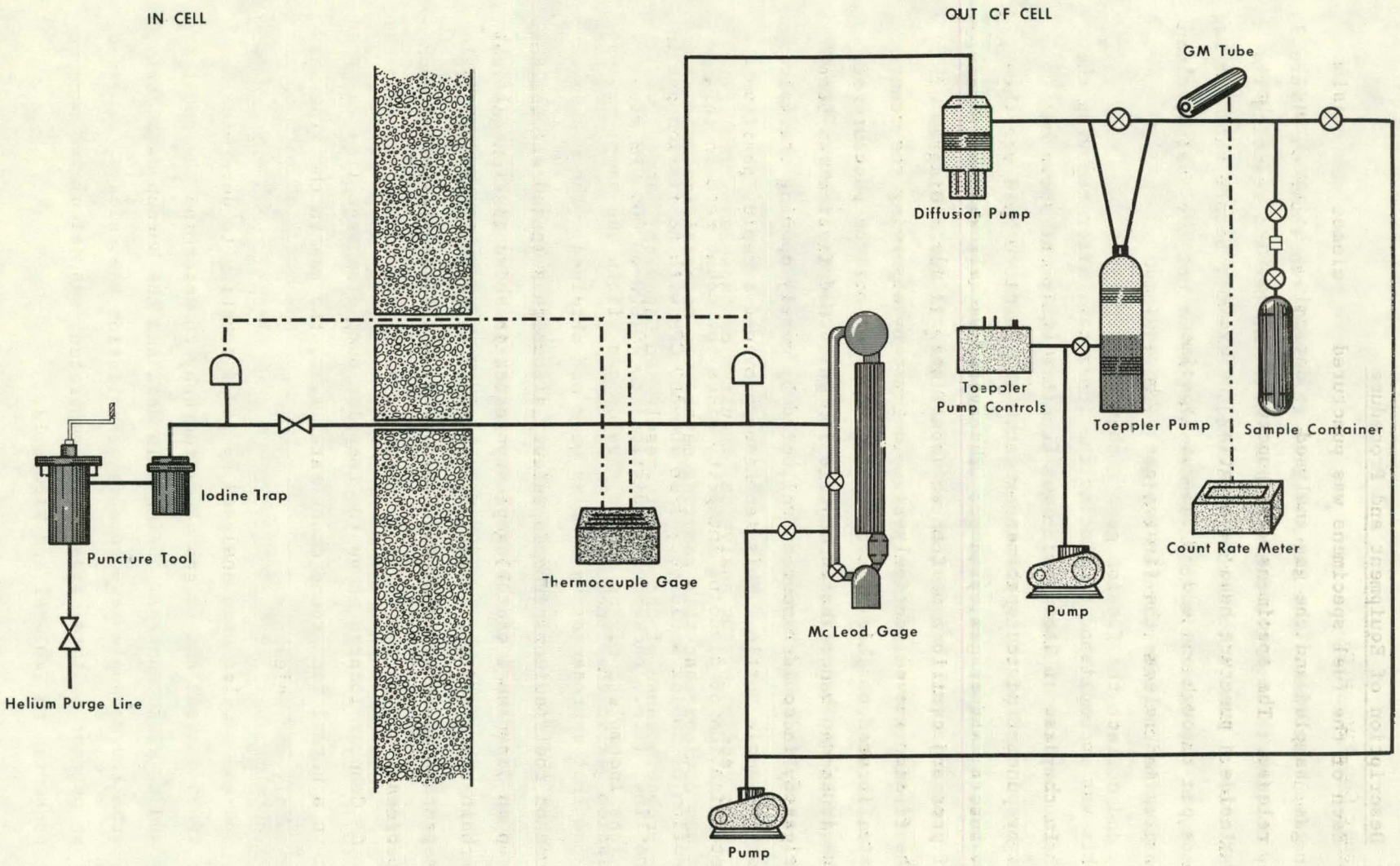

Figure 11. FISSION GAS COLLECTION SYSTEM

E. Fission Gas Release Determination

1. Description of Equipment and Procedure

Each of the fuel specimens was punctured to release the fission gas, sampled and the gas analysed to determine the percentage release. The specimens were punctured by sealing the specimen inside a puncture head, evacuating the system and then driving a pin through one end of the fuel specimen to rupture the end plug and release the fission gas. The equipment used to release and collect the fission gas is shown on Figure 11.

In the case of Capsules I and II, the released gas was sampled by puncturing the specimen, and then allowing the gas to diffuse into a 1-liter gas cylinder. The system was allowed to come to pressure equilibrium after which the gas cylinder was valved off and removed for analysis. The system had been previously calibrated so that the volume of the various parts of the system was known, hence the percentage of the total gas collected in the gas cylinder was known.

Upon receipt of the analytical results for Capsules I and II, it was obvious that this sampling method was not satisfactory. The probable cause of the erratic results on Capsules I and II was the incomplete mixing of the fission gas within the sampling system so that representative samples were not obtained. The system was then modified to include a mercury diffusion pump and a toeppler pump just ahead of the sample container as shown on Figure 11. Using this system, it was then possible to pump all of the fission gas out of the sample, and collect it in the gas cylinder. In operation, the pumping was continued until the count rate from the GM Counter located above the toeppler pump discharge line returned to a normal background count rate; i.e., the gas in the line was mainly air inleakage.

The gas samples were analysed by gamma counting to determine the Kr-85 content and by gas chromatography to determine the total Kr and total Xe content. Using this data and the burnup data derived from thermocouple measurements, the fission gas release, expressed as percent of total fission gas generated, was calculated, and is presented in Table VI and Figure 12.

TABLE VI

FISSION GAS RELEASE DATA

Specimen Number	Burnup $\left(\frac{MWD}{T}\right)$[b]	Average Heat Flux (Btu/hr-ft^2)	Average Surface Temperature ($^\circ$F)[c]	Ave. Density (% of theor.)	Percent Fission Gas Release				Xe/Kr Ratio
					Kr-85	Total Kr	Total Xe	Average	
I-1-P[a]	16,600	1.30 x 10^6	970	93.5	0.163	(h)			
2-P	13,600	1.11 "	830	92.5	23.23				
3-P	8,700	0.75 "	750	93.3	20.64				
4-P	4,700	0.40 "	650	92.7	5.07				
II-1-S	19,400	1.28 "	1050	75	(c)				
2-S	16,100	1.09 "	910	75	3.01				
3-S	10,700	0.73 "	830	75	2.15				
4-S	6,600	0.45 "	750	75	51.52				
III-1-S	26,000	1.06 "	760	75	34.8	41.8	43.9	40.2	9.9
2-P	18,800	0.96 "	730	93.3	36.6	42.2	42.4	40.4	9.4
3-P	15,100	0.77 "	670	92.3	47.2	52.8	52.1	50.7	9.3
4-S	11,700	0.48 "	500	75	57.30	(c)	(c)	57.3	
IV-1-S	19,100	0.78 "	820	75	23.1	49.5	52.3	41.6	9.9
2-P	14,100	0.71 "	910	90.7	35.70	45.2	46.3	42.4	9.5
3-P	10,900	0.55 "	820	89.0	38.3	52.9	51.3	47.5	9.1
4-S	9,000	0.37 "	660	75	23.0	26.2	26.1	25.1	9.4
V-1-S	99,000	1.27 "	1060	75	40.6	49.6	40.2	43.4	7.6
2-P	77,400	1.30 "	1020	95.8	34.7	21.9	20.8	25.8	8.8
3-P	54,400	0.92 "	880	94.5	36.6	35.1	31.8	34.5	8.5
4-S	42,700	0.55 "	650	75	59.0	70.0	65.3	64.8	8.7
VI-1-S	69,100	0.89 "	1030	75	47.6	42.1	40.4	43.4	9.0
2-P	41,600	0.68 "	950	96	33.0	33.9	34.2	33.7	9.5
3-P	34,900	0.57 "	950	95.3	(c)	(c)	(c)		
4-S	30,900	0.40 "	680	75	57.7	45.8	44.2	49.2	9.1
VII-1-S	70,300	1.31 "	990	75	27.6	34.0	36.2	32.6	9.9
2-P	49,900	1.32 "	950	94.7	33.1	52.4	52.9	46.1	9.4
3-P	38,900	0.92 "	790	96	31.1	44.0	44.5	39.9	9.4
4-S	29,600	0.55 "	630	75	47.9	53.3	53.1	51.4	9.3
VIII-1-S	45,200	0.83 "	930	75	54.0	58.9	66.9	59.9	10.6
2-P	28,300	0.66 "	920	94.2	(c)	(c)	(c)		
3-P	23,100	0.54 "	840	94.3	42.7	(c)	(c)	42.7	
4-S	19,300	0.36 "	590	75	61.3	(c)	(c)	61.3	

TABLE VI (Continued)

Specimen Number	Burnup (MWD/T)[b]	Average Heat Flux (Btu/hr-ft^2)	Average Surface Temperature (°F)[d]	Ave. Density (% of theor.)	Percent Fission Gas Release: Kr-85	Total Kr	Total Xe	Average	Xe/Kr Ratio
IX-1-P	47,500	1.36×10^6	930	86.5	(c)	(c)	(c)		
2-P[e]	38,300	1.19 "	(f)	94.8	42.1	38.4	28.3	36.3	6.9
3-P	34,500	0.95 "	740	83.7	11.7	9.5	9.8	10.3	9.5
4-P[e]	17,600	0.65 "	(f)	95.8	33.2	33.8	35.6	34.2	8.6
X-1-S[g]	36,300	0.88 "		75	21.9	30.9	31.9	28.2	9.9
2-P	23,700	0.75 "		96	34.2	26.7	24.9	28.6	8.6
3-P	16,800	0.54 "		96.5	27.3	34.2	34.3	31.9	9.3
4-S	15,000	0.37 "		75	(c)	61.0	59.3	60.1	9.1

(a) P - Pelleted Specimen
S - Swaged Specimen

(b) T - Tons of Pu & U (2000#/ton)

(c) No sample

(d) Temperature at inner surface of cladding

(e) These specimens had no gas plenum

(f) Cladding thermocouple failed

(g) Estimated data - Majority of thermocouples failed during irradiation

(h) Analysis by gas chromatography not performed on Capsules I and II

(i) Doubtful sampling accuracy on Capsules I and II. System revised for remainder of capsules.

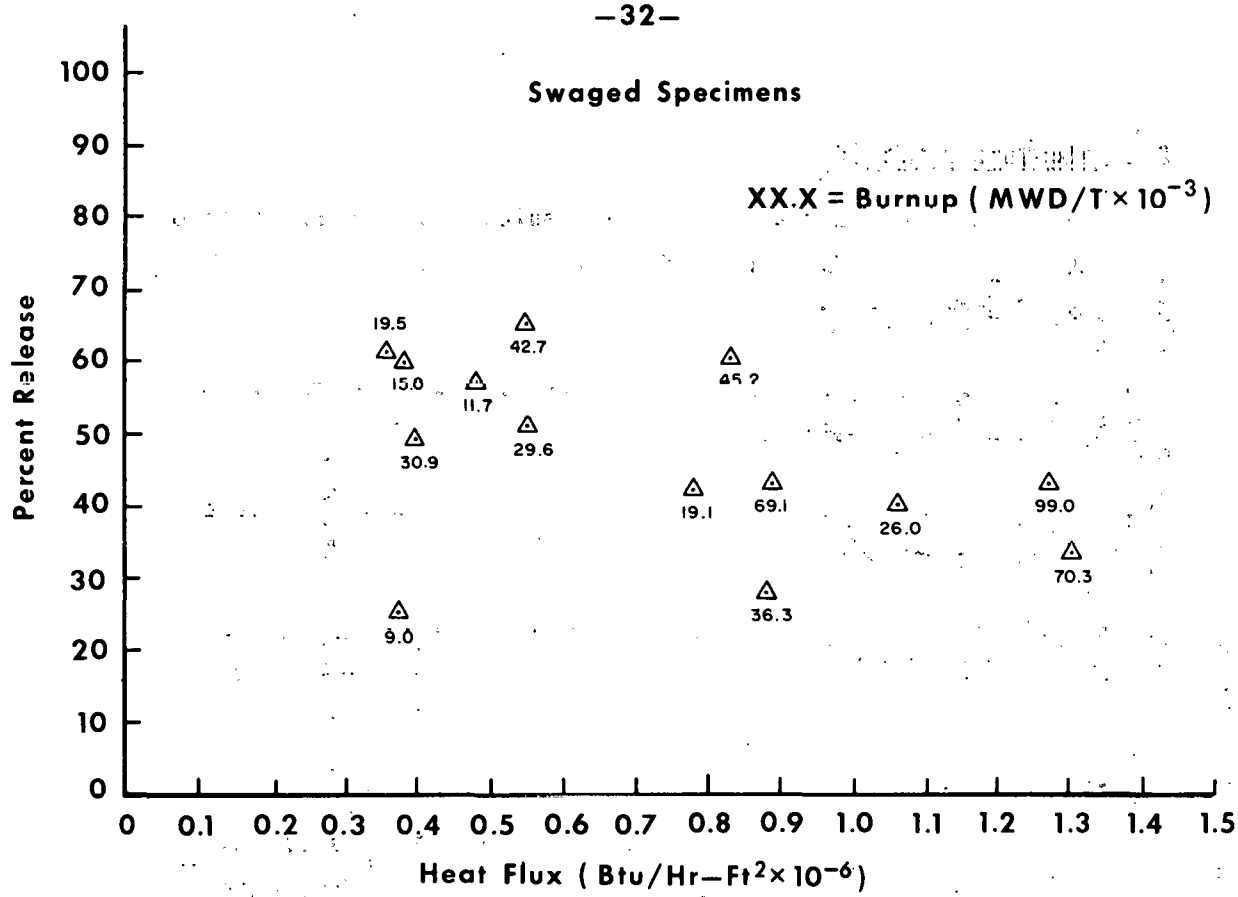

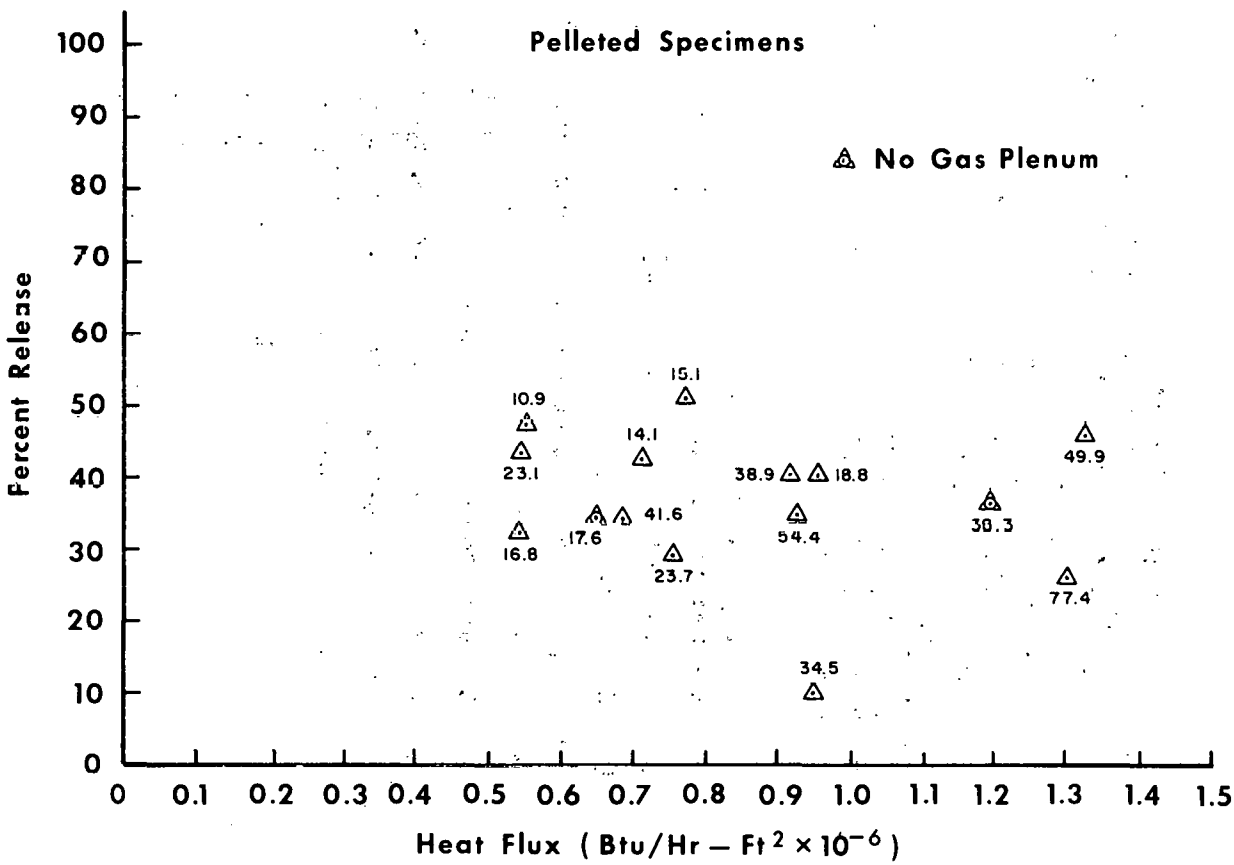

Figure 12. FISSION GAS RELEASE DATA, PERCENT RELEASE VERSUS HEAT FLUX

2. Calculation Method

The calculation of the percentage fission gas release is complicated by several factors in this particular fuel. Among these complicating factors are:

a. Data for the fission yield of the krypton isotopes from plutonium fission are not directly available.

b. The U-235/Pu-239 fission ratio does not remain constant during irradiation.

c. Xe-136 is formed by U-235 and Pu-239 fission and by neutron capture in Xe-135. Thus, the amount of Xe-136 formed is a function of both burnup and neutron flux.

d. The difference in size between Xe atoms and Kr atoms (1.90 A and 1.69 A respectively) indicates that the fractional release of these two isotopes might differ. Data by Markowitz[6] shows the diffusion coefficient of Xe to be an order of magnitude lower than that of Kr.

Obviously certain assumptions had to be made, and a fixed basis used for the calculation of the percentage fission gas release. A discussion of the assumptions made is as follows:

a. Fission Yields

The thermal fission yields of the noble gas isotopes from U-235 and Pu-239 used in the fission gas release calculations are presented in Table VII:

TABLE VII

NOBLE GAS FISSION YIELDS FROM URANIUM AND PLUTONIUM

Isotope	Fission Yield, %[7] U-235	Pu-239
Kr-83	0.544	0.29
Kr-84	1.00	0.47
Kr-85	0.293	0.127
Kr-86	2.02	0.76
Total Kr	3.857	1.647
Xe-131	2.93	3.78
Xe-132	4.38	5.26
Xe-134	8.06	7.47
Xe-136	6.46	6.63
Total Xe	21.83	23.14

b. U-235/Pu-239 Fission Ratio

Using a thermal neutron fission cross-section of 489 and 735 barns for U-235 and Pu-239 respectively, the initial U 235/Pu-239 fission ratio of this fuel is calculated to be 1.36. As burnup progresses, this fission ratio will increase since Pu-239 is relatively more rapidly depleted than U-235 because of its higher absorption cross-section. The picture is further complicated by the fact that this

fuel contains a high percentage of fissionable material and, hence, the self shielding in the fuel is quite high. An approximate calculation indicates that the fission ratio would rise to 2.13 at 100,000 MWD/T if burnup is assumed to be restricted to the fuel in an annular cross-section with a depth equal to half the fuel radius. The maximum effect would be seen in the Kr-85 fission yield which would increase from 0.222% to 0.240%. Since this effect of changing fission ratio has to be integrated over the entire burnup range, the error introduced by using the initial fission ratio of 1.36 is less than 10% at the highest burnup, and insignificant at the lower burnups.

Since the fission ratio for this fuel is assumed to be 1.36 throughout the entire irradiation, the composite fission yields used are as follows:

Kr-85	0.222%
Total Kr	2.92%
Total Xe	22.39%

c. Xe-136 Formation

In addition to the Xe formed by fissioning, Xe is also formed by neutron capture in the 9.2 hour Xe-135 to form Xe-136. The thermal fission yield of Xe-135 is 6.3% for U-235 and 5.99% for Pu-239 so that the composite fission yield of Xe-135 is 6.16%. Assuming a volume average neutron flux of 3×10^{13} $n/cm^2/sec$, the conversion of Xe-135 to Xe-136 would be about 80% so that the total Xe yield is 27.32%. Thus, the data used to calculate percentage release was as follows:

Isotope	Total Yield (Atoms/Atom Fissioned)
Kr-85	0.00222
Total Kr	0.0292
Total Xe	0.2732

From the above data, it can be seen that the theoretical total Xe/total Kr ratio is 9.4 which compares well with the measured ratio as shown in Table VI.

d. Relative Release of Kr and Xe

The analysis of the fission gas samples employed two different techniques. After thoroughly mixing the gas from a gas cylinder, an aliquot was taken and gamma counted to determine the Kr-85 content. This same sample was then analyzed for total Kr and Xe by gas chromatography. It can be seen from the data in Table VI that the percentage release for Kr and Xe was very nearly equal in most cases with the Xe/Kr ratio being very close to the predicted value of 9.4. Thus, it appears that in this case, the difference in size between the Kr and Xe atoms had no effect upon their release rate or conversely, fission gas release was not controlled by a diffusion mechanism in this fuel.

3. Discussion of Results

Examination of the fission gas release data shows several items of interest. First, it is noted that all the percentage releases fall within the range of 10 to 65%. The average release was 47% and 36% for the swaged and pelleted specimens respectively. Further, it is noted that the percentage release does not seem to follow any pattern with respect to burnup, heat flux or $\int k d\theta$. A plot of percentage fission gas release vs. heat flux and burnup shows no apparent correlation and also shows little difference between the pelleted and swaged specimens. This "scatter" in the fission gas release data is consistent with other data collected for UO_2 fission gas release; however, the percentage release is greater than the observed release from UO_2 operated under similar heat flux conditions[8,9].

This scatter in the data and the deviation from UO_2 behavior may be due to any one, or a combination of other experimental parameters such as:

a. The combination of high burnup and high power density.

b. The uncertainty as to the fuel-to-clad gap condition in the specimens during irradiation, and hence an uncertainty as to the temperature conditions.

c. The presence of Pu in this fuel and its attendant effect upon melting points, thermal conductivity, stability of the PuO_2-UO_2 system, etc.

From a practical standpoint, concern about high fission gas release data is lessened by the fact that the experiment also showed that the gas plenum offers one design method for accommodating the fission gas pressure.

F. Sectioning

After puncturing, the specimens were sectioned by cutting through the cladding and fuel with a tubing cutter mounted on the lathe shown in Figure 5. The length of the cut sections was measured by photographing the sections adjacent to a machinist's scale, as shown in Figure 13, in order to determine the exact location of the sectioning cuts. The cladding was also checked for warpage and bulging at this time. No cladding defects or deformations were observed. The surfaces exposed by the sectioning operation were then visually examined at 30X magnification and photographed. Photographs of the fuel cross-sections in the"as cut" condition are shown in Figures 14 through 50.

In addition to photographing the exposed fuel surfaces, the size and depth of the central void was measured. The diameter of the central void was measured by scaling off the void dimensions from the "as cut" photographs. The depth of the void was measured by probing the void with a fine wire. In this way both the length and position of the central void within the fuel could be determined. The position of the central void is shown on the sectioning diagrams (Figures 14 through 50). This latter technique was not successful in all cases due to the size of the void. In these cases, the minimum void length was determined by visual observation of the void at the various surfaces. The physical dimensions of the active fuel zone and the central void are given in Table V (pages 24 and 25)

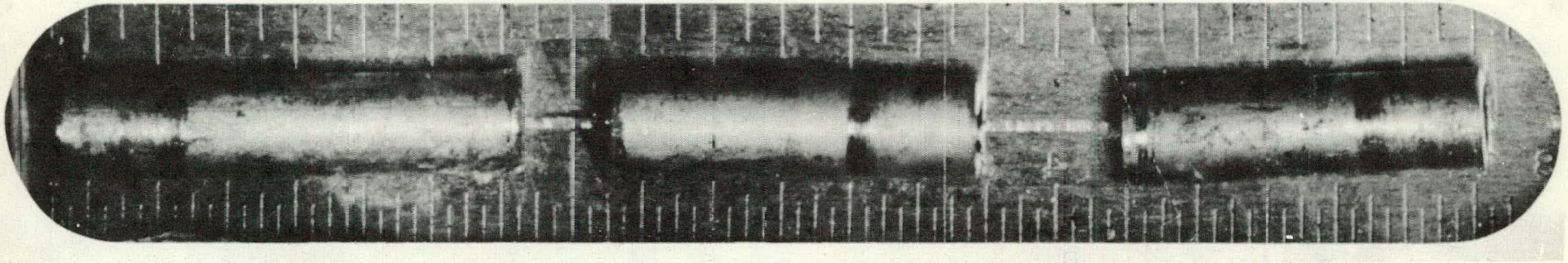

Figure 13. FUEL SPECIMEN AFTER SECTIONING

Specimen I-1-P	
Burnup	16,600 $\frac{MWD}{T}$
Heat Flux	1.41×10^6 BTU/HR - FT^2
Cladding Surface Temp.	1040°F
Fission Gas Release	—— %

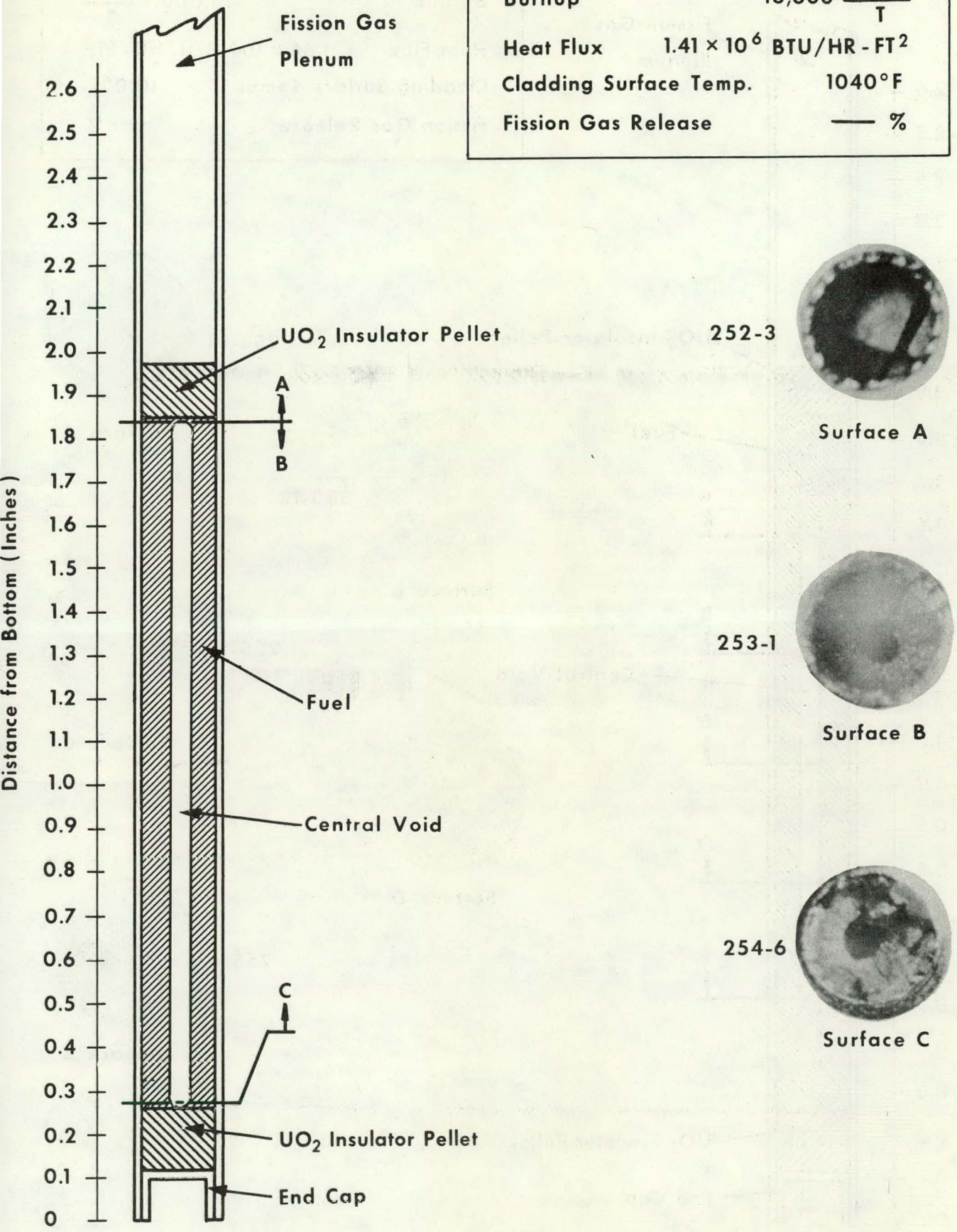

Figure 14 SECTIONING DIAGRAM AND FUEL CROSS SECTIONS, SPECIMEN I-1-P

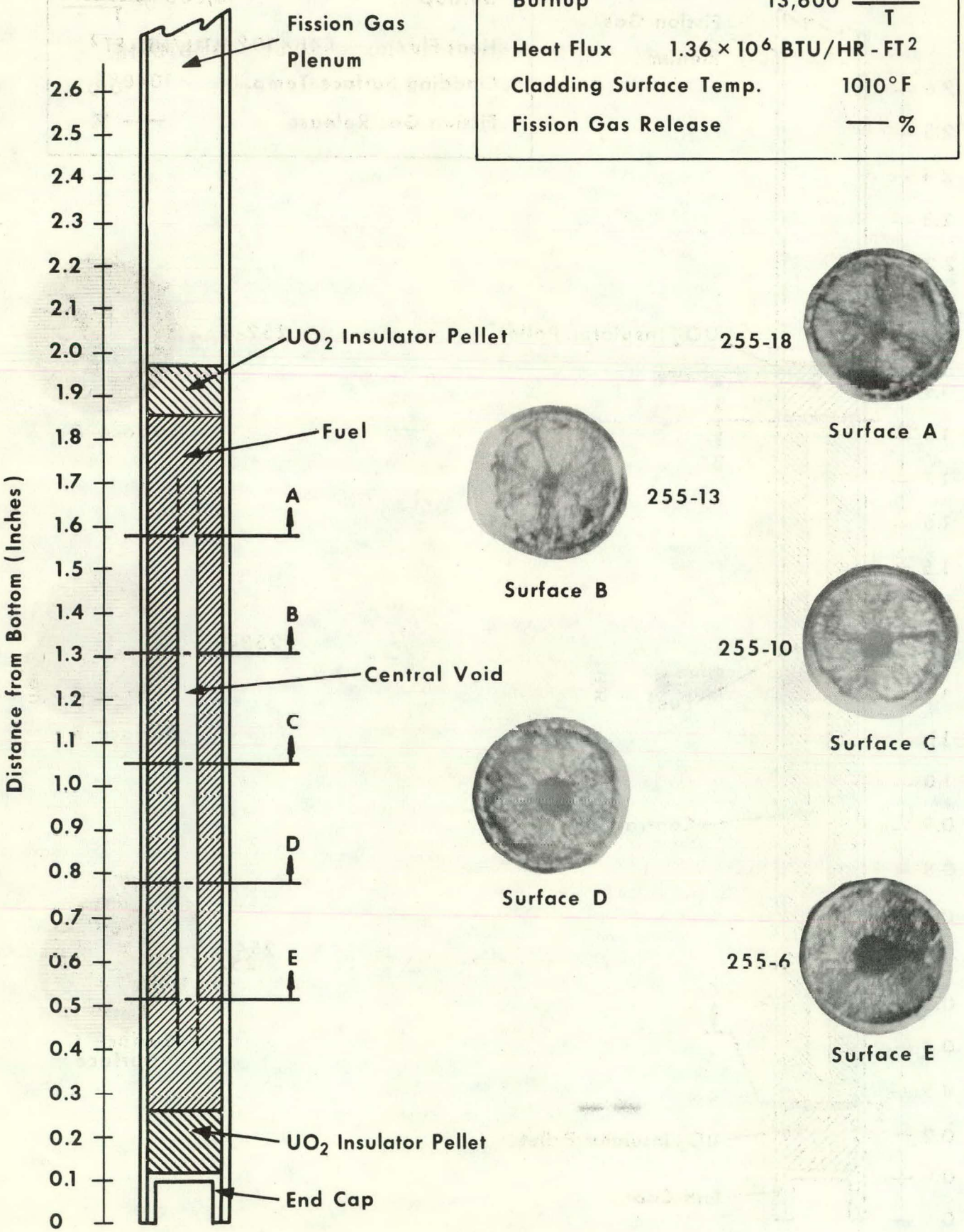

Figure 15. SECTIONING DIAGRAM AND FUEL CROSS SECTIONS, SPECIMEN I-2-P

Specimen I-4-P	
Burnup	4,700 $\frac{MWD}{T}$
Heat Flux	0.62×10^6 BTU/HR - FT^2
Cladding Surface Temp.	1010° F
Fission Gas Release	— %

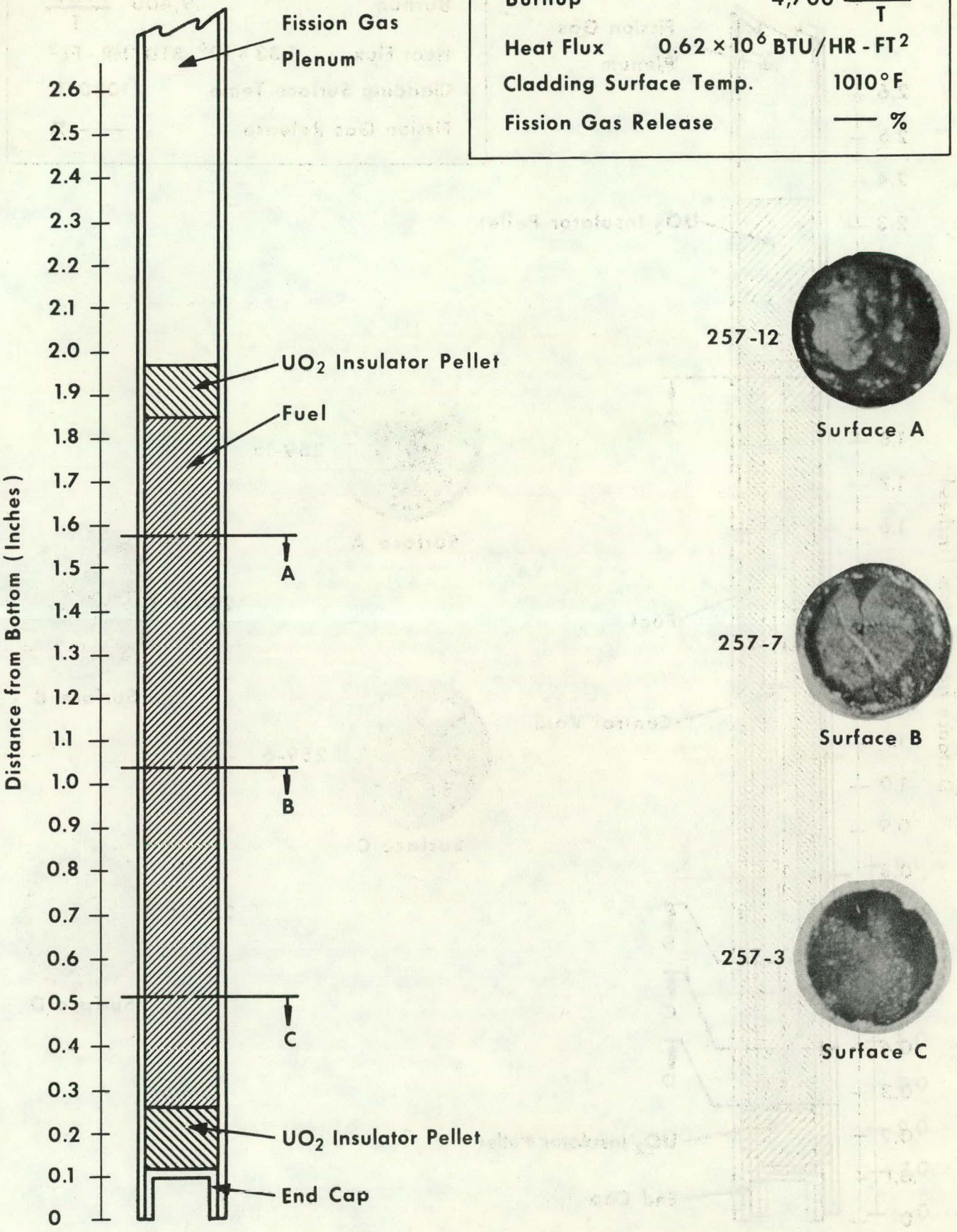

Figure 16. SECTIONING DIAGRAM AND FUEL CROSS SECTIONS, SPECIMEN I-4-P

Specimen II-1-S	
Burnup	19,400 MWD/T
Heat Flux	1.33×10^6 BTU/HR - FT^2
Cladding Surface Temp.	1080°F
Fission Gas Release	—— %

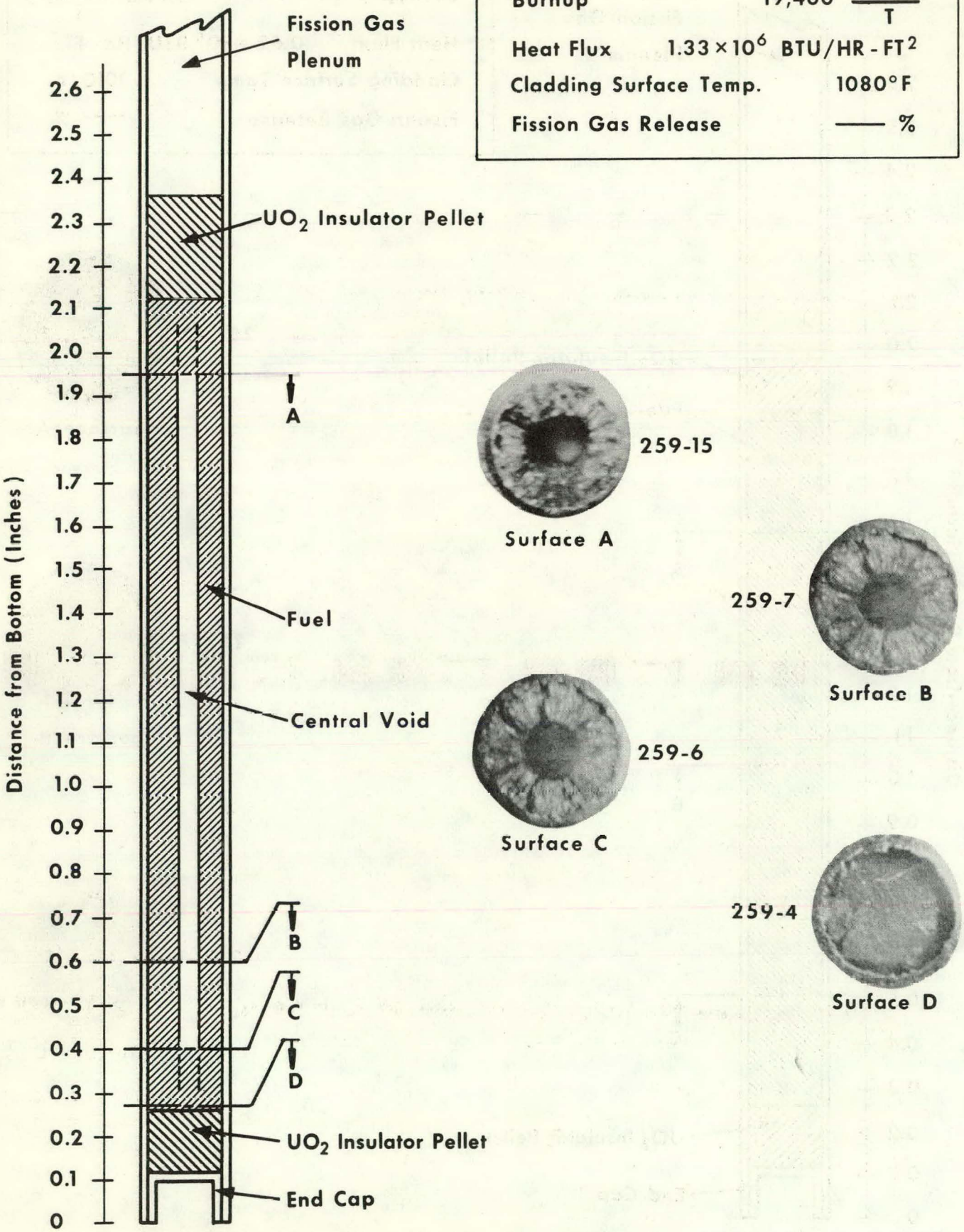

Figure 17. SECTIONING DIAGRAM AND FUEL CROSS SECTIONS, SPECIMEN II-1-S

Specimen II-4-S	
Burnup	6,600 $\frac{MWD}{T}$
Heat Flux	0.72×10^6 BTU/HR-FT^2
Cladding Surface Temp.	1130°F
Fission Gas Release	—— %

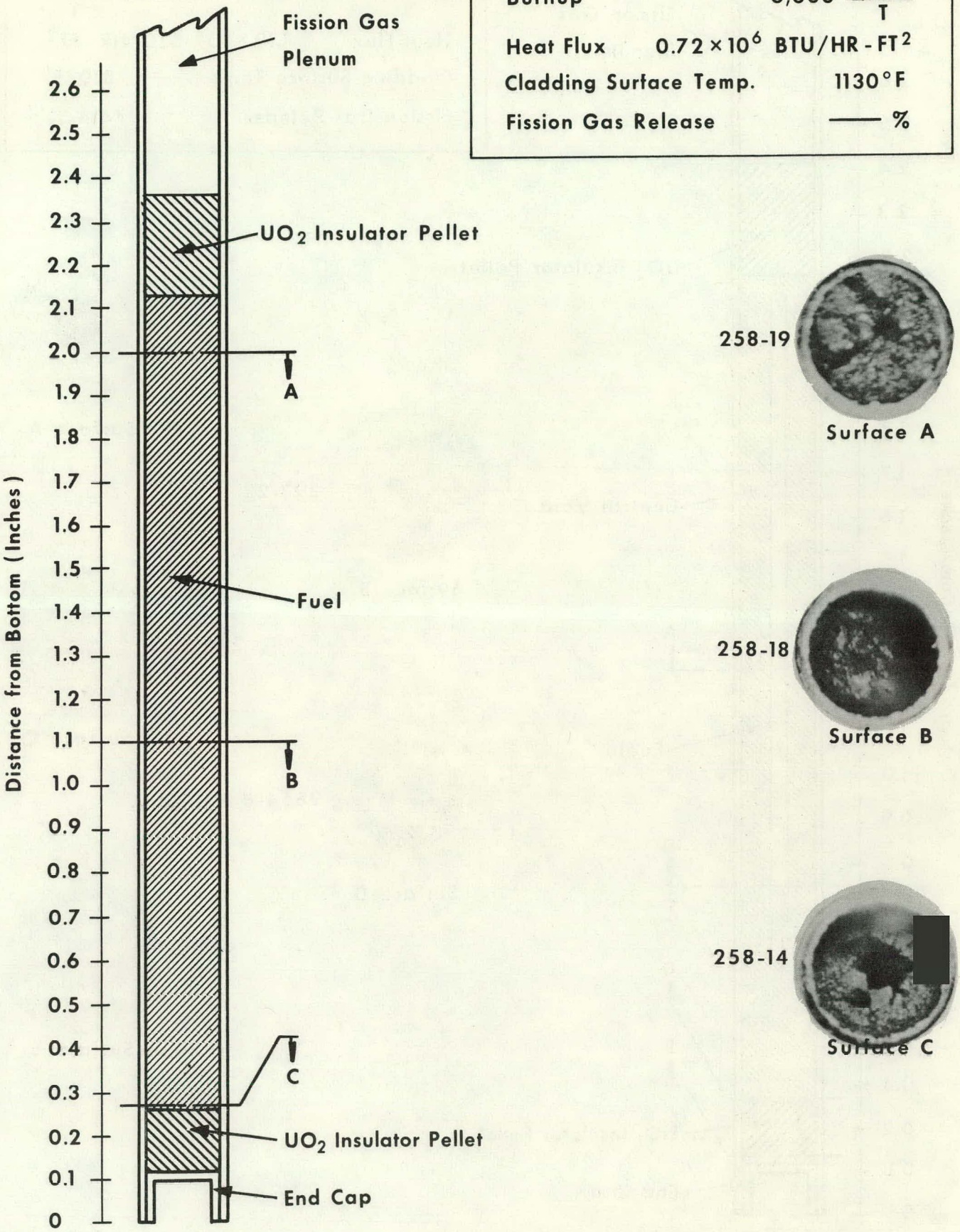

Figure 18. SECTIONING DIAGRAM AND FUEL CROSS SECTIONS, SPECIMEN II-4-S

Specimen III-1-S	
Burnup	26,000 MWD/T
Heat Flux	1.19×10^6 BTU/HR - FT^2
Cladding Surface Temp.	810°F
Fission Gas Release	44.4 %

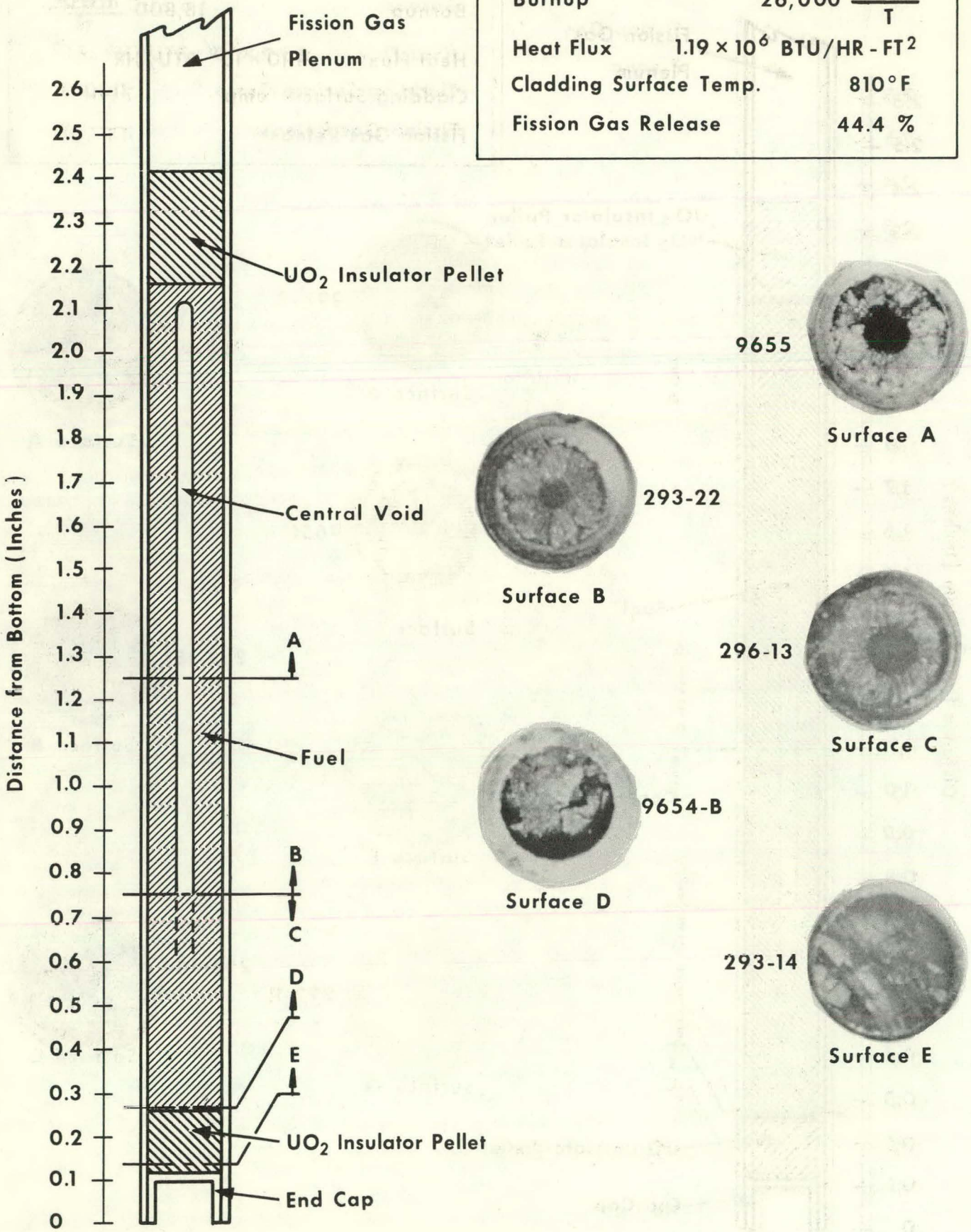

Figure 19. SECTIONING DIAGRAM AND FUEL CROSS SECTIONS, SPECIMEN III-1-S

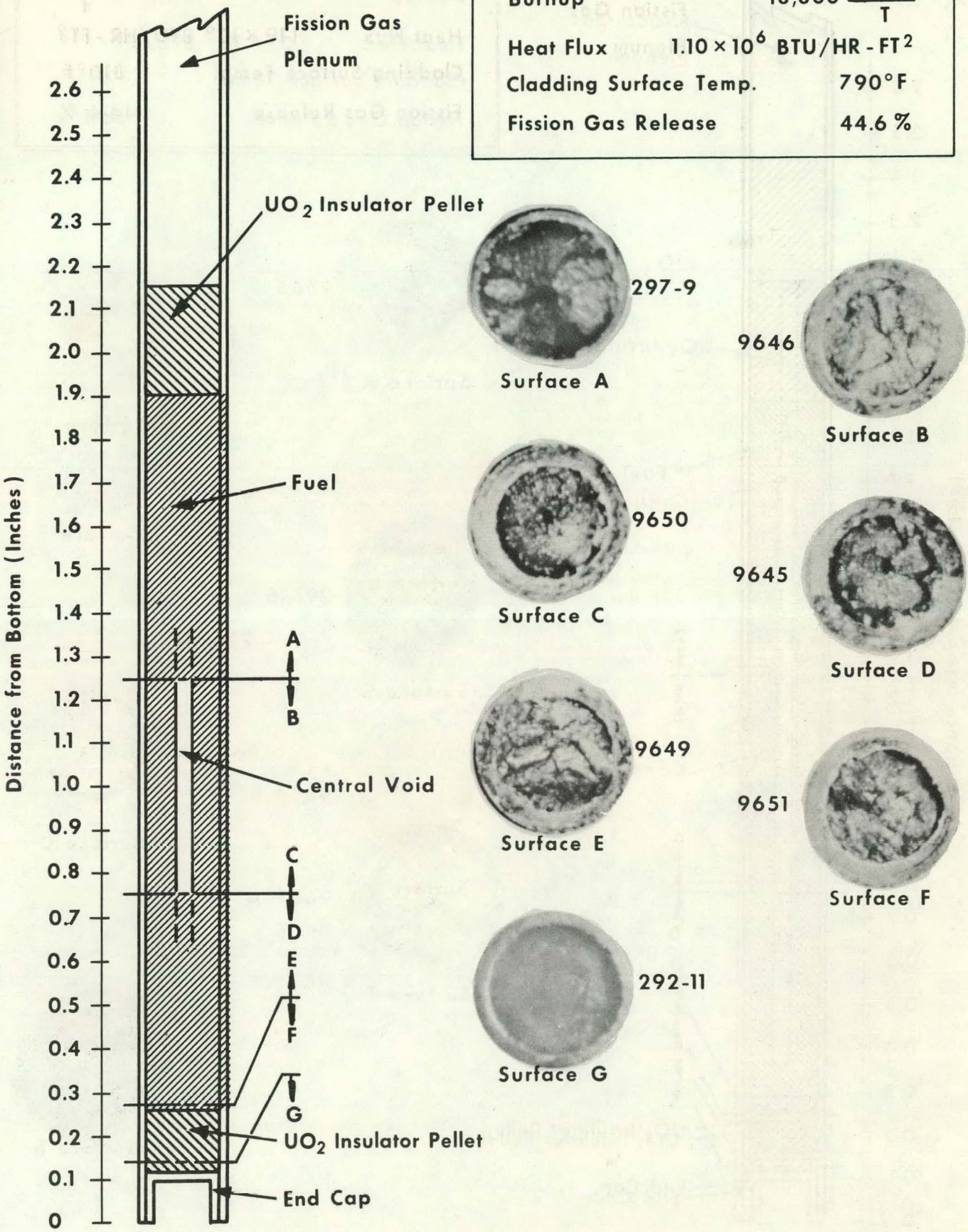

Figure 20. SECTIONING DIAGRAM AND FUEL CROSS SECTIONS, SPECIMEN III-2-P

Specimen III-3-P	
Burnup	15,100 $\frac{MWD}{T}$
Heat Flux	1.02×10^6 BTU/HR - FT^2
Cladding Surface Temp.	820°F
Fission Gas Release	56.1 %

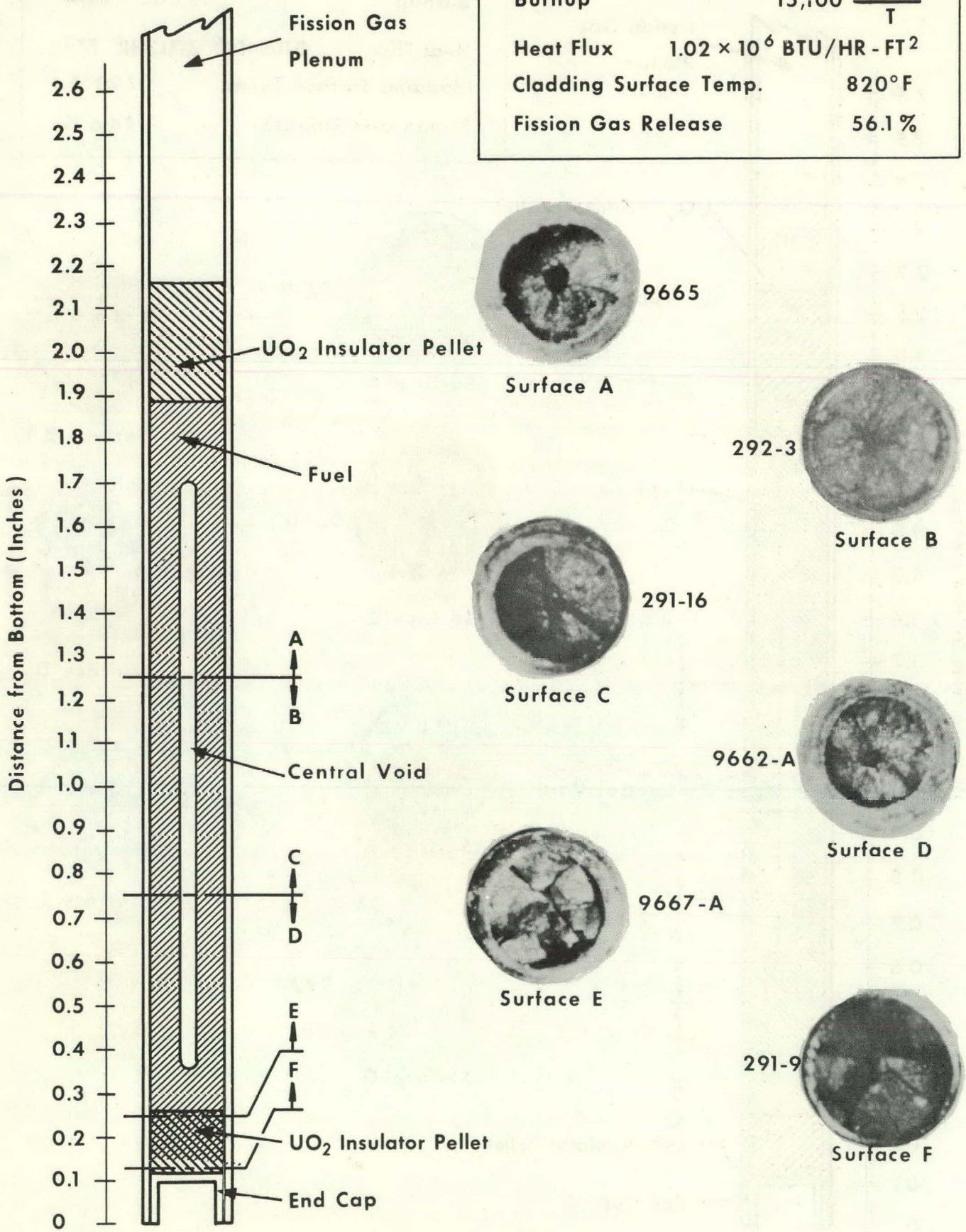

Figure 21. SECTIONING DIAGRAM AND FUEL CROSS SECTIONS, SPECIMEN III-3-P

Specimen III-4-S	
Burnup	11,700 $\frac{MWD}{T}$
Heat Flux	0.75×10^6 BTU/HR - FT^2
Cladding Surface Temp.	710°F
Fission Gas Release	66.6 %

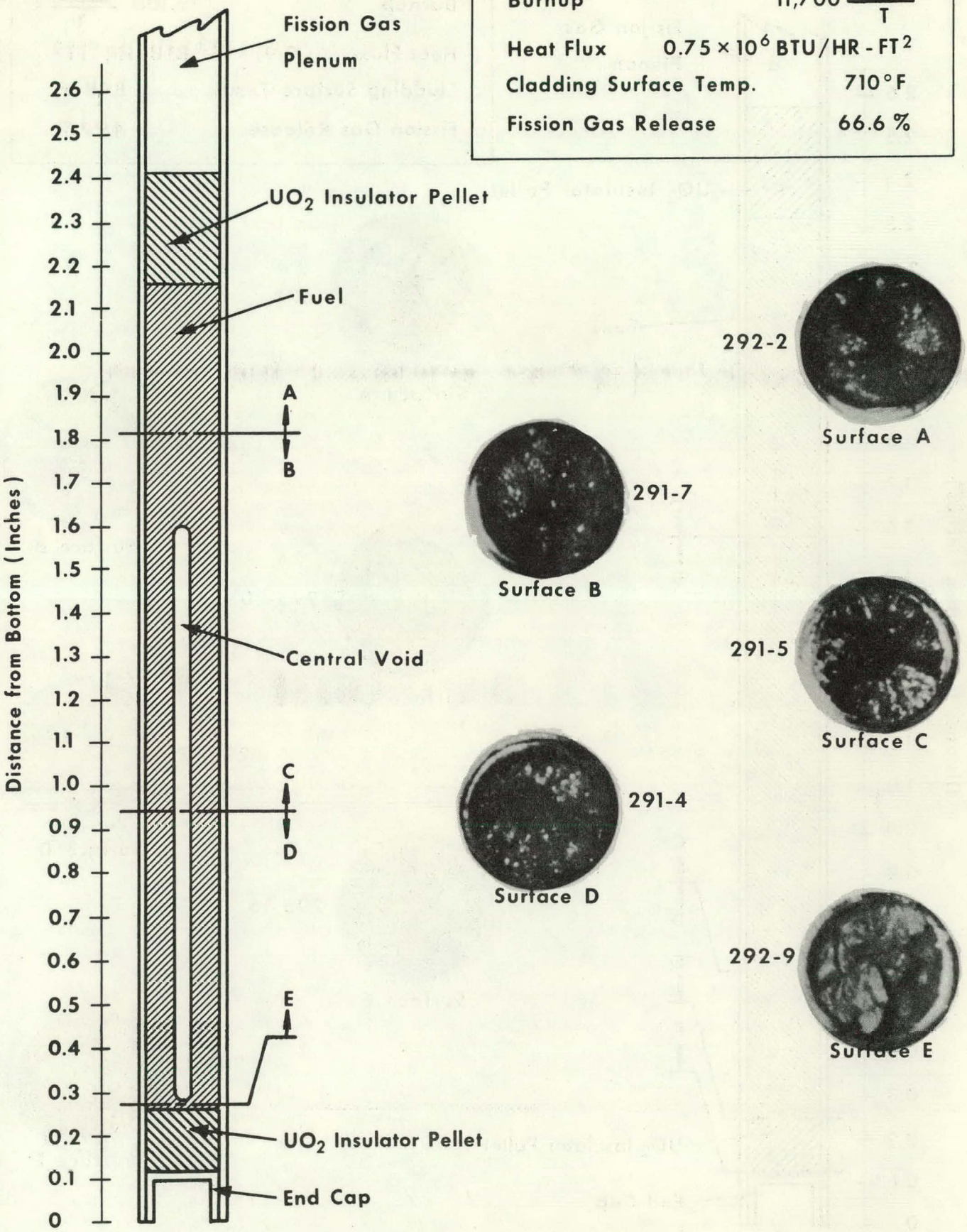

Figure 22. SECTIONING DIAGRAM AND FUEL CROSS SECTIONS, SPECIMEN III-4-S

Specimen IV-1-S	
Burnup	19,100 $\frac{MWD}{T}$
Heat Flux	0.91×10^6 BTU/HR - FT^2
Cladding Surface Temp.	890°F
Fission Gas Release	45.7 %

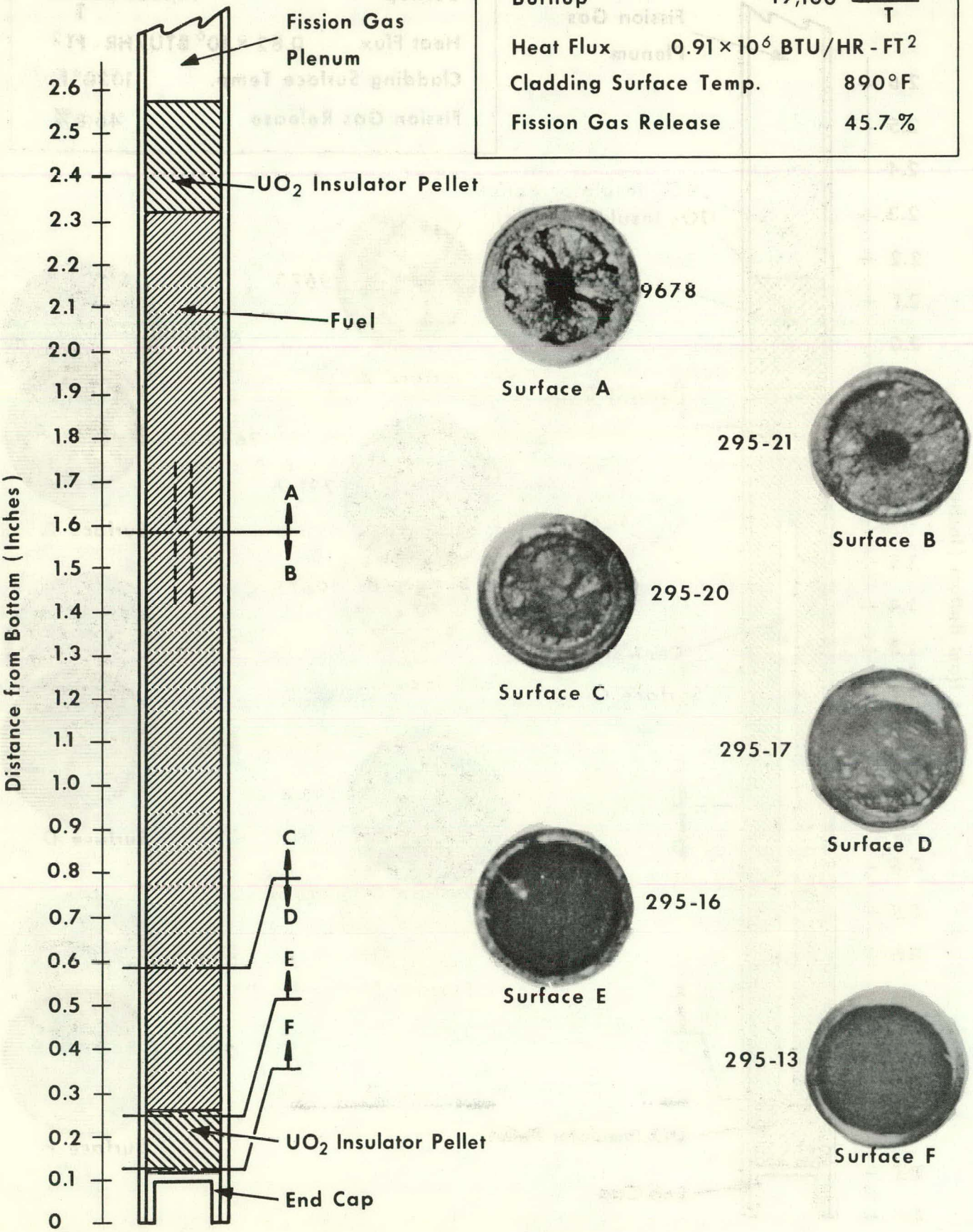

Figure 23. SECTIONING DIAGRAM AND FUEL CROSS SECTIONS, SPECIMEN IV-1-S

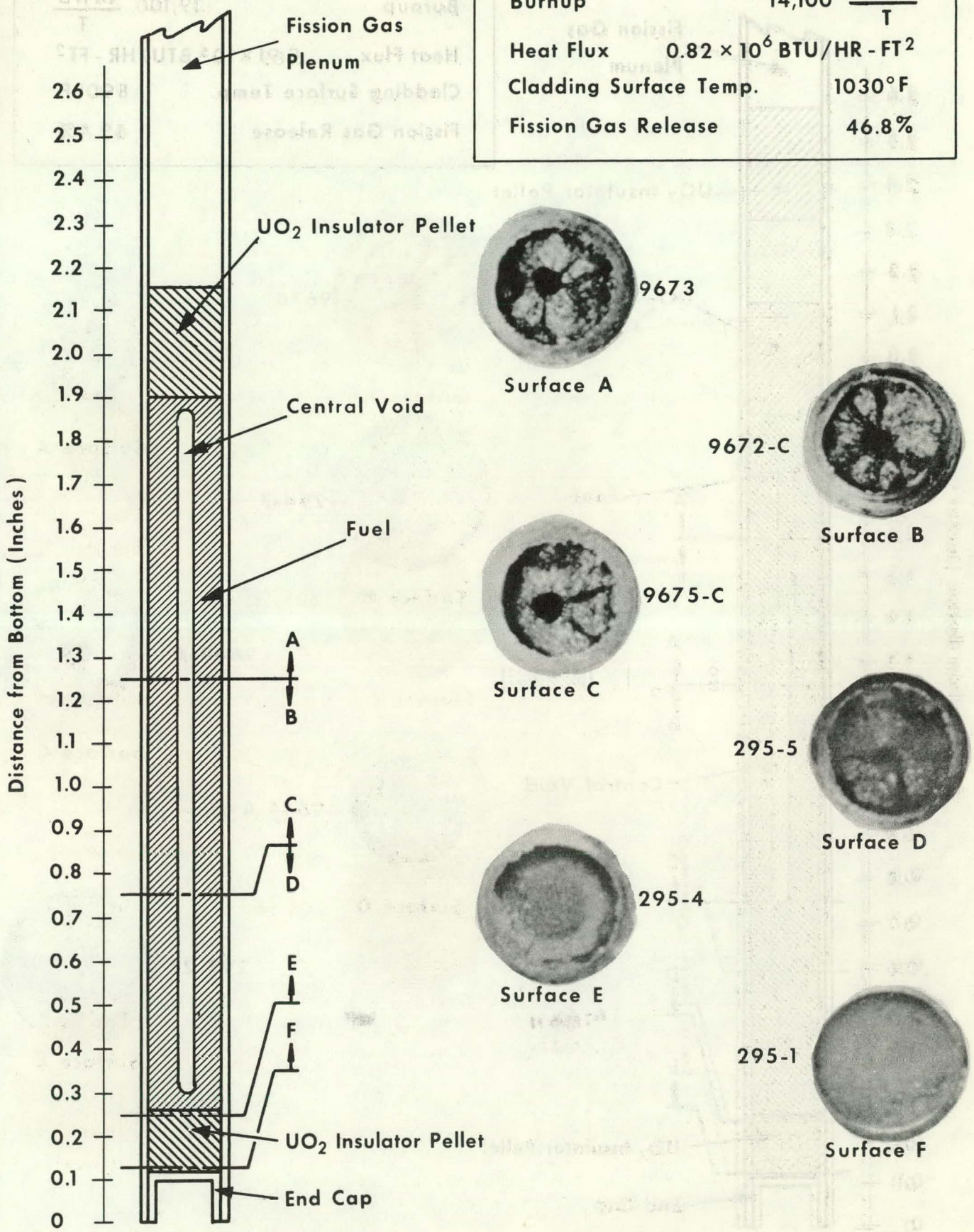

Figure 24. SECTIONING DIAGRAM AND FUEL CROSS SECTIONS, SPECIMEN IV-2-P

Specimen IV-3-P	
Burnup	10,900 MWD/T
Heat Flux	0.69×10^6 BTU/HR - FT^2
Cladding Surface Temp.	990°F
Fission Gas Release	52.4%

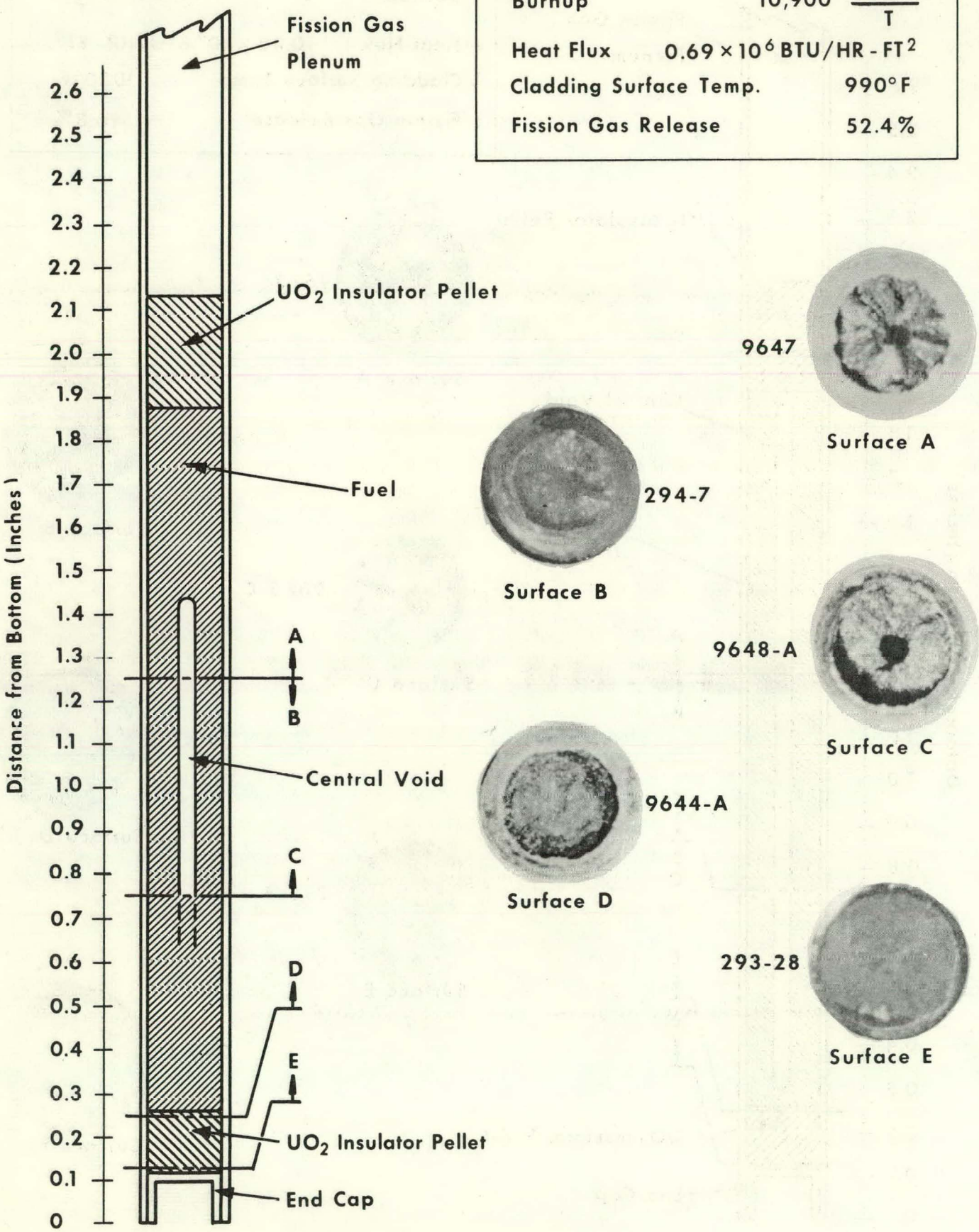

Figure 25. SECTIONING DIAGRAM AND FUEL CROSS SECTIONS, SPECIMEN IV-3-P

Specimen IV-4-S	
Burnup	9,000 $\frac{MWD}{T}$
Heat Flux	0.53×10^6 BTU/HR - FT^2
Cladding Surface Temp.	880°F
Fission Gas Release	27.8%

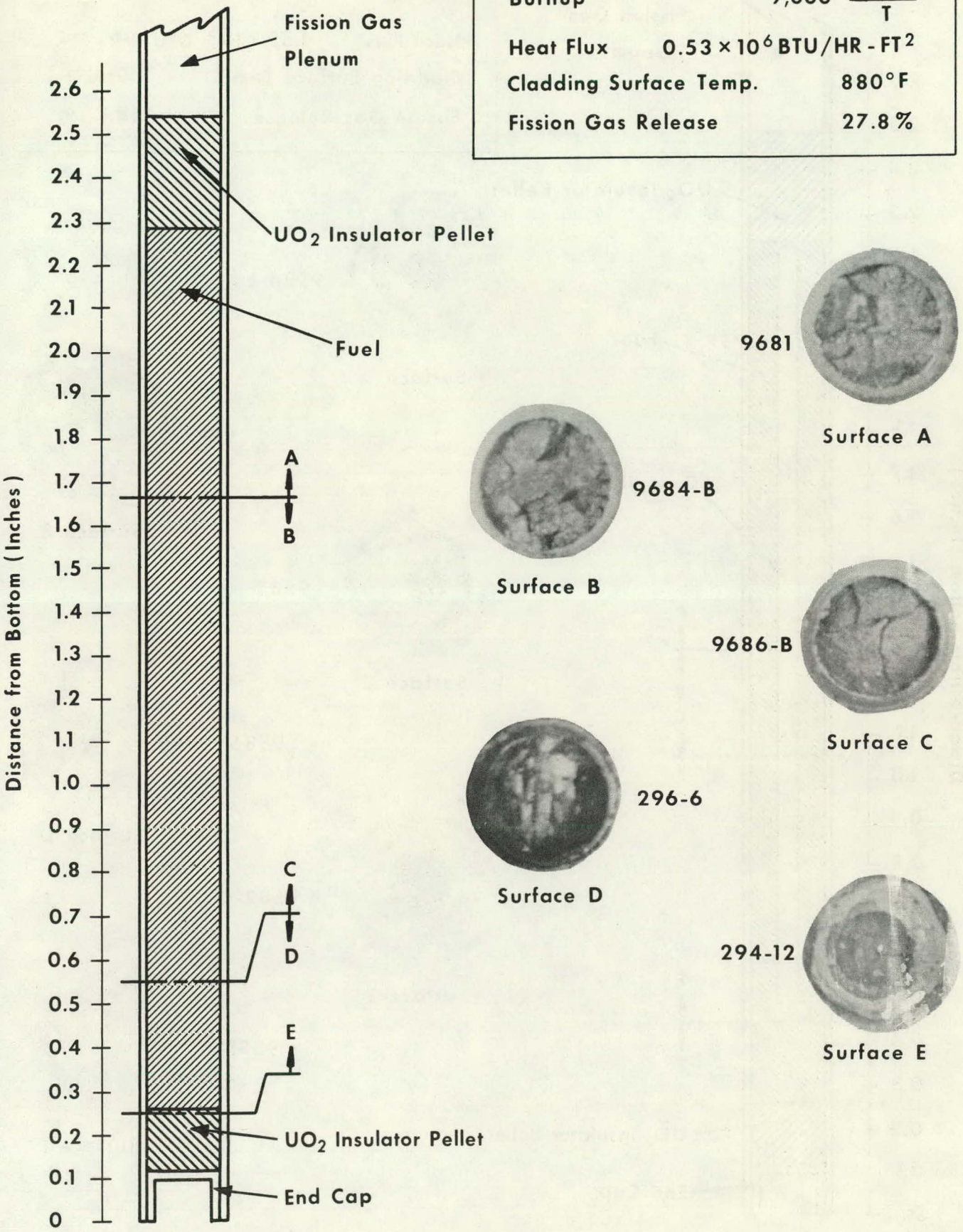

Figure 26. SECTIONING DIAGRAM AND FUEL CROSS SECTIONS, SPECIMEN IV-4-S

Specimen V-1-S	
Burnup	99,000 MWD/T
Heat Flux	1.52×10^6 BTU/HR - FT^2
Cladding Surface Temp.	1260°F
Fission Gas Release	48.1 %

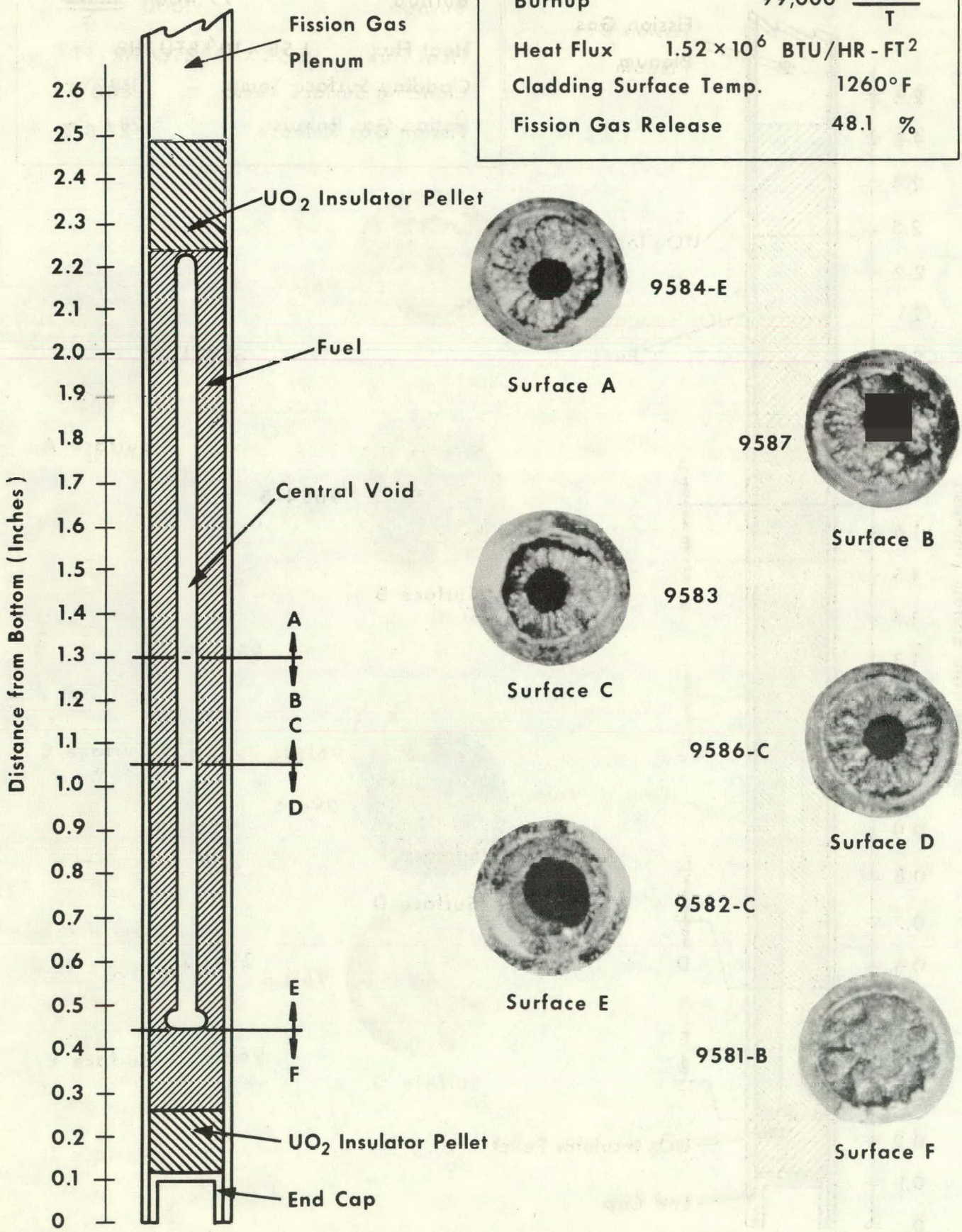

Figure 27. SECTIONING DIAGRAM AND FUEL CROSS SECTIONS, SPECIMEN V-1-S

Specimen V-2-P		
Burnup	77,400	MWD/T
Heat Flux	1.58×10^6	BTU/HR - FT^2
Cladding Surface Temp.	1180	°F
Fission Gas Release	28.8	%

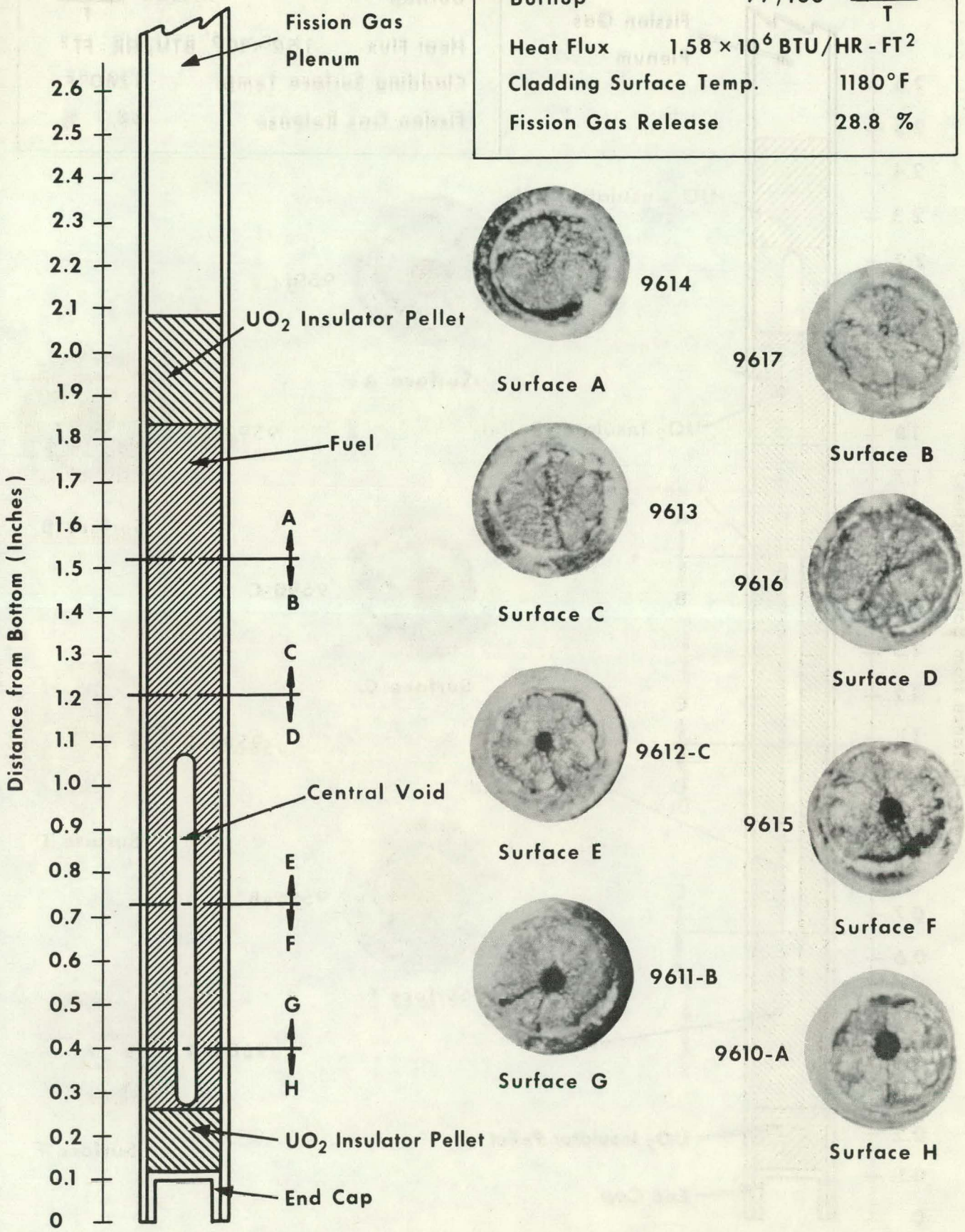

Figure 28. SECTIONING DIAGRAM AND FUEL CROSS SECTIONS, SPECIMEN V-2-P

Specimen V-3-P	
Burnup	54,400 MWD/T
Heat Flux	1.28×10^6 BTU/HR - FT^2
Cladding Surface Temp.	1130 °F
Fission Gas Release	38.3 %

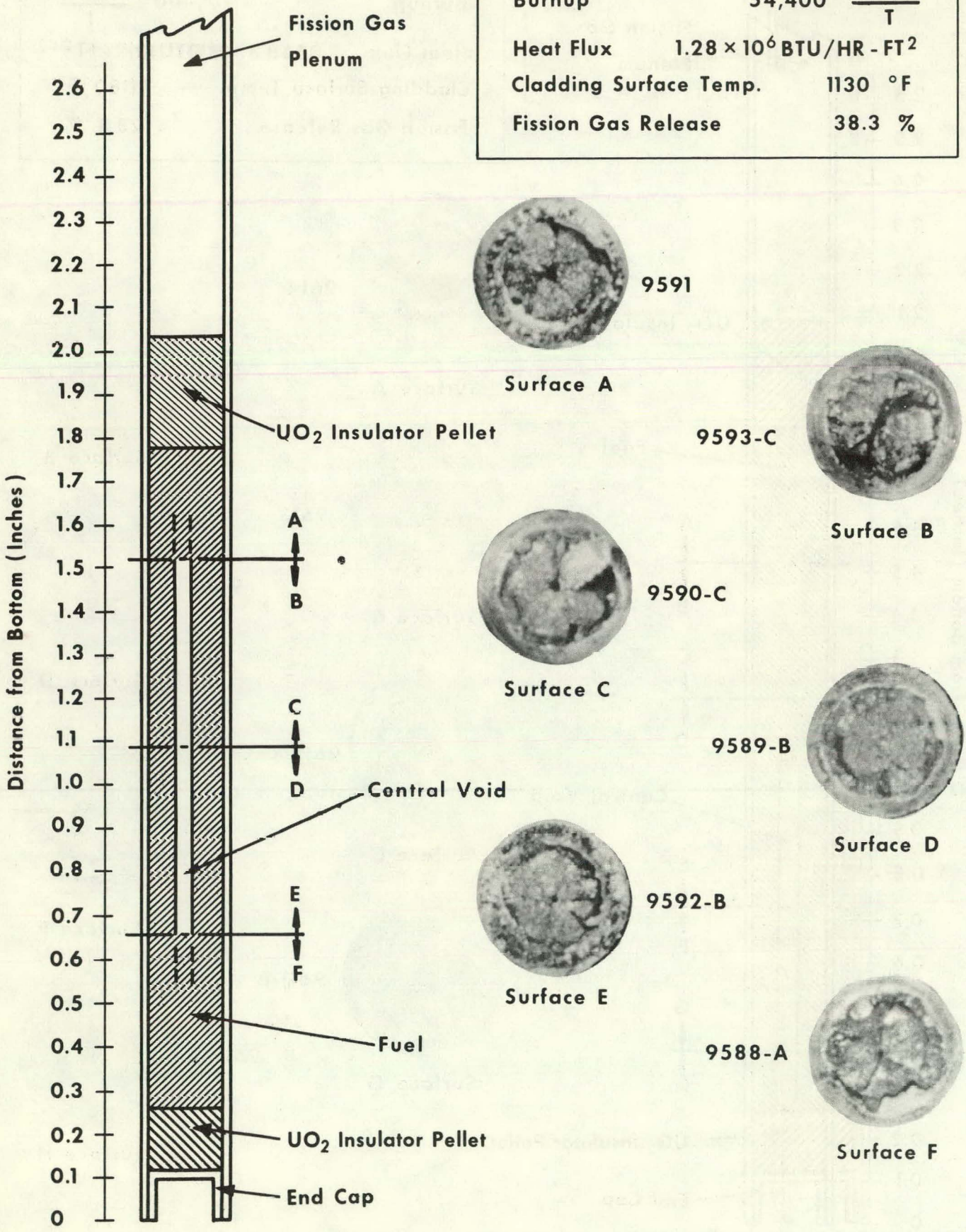

Figure 29. SECTIONING DIAGRAM AND FUEL CROSS SECTIONS, SPECIMEN V-3-P

Specimen V-4-S		
Burnup	42,700	MWD/T
Heat Flux	0.86×10^6	BTU/HR-FT^2
Cladding Surface Temp.	930	°F
Fission Gas Release	71.7	%

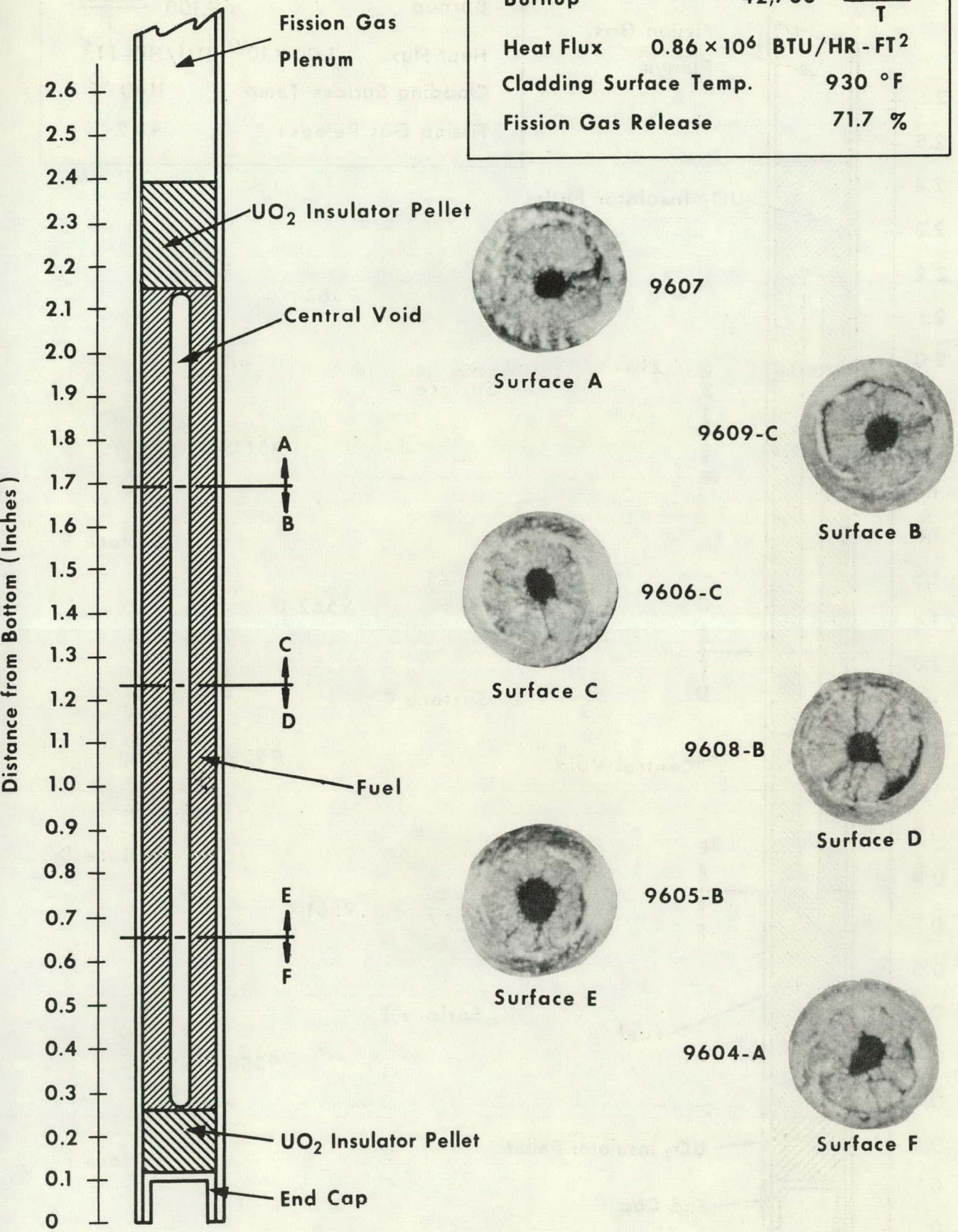

Figure 30. SECTIONING DIAGRAM AND FUEL CROSS SECTIONS, SPECIMEN V-4-S

Specimen VI-1-S	
Burnup	69,100 $\frac{MWD}{T}$
Heat Flux	1.00×10^6 BTU/HR-FT^2
Cladding Surface Temp.	1140 °F
Fission Gas Release	48.2 %

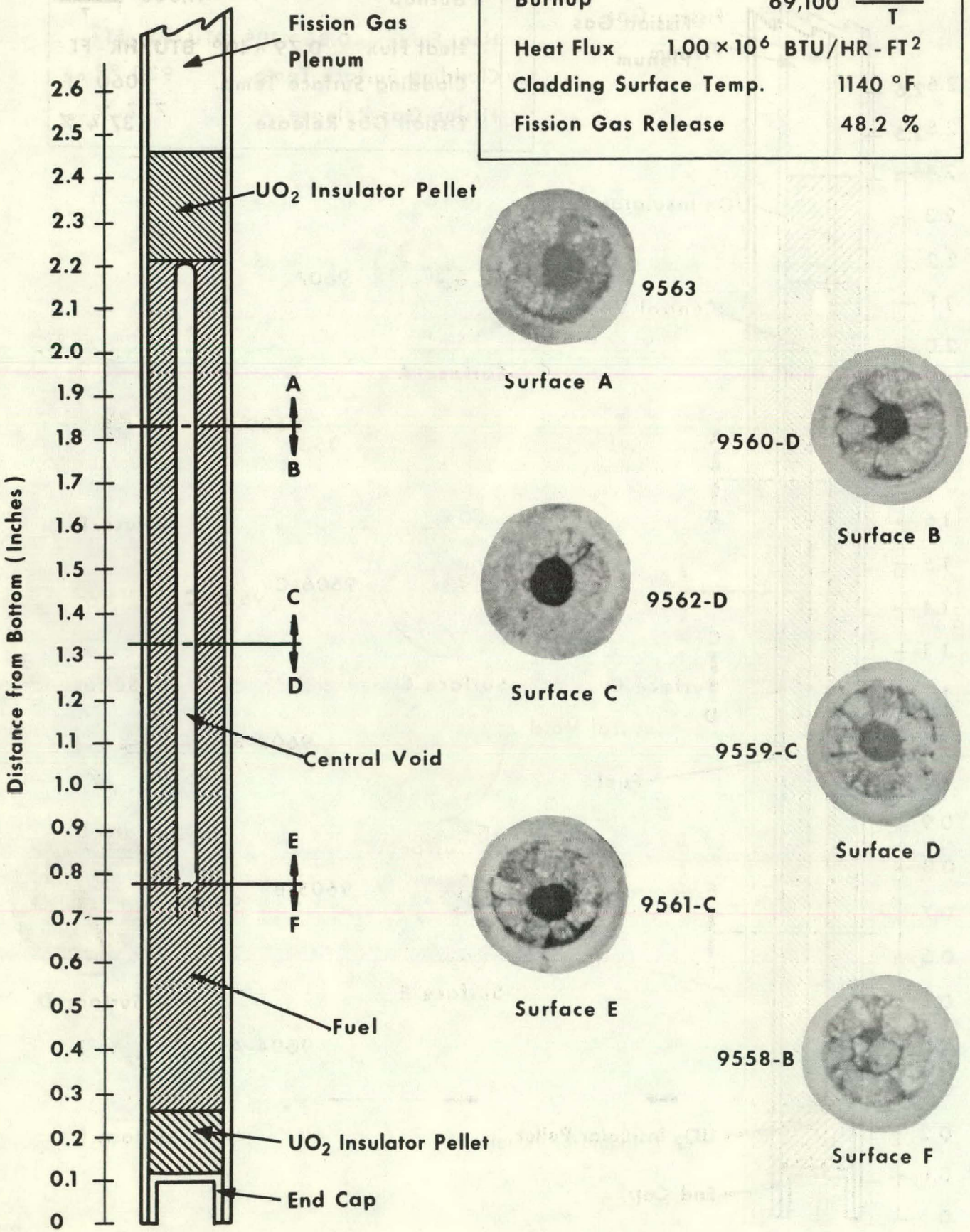

Figure 31. SECTIONING DIAGRAM AND FUEL CROSS SECTIONS, SPECIMEN VI-1-S

Specimen VI-2-P	
Burnup	41,600 MWD/T
Heat Flux	0.79×10^6 BTU/HR-FT^2
Cladding Surface Temp.	1060 °F
Fission Gas Release	37.4 %

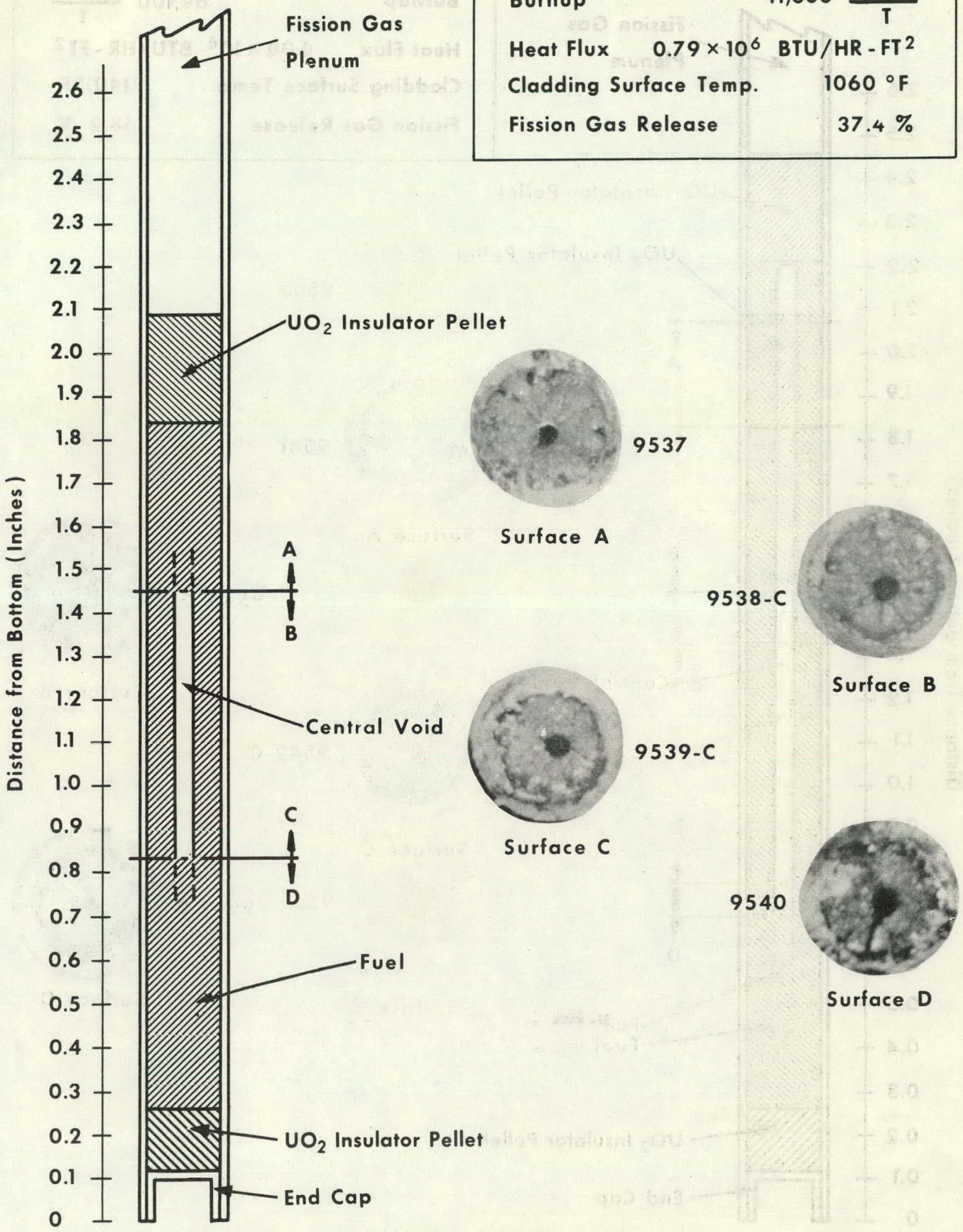

Figure 32. SECTIONING DIAGRAM AND FUEL CROSS SECTIONS, SPECIMEN VI-2-P

Specimen VI-3-P	
Burnup	34,900 MWD/T
Heat Flux	0.76×10^6 BTU/HR-FT^2
Cladding Surface Temp.	1210°F
Fission Gas Release	— %

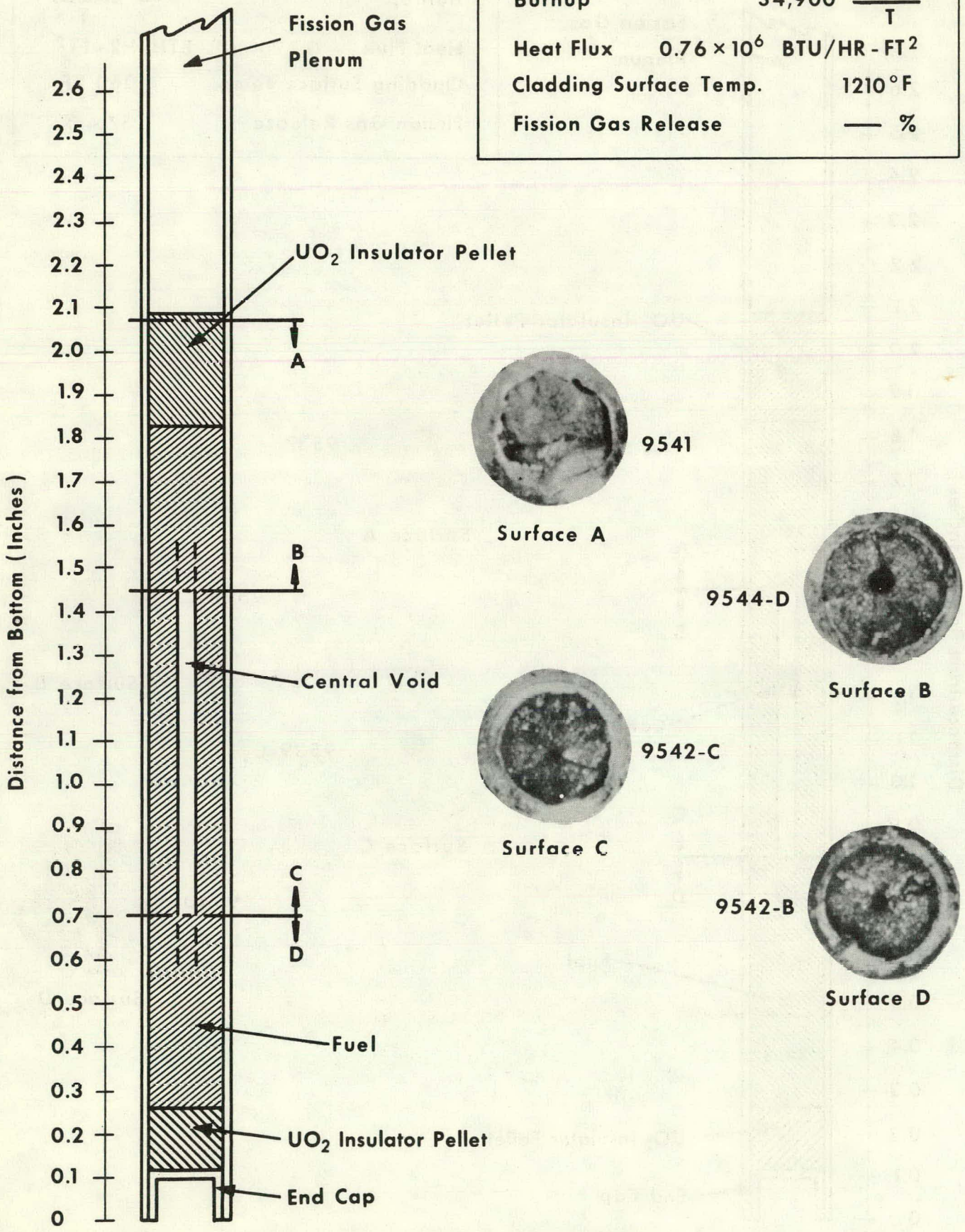

Figure 33. SECTIONING DIAGRAM AND FUEL CROSS SECTIONS, SPECIMEN VI-3-P

Specimen VI-4-S	
Burnup	30,900 MWD/T
Heat Flux	0.62×10^6 BTU/HR - FT^2
Cladding Surface Temp.	980°F
Fission Gas Release	54.8 %

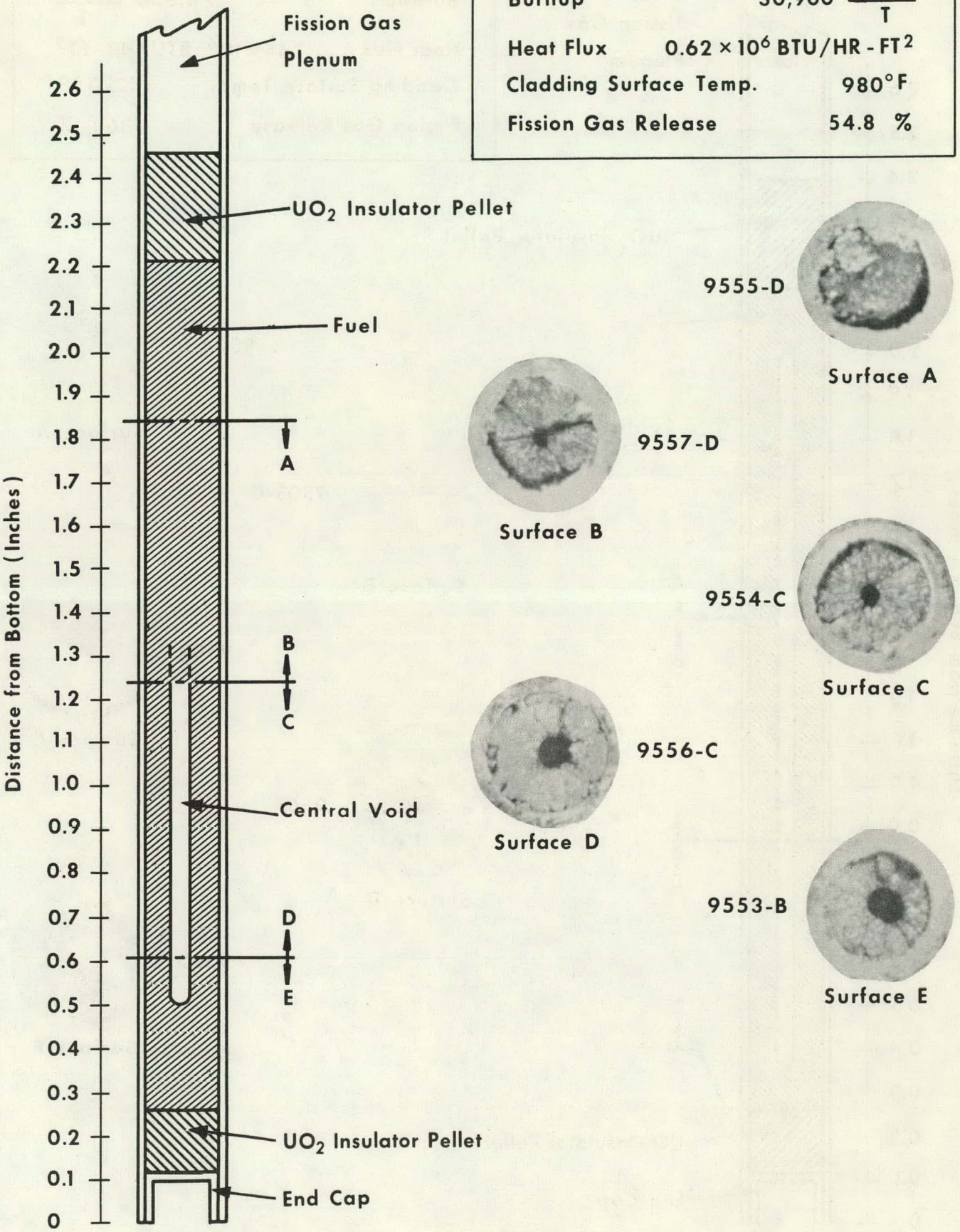

Figure 34. SECTIONING DIAGRAM AND FUEL CROSS SECTIONS, SPECIMEN VI-4-S

Specimen VII-1-S	
Burnup	70,300 MWD/T
Heat Flux	1.44×10^6 BTU/HR-FT^2
Cladding Surface Temp.	1220°F
Fission Gas Release	36.1 %

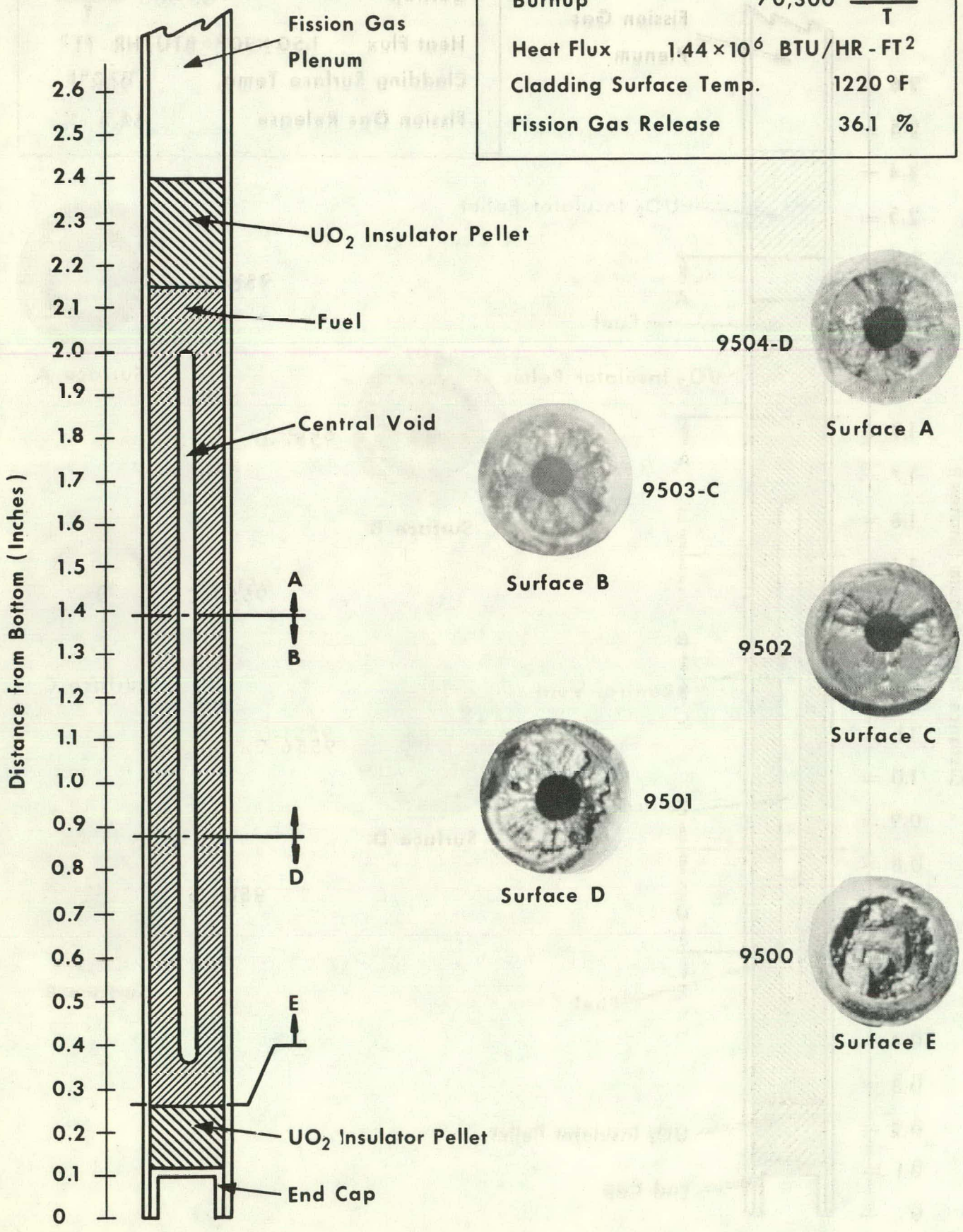

Figure 35. SECTIONING DIAGRAM AND FUEL CROSS SECTIONS, SPECIMEN VII-1-S

Specimen VII-2-P		
Burnup	49,900	MWD/T
Heat Flux	1.50×10^6	BTU/HR-FT^2
Cladding Surface Temp.	1170°F	
Fission Gas Release	44.2	%

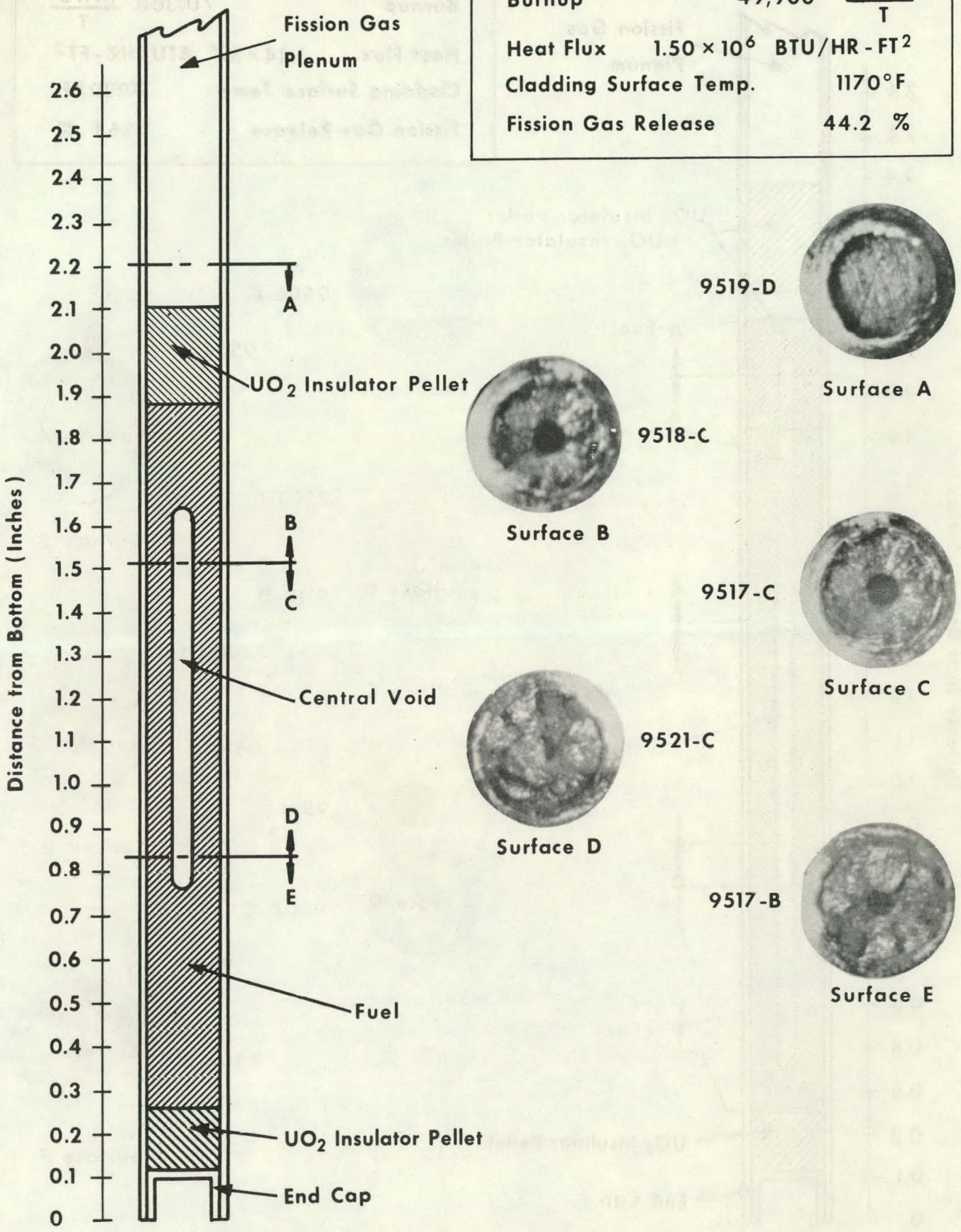

Figure 36. SECTIONING DIAGRAM AND FUEL CROSS SECTIONS, SPECIMEN VII-2-P

Specimen VII-3-P	
Burnup	38,900 MWD/T
Heat Flux	1.24×10^6 BTU/HR-FT^2
Cladding Surface Temp.	1080 °F
Fission Gas Release	44.0 %

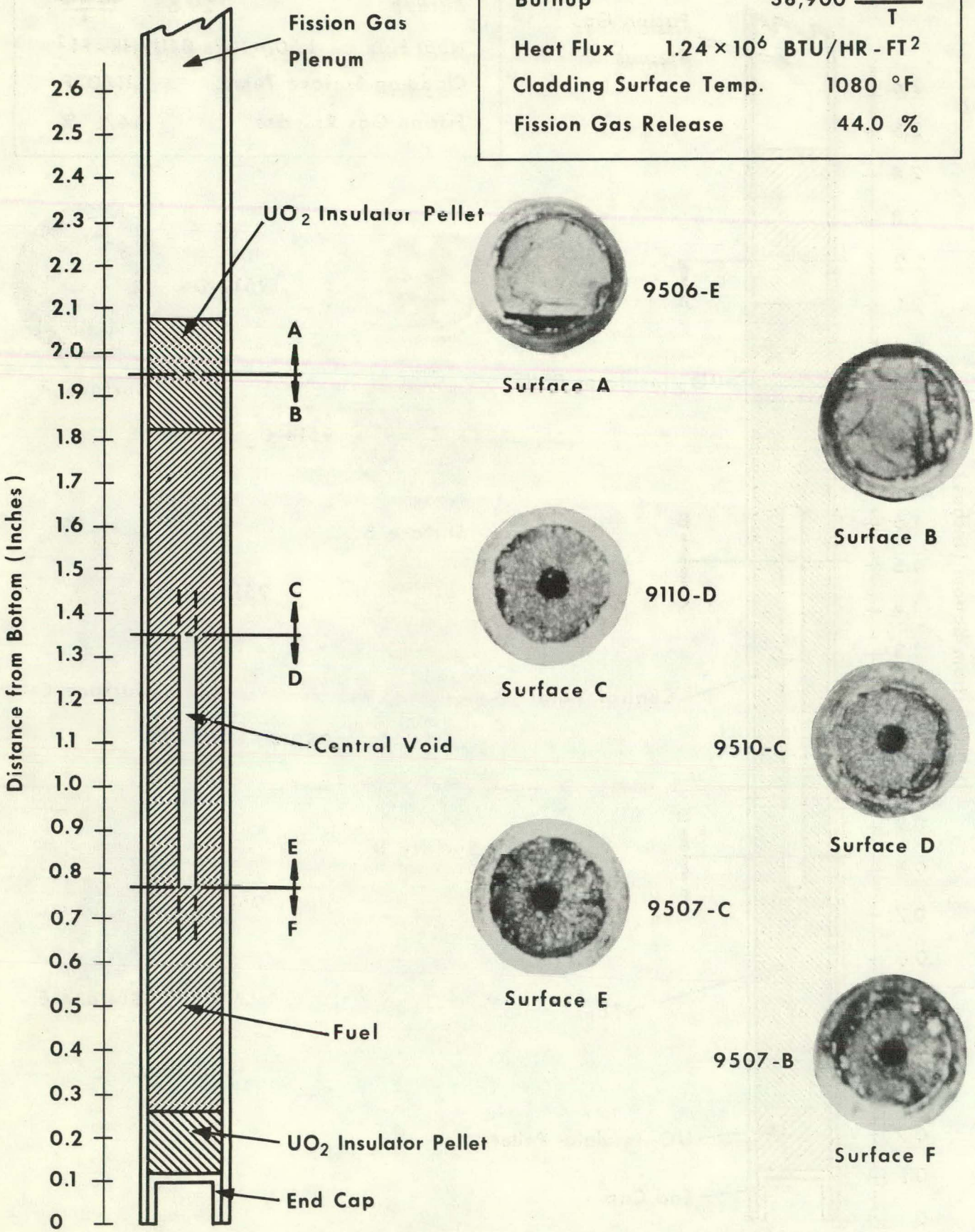

Figure 37. SECTIONING DIAGRAM AND FUEL CROSS SECTIONS, SPECIMEN VII-3-P

Specimen VII-4-S	
Burnup	29,600 $\frac{MWD}{T}$
Heat Flux	0.86×10^6 BTU/HR - FT^2
Cladding Surface Temp.	950 °F
Fission Gas Release	57.0 %

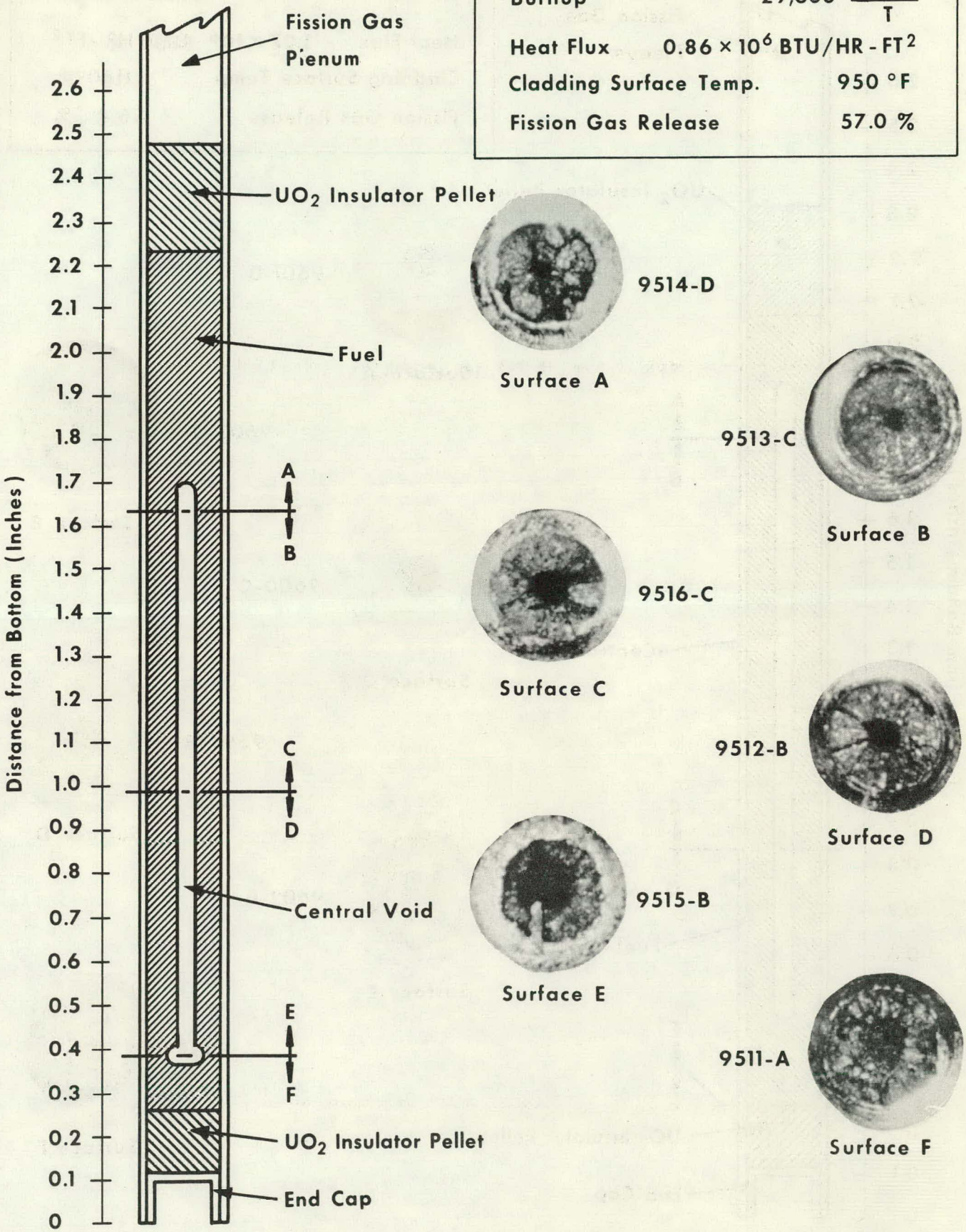

Figure 38. SECTIONING DIAGRAM AND FUEL CROSS SECTIONS, SPECIMEN VII-4-S

Specimen VIII-1-S	
Burnup	45,200 MWD/T
Heat Flux	1.07×10^6 BTU/HR-FT^2
Cladding Surface Temp.	1180 °F
Fission Gas Release	66.4 %

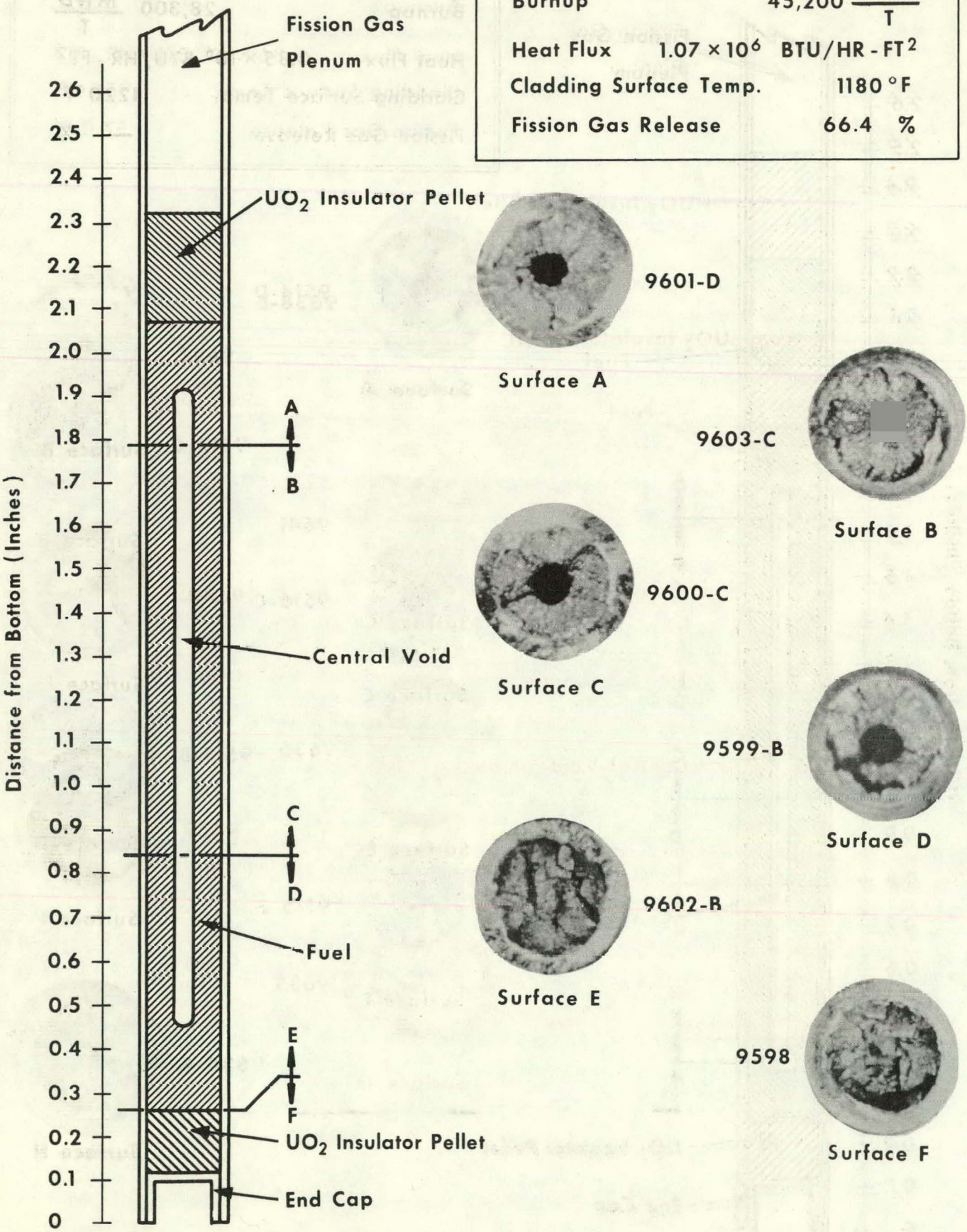

Figure 39. SECTIONING DIAGRAM AND FUEL CROSS SECTIONS, SPECIMEN VIII-1-S

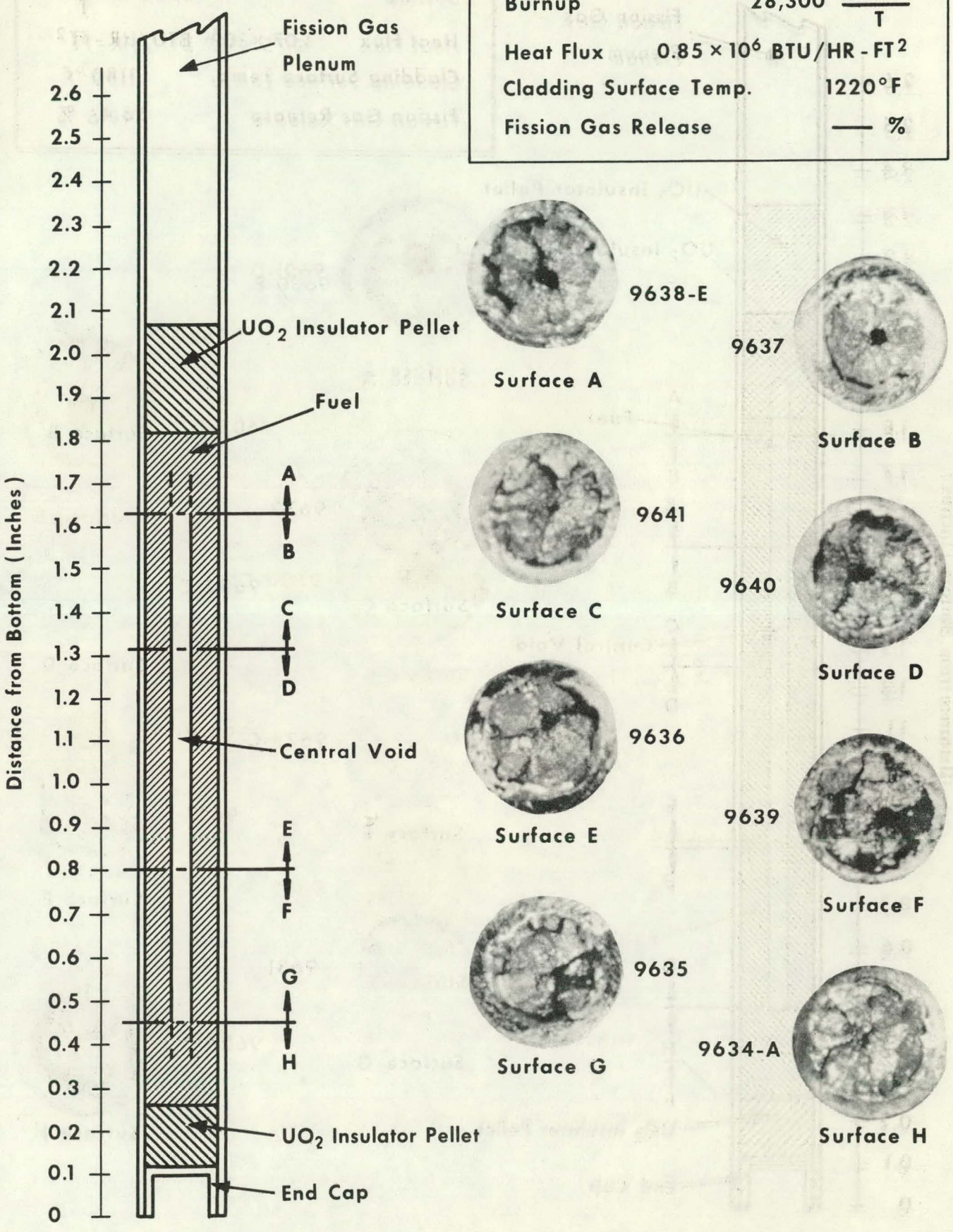

Figure 40. SECTIONING DIAGRAM AND FUEL CROSS SECTIONS, SPECIMEN VIII-2-P

Specimen VIII-3-P	
Burnup	23,100 MWD/T
Heat Flux	0.75×10^6 BTU/HR-FT^2
Cladding Surface Temp.	1150 °F
Fission Gas Release	49.6 %

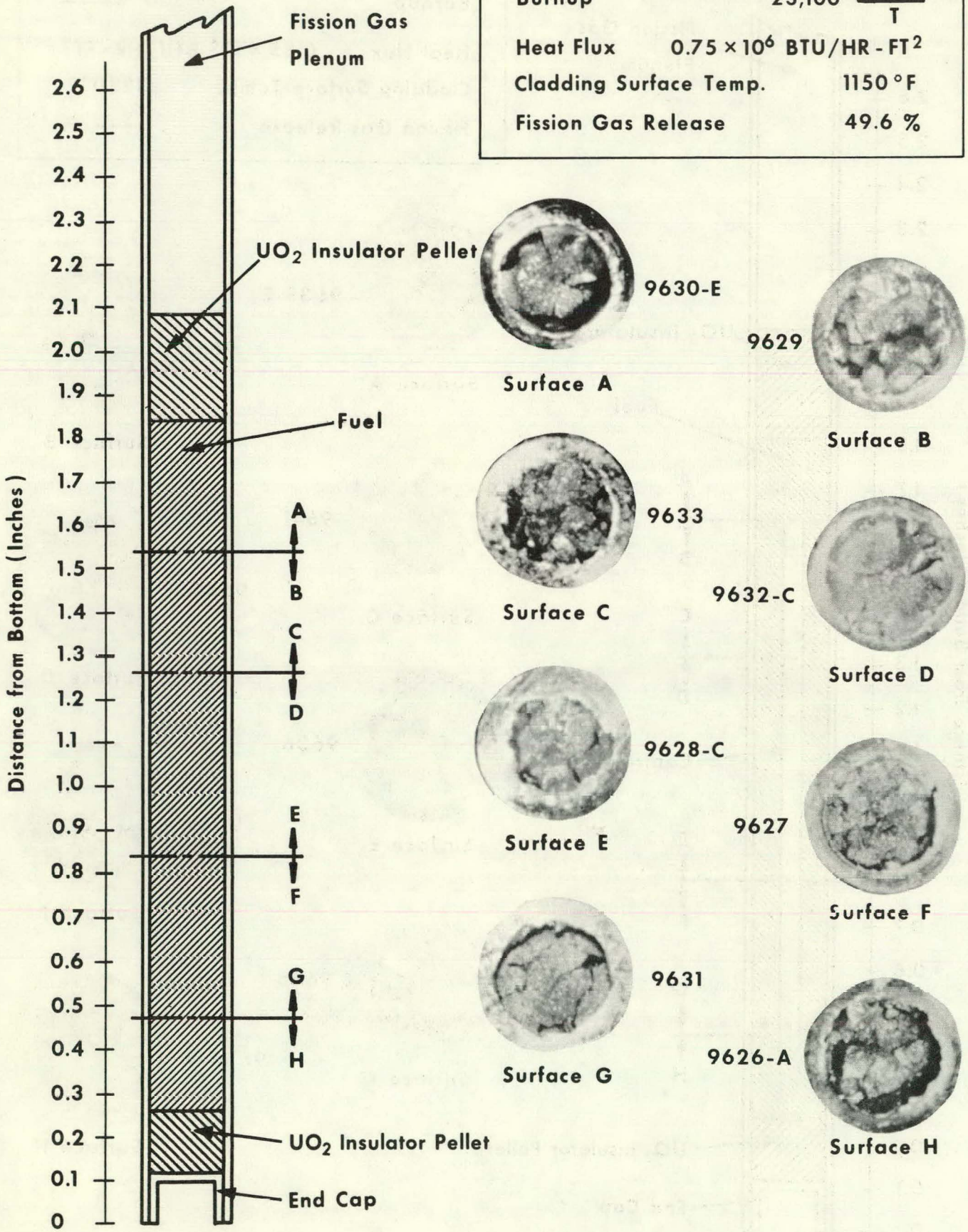

Figure 41. SECTIONING DIAGRAM AND FUEL CROSS SECTIONS, SPECIMEN VIII-3-P

Specimen VIII-4-S

Burnup	19,300 MWD/T
Heat Flux	0.50×10^6 BTU/HR-FT^2
Cladding Surface Temp.	820°F
Fission Gas Release	71.3 %

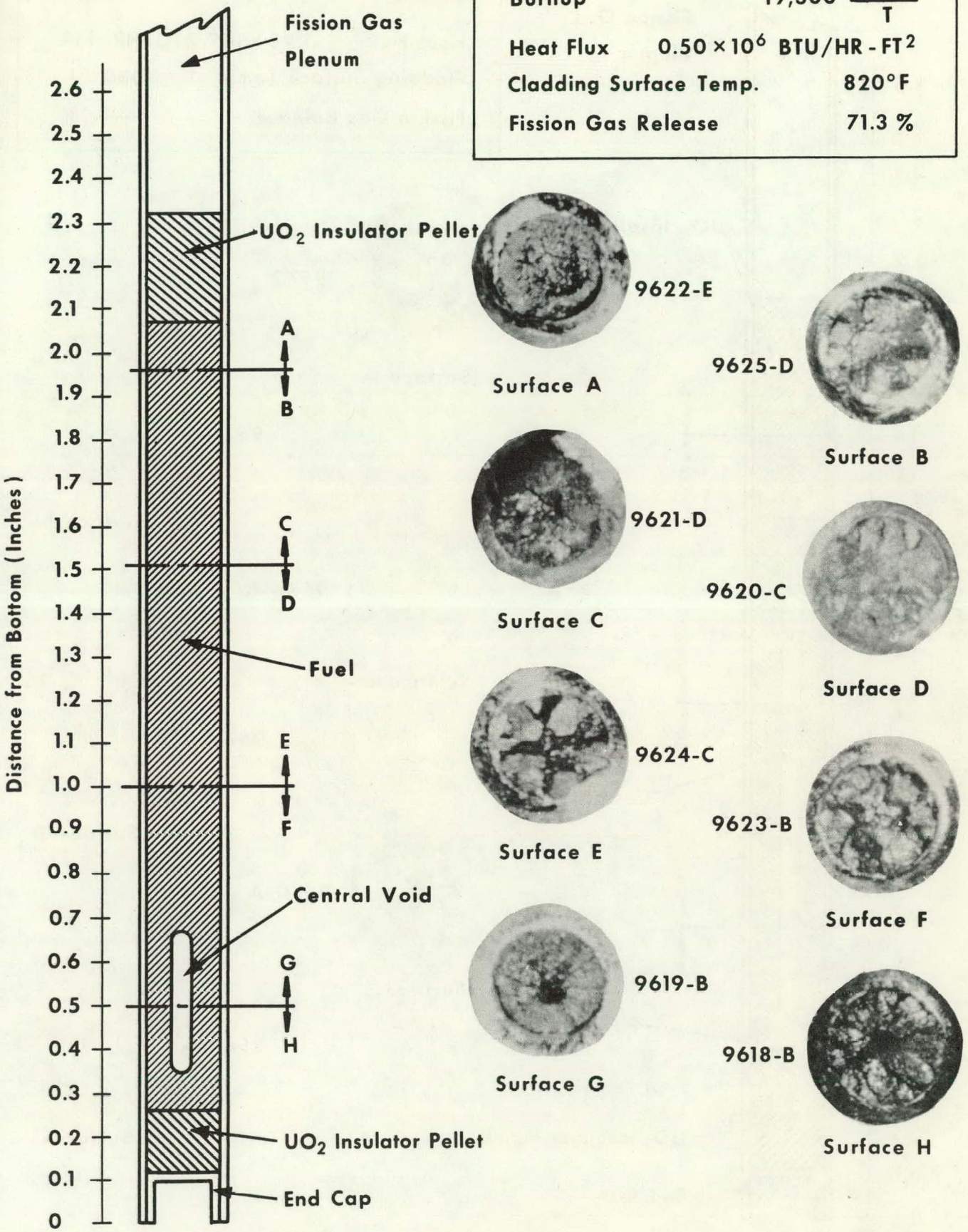

Figure 42. SECTIONING DIAGRAM AND FUEL CROSS SECTIONS, SPECIMEN VIII-4-S

Specimen IX-1-P		
Burnup	47,600	MWD/T
Heat Flux	1.23×10^6	BTU/HR-FT^2
Cladding Surface Temp.	1030	°F
Fission Gas Release	——	%

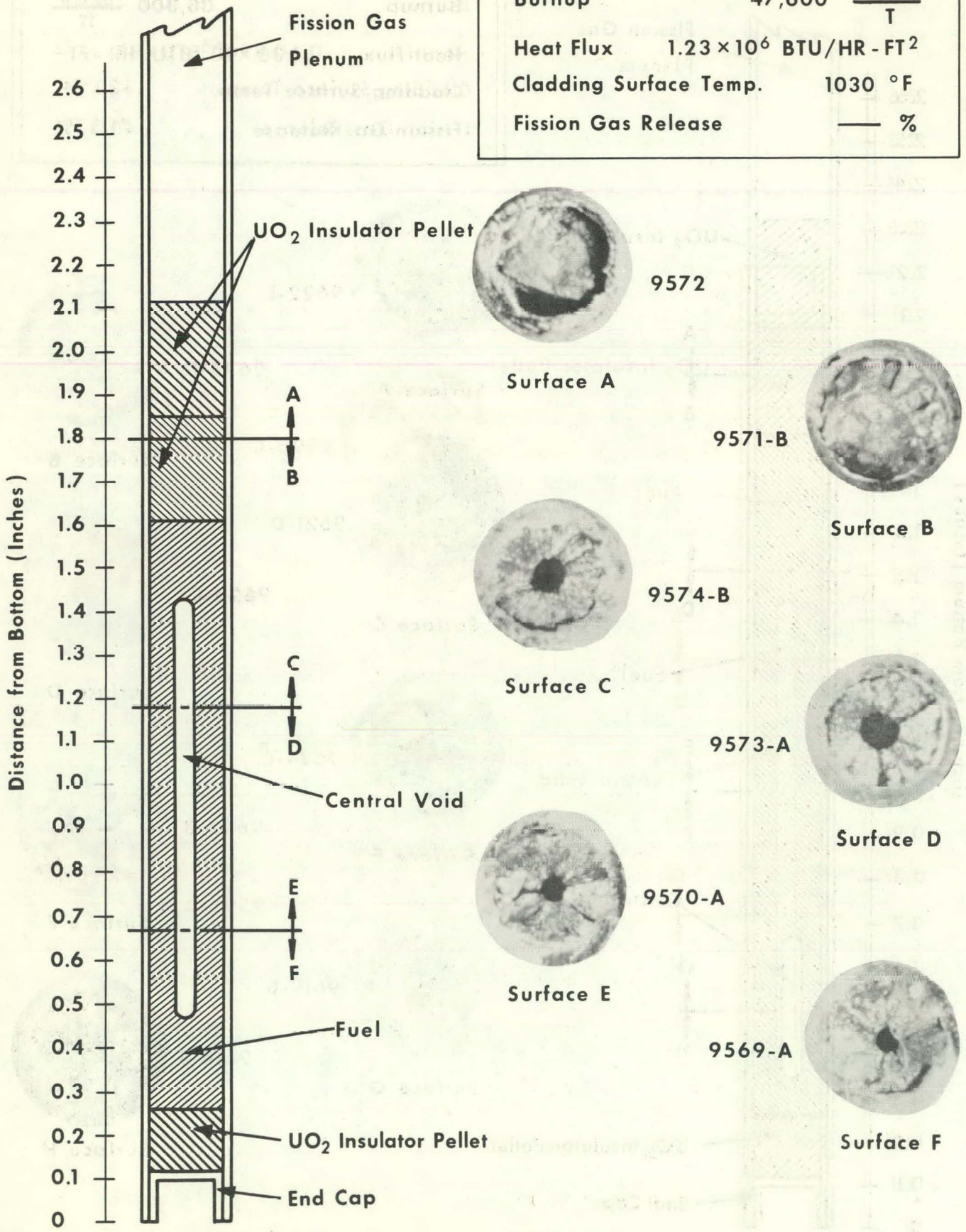

Figure 43. SECTIONING DIAGRAM AND FUEL CROSS SECTIONS, SPECIMEN IX-1-P

Specimen IX-2-P	
Burnup	38,300 MWD/T
Heat Flux	1.36×10^6 BTU/HR-FT^2
Cladding Surface Temp.	—— °F
Fission Gas Release	40.3 %

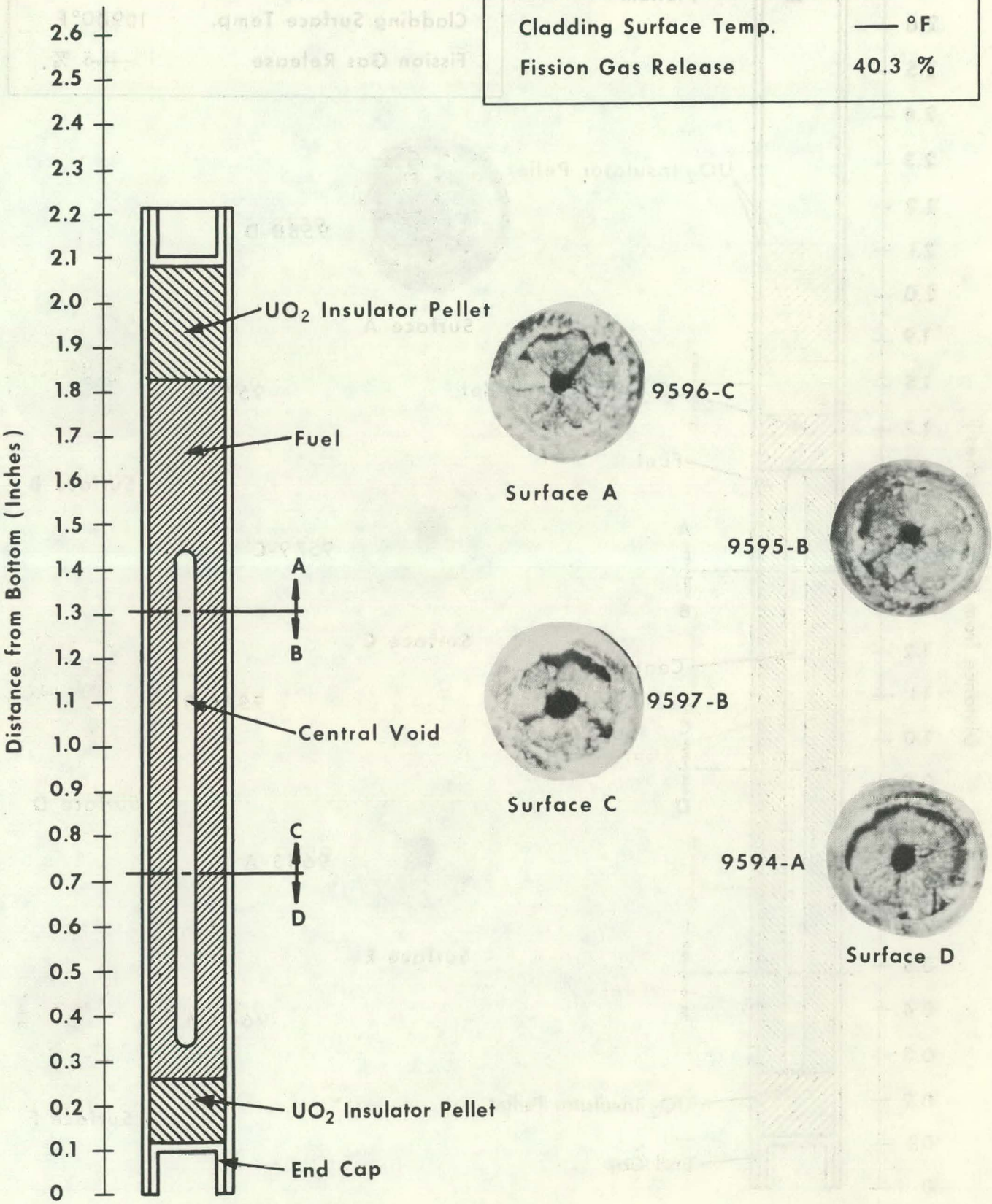

Figure 44. SECTIONING DIAGRAM AND FUEL CROSS SECTIONS, SPECIMEN IX-2-P

Specimen IX-3-P		
Burnup	34,500	MWD/T
Heat Flux	1.10×10^6	BTU/HR-FT^2
Cladding Surface Temp.	970°F	
Fission Gas Release	11.5 %	

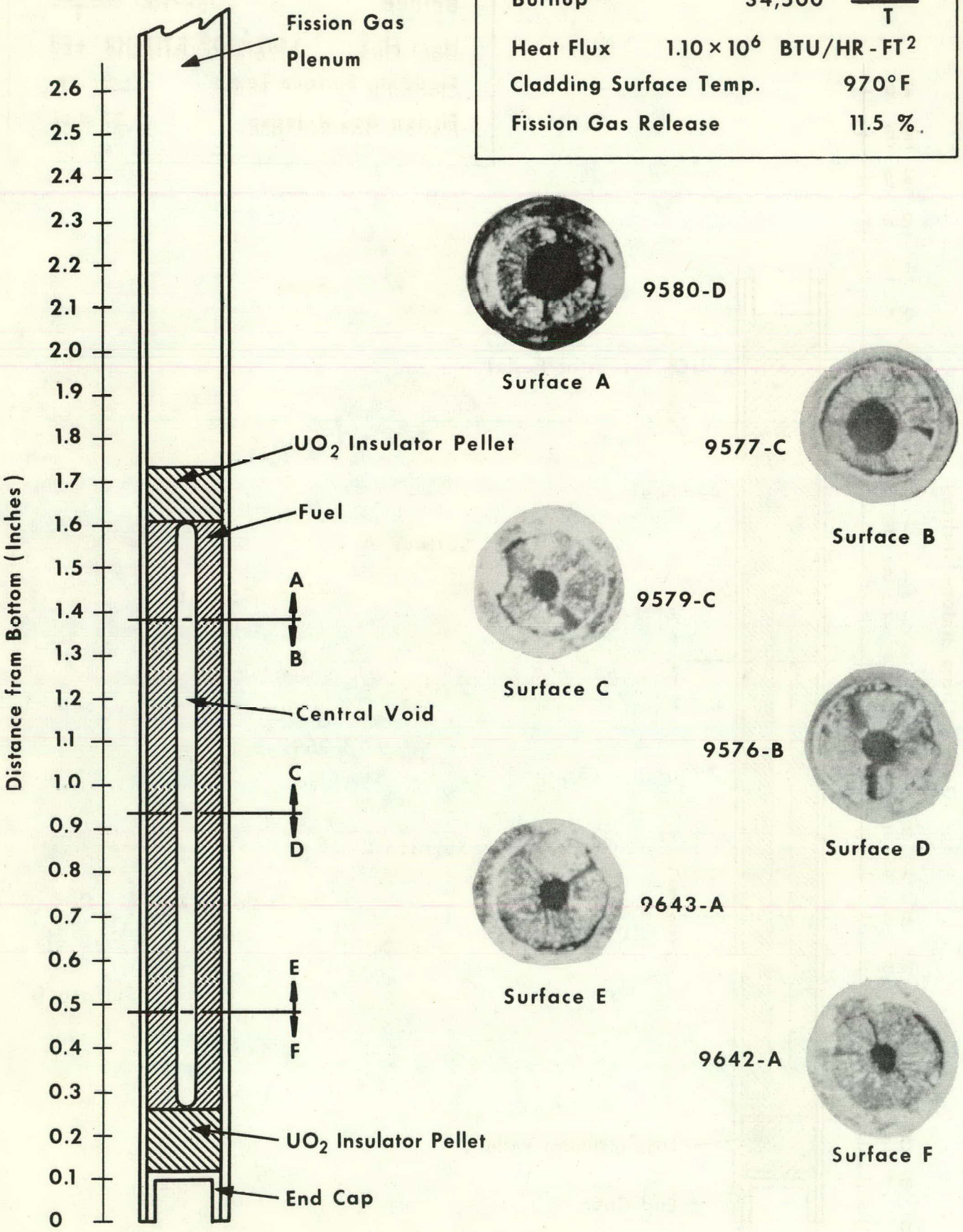

Figure 45. SECTIONING DIAGRAM AND FUEL CROSS SECTIONS, SPECIMEN IX-3-P

Specimen IX-4-P		
Burnup	17,600	MWD/T
Heat Flux	1.00×10^6	BTU/HR - FT^2
Cladding Surface Temp.	——	°F
Fission Gas Release	37.9	%

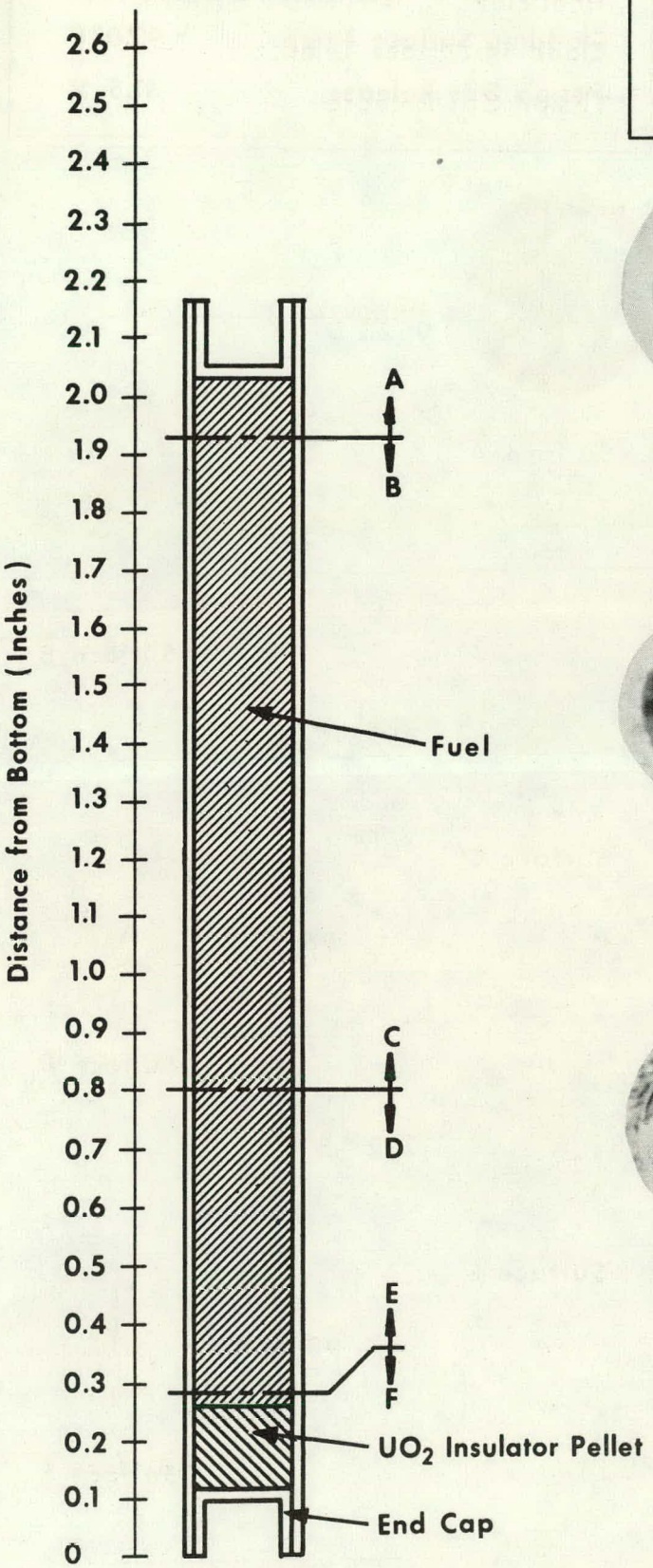

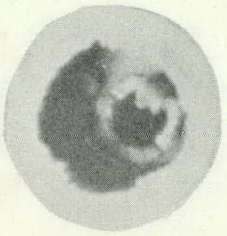

9563

Surface A

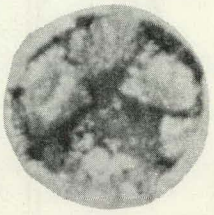

9565-C

Surface B

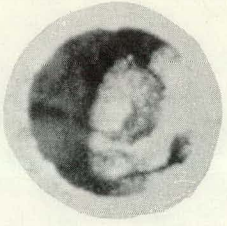

9566-C

Surface C

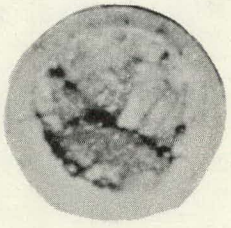

9567-B

Surface D

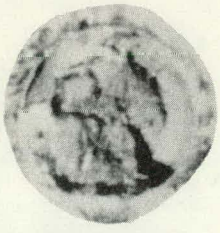

9568-B

Surface E

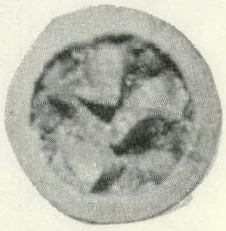

9564-A

Surface F

Figure 46. SECTIONING DIAGRAM AND FUEL CROSS SECTIONS, SPECIMEN IX-4-P

Specimen	X-1-S	
Burnup	36,300	MWD/T
Heat Flux	0.91×10^6	BTU/HR-FT^2
Cladding Surface Temp.	—	°F
Fission Gas Release	31.1	%

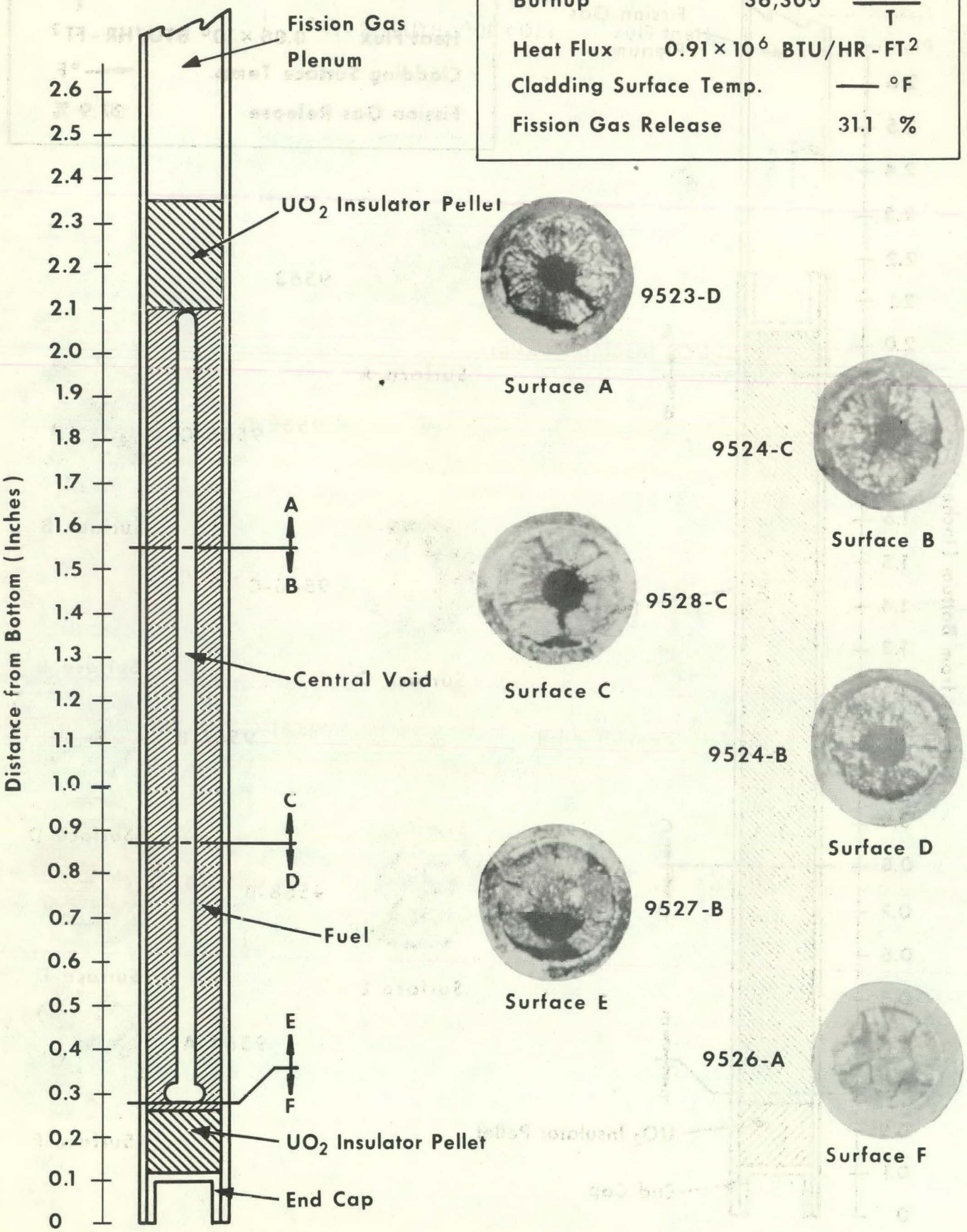

Figure 47. SECTIONING DIAGRAM AND FUEL CROSS SECTIONS, SPECIMEN X-1-S

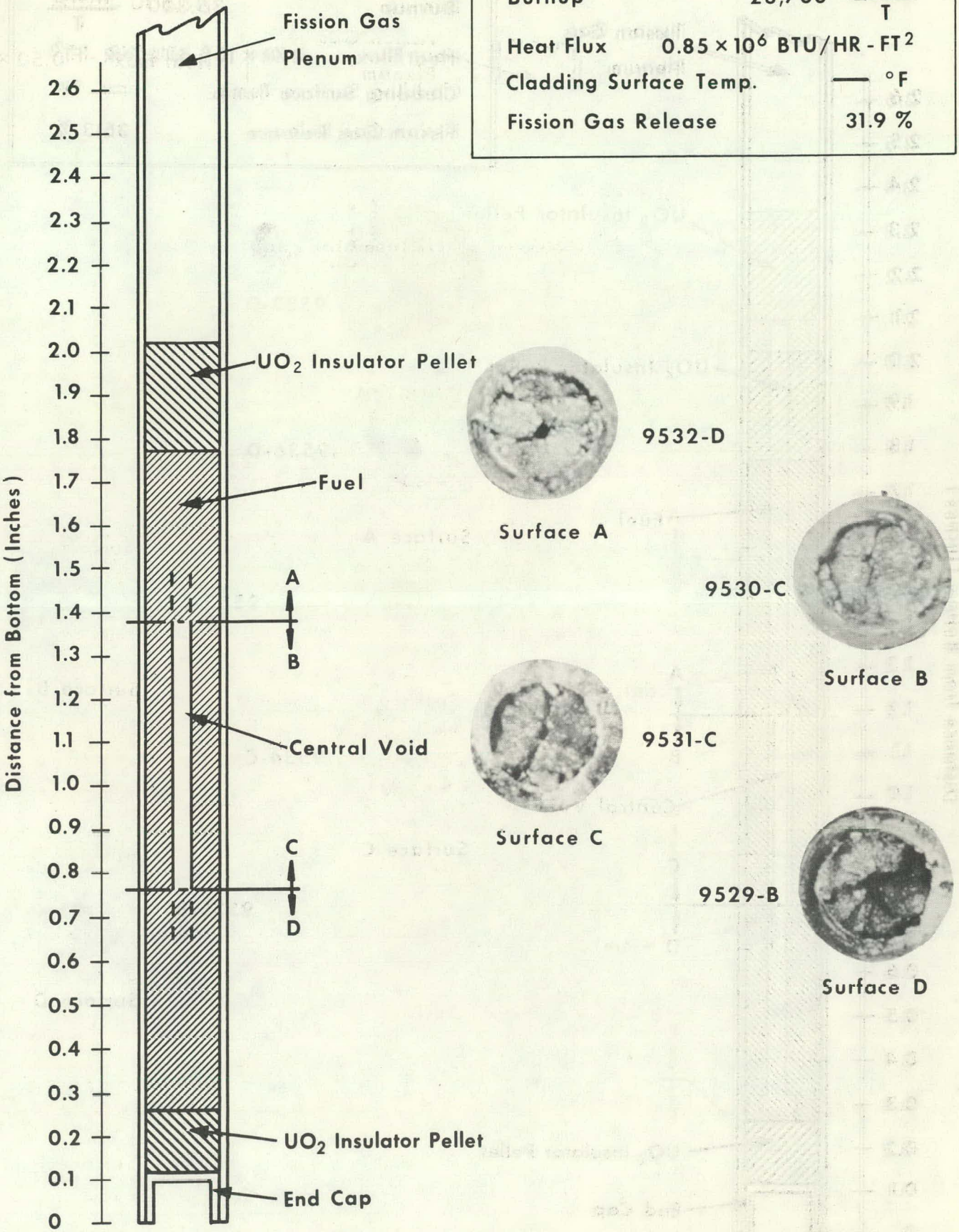

Figure 48. SECTIONING DIAGRAM AND FUEL CROSS SECTIONS, SPECIMEN X-2-P

Specimen X-3-P	
Burnup	16,800 $\frac{MWD}{T}$
Heat Flux	0.71×10^6 BTU/HR - FT^2
Cladding Surface Temp.	— °F
Fission Gas Release	35.3 %

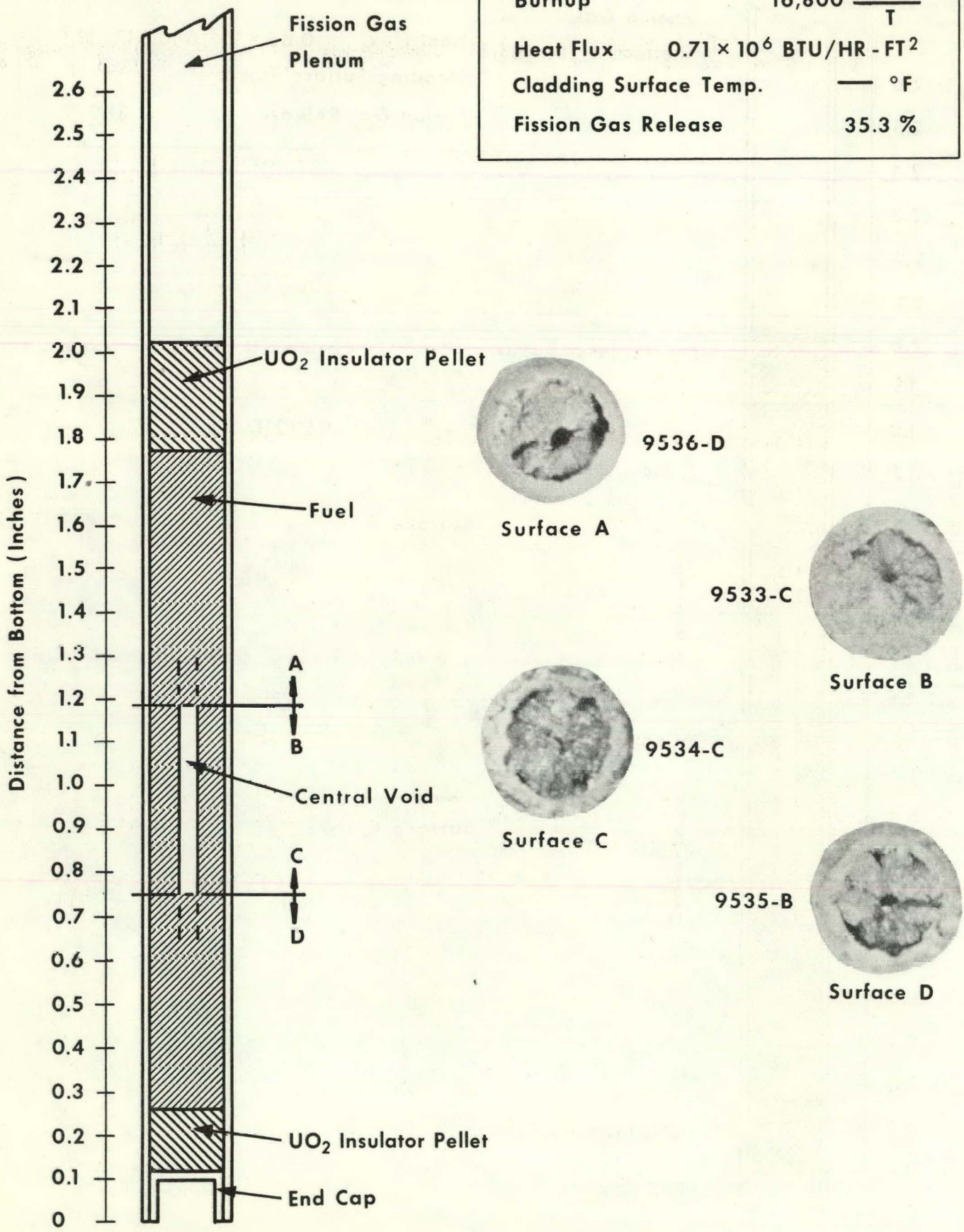

Figure 49. SECTIONING DIAGRAM AND JEL CROSS SECTIONS, SPECIMEN X-3-P

Specimen X-4-S	
Burnup	15,000 MWD/T
Heat Flux	0.57×10^6 BTU/HR-FT^2
Cladding Surface Temp.	— °F
Fission Gas Release	65.1 %

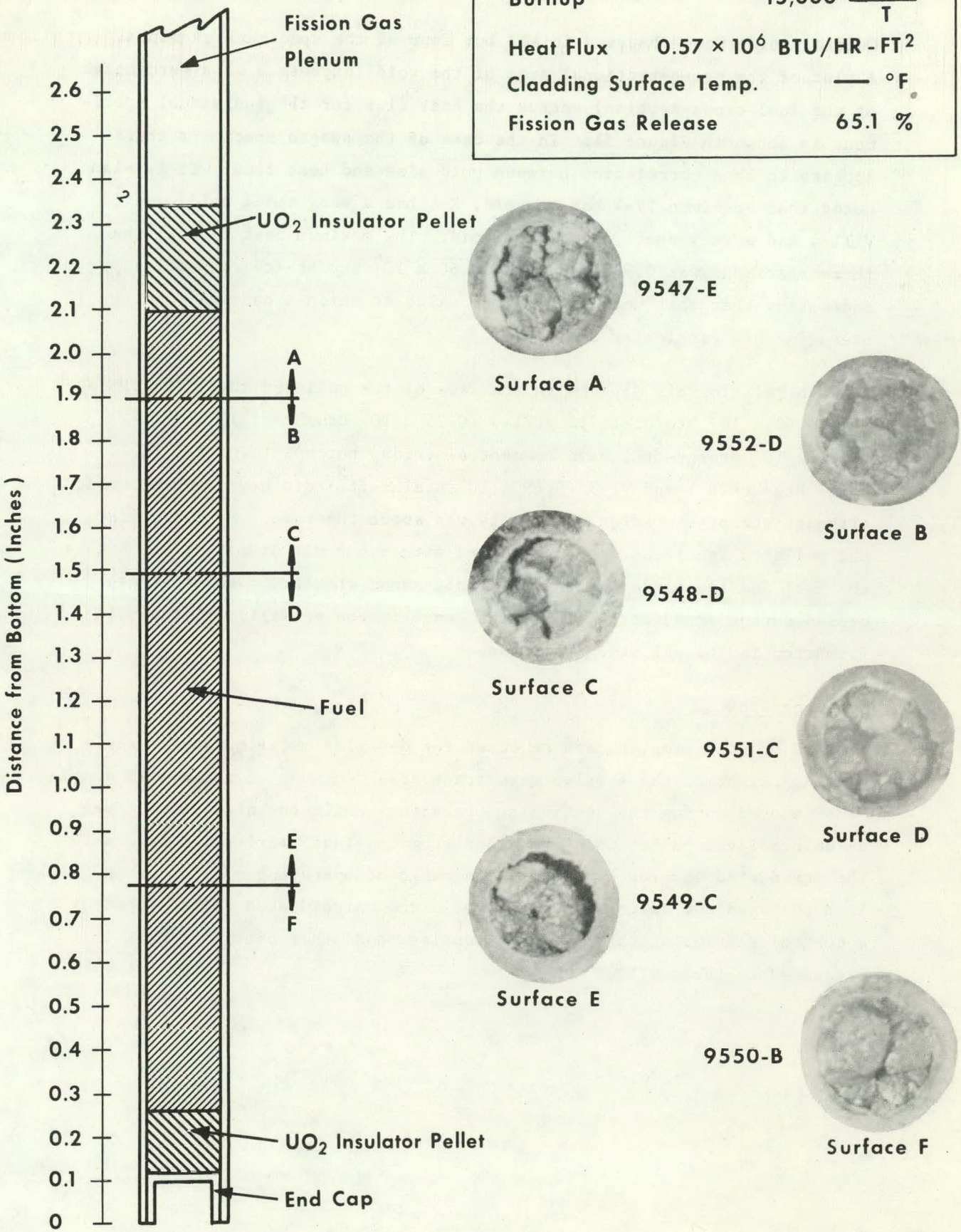

Figure 50. SECTIONING DIAGRAM AND FUEL CROSS SECTIONS, SPECIMEN X-4-S

Central voids were observed in all but four of the specimens examined. A plot of the cross-sectional area of the void (expressed as a percentage of the fuel cross-section) versus the heat flux for the individual specimens is shown in Figure 51. In the case of the swaged specimens there appears to be a correlation between void size and heat flux. It is also noted that specimen IV-4 has no void, X-4 had a very small void, and VIII-4 had a very short, localized void. The maximum heat flux in the three specimens was 0.53, 0.57, and 0.50 x 10^6 Btu/hr-ft^2 respectively, indicating that this heat flux is the value at which a central void appears in this particular fuel.

No such relationship appears in the case of the pelleted fuel. Specimens I-4 (0.62 x 10^6 Btu/hr-ft^2), VIII-3 (0.75 x 10^6 Btu/hr-ft^2), and IX-4 (0.86 x 10^6 Btu/hr-ft^2) have no central voids, but specimens X-3 (0.71 x 10^6 Btu/hr-ft^2) and VI-3 (0.69 x 10^6 Btu/hr-ft^2) did have central voids although the pre-irradiation density was about the same. However, since the pelleted specimens were fabricated with a 6-8 mil diametral gap between the fuel and the cladding, and it is not known whether or not this gap closed during irradiation, this might explain the anomalies in the void formation in the pelleted specimens.

G. Metallography

A total of nine samples were selected for detailed metallographic examination. Eight of the samples were transverse sections of irradiated specimens removed during the sectioning operations while the ninth sample was an unirradiated pellet which remained from the fuel fabrication program. The irradiated samples covered a wide range of operating conditions in both pelleted and swaged specimens while the unirradiated pellet acted as a control sample. Location of the samples, and other pertinent data is presented in Table VIII.

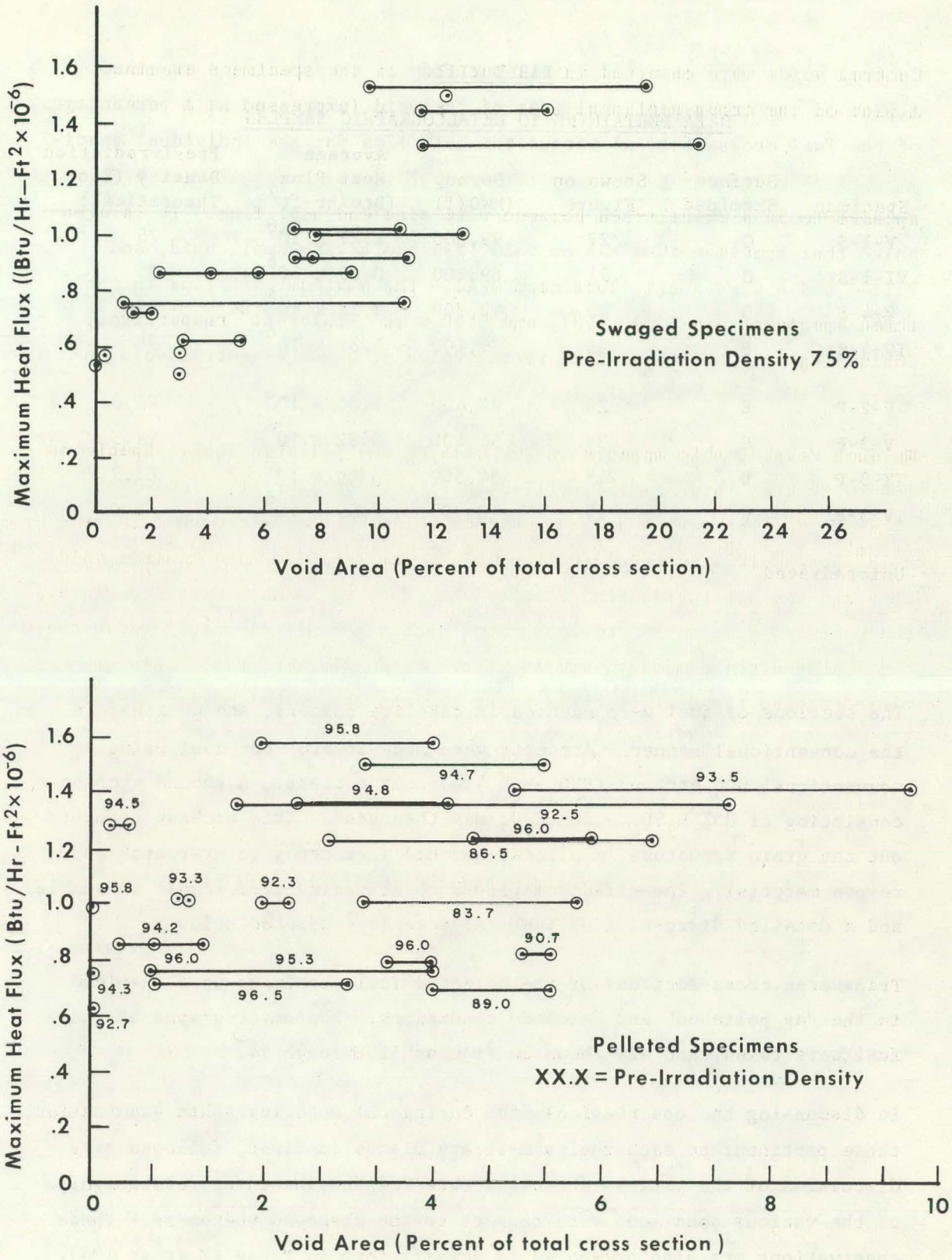

Figure 51. CENTRAL VOID DATA, HEAT FLUX VERSUS VOID AREA

TABLE VIII

DATA PERTAINING TO METALLOGRAPHIC SAMPLES

Specimen	Surface Examined	Shown on Figure	Burnup (MWD/T)	Average Heat Flux ($Btu/hr-ft^2$)	Pre-Irradiation Density (% of Theoretical)
V-1-S	C	27	99,000	1.27×10^6	~ 75
VI-1-S	C	31	69,100	0.89×10^6	~ 75
V-4-S	D	30	42,700	0.55×10^6	~ 75
IV-4-S	B	26	9,100	0.37×10^6	~ 75
V-2-P	E	28	77,400	1.30×10^6	95.8
V-3-P	C	29	54,400	0.92×10^6	94.5
IX-3-P	D	45	34,500	0.95×10^6	83.7
IV-3-P	C	25	10,900	0.55×10^6	89.0
Unirradiated			0	-	93.7

The sections of fuel were mounted in bakelite holders, and polished in the conventional manner. Attempts were made to etch the fuel using a conventional UO_2 etchant (HNO_3-H_2O_2) without success. A second etchant consisting of 80% H_2SO_4 - 20% H_2O_2 was then used. This etchant brought out the grain structure in places, but had a tendency to over etch and remove material. The effect of this etchant varied from sample to sample, and a detailed discussion of these effects is presented below.

Transverse cross-sections of the selected fuel specimens were examined in the "as polished" and "etched" conditions. Photomicrographs of the fuel were taken, and are shown on Figures 52 through 74.

In discussing the observations made during the metallographic examination, those pertinent to each fuel sample are discussed first, followed by a discussion of the various phenomena observed and the inter-relationships of the various specimens with respect to the observed phenomena. These observations are also presented in summary form in Table IX. (page 105).

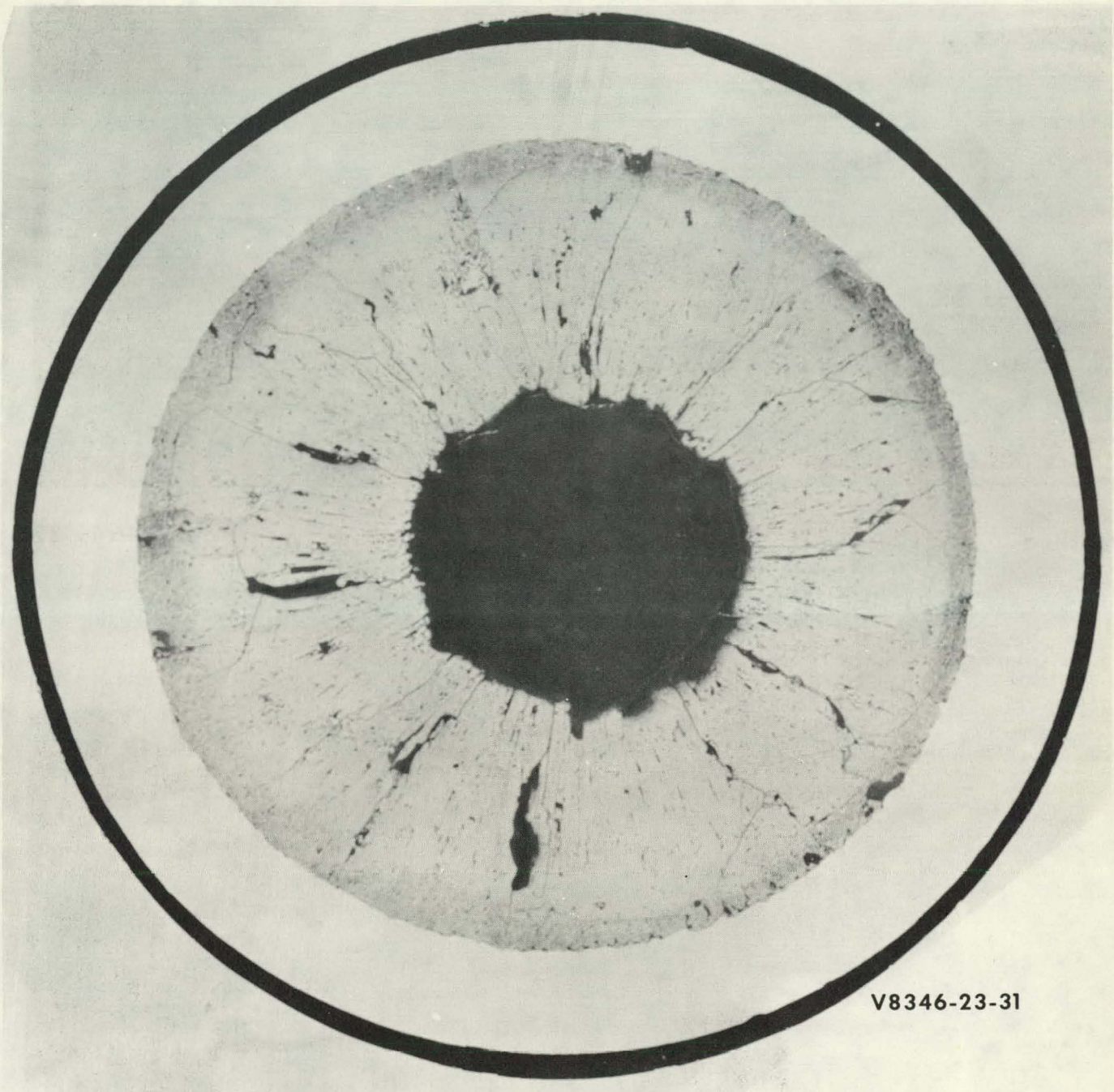

Figure 52. SPECIMEN V-1-S. (99,000 MWD/T), TRANSVERSE CROSS SECTION THROUGH FUEL AND CLADDING

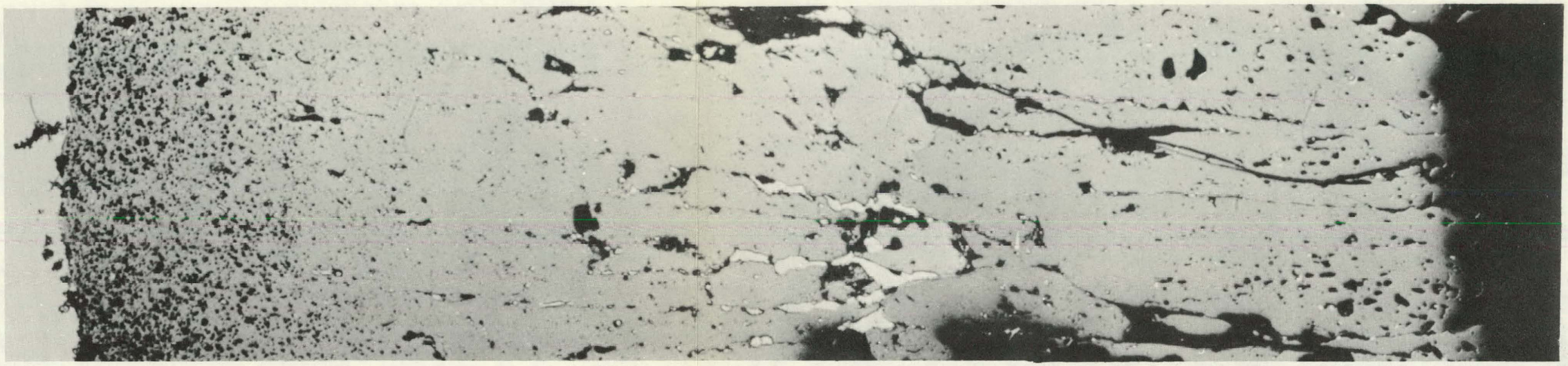

250X As Polished V8346-19-22

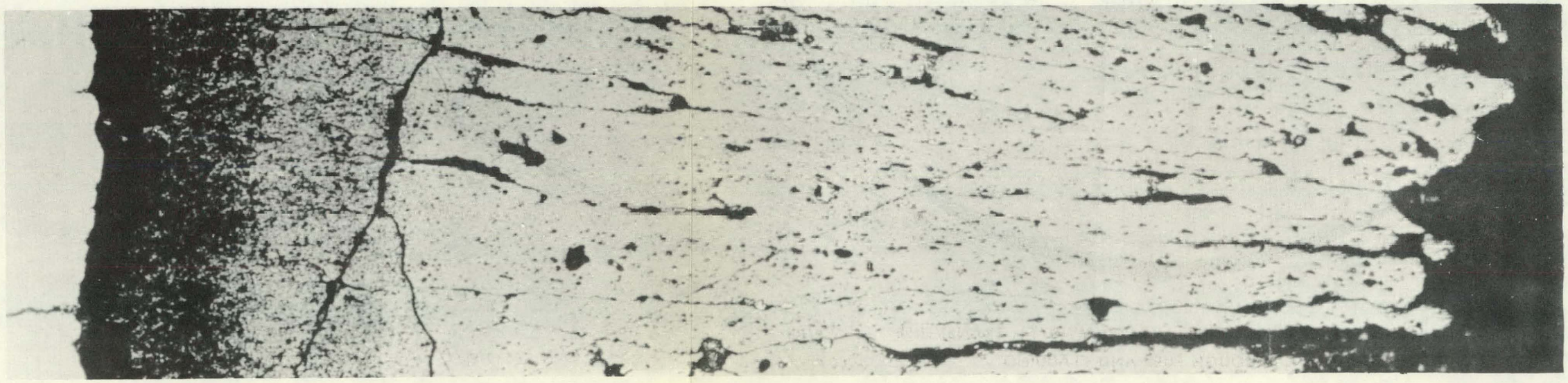

250X Etched V8346-15-18

Figure 53. SPECIMEN V-1-S. (99,000 MWD/T), EDGE TO CENTER PHOTOGRAPHS OF FUEL

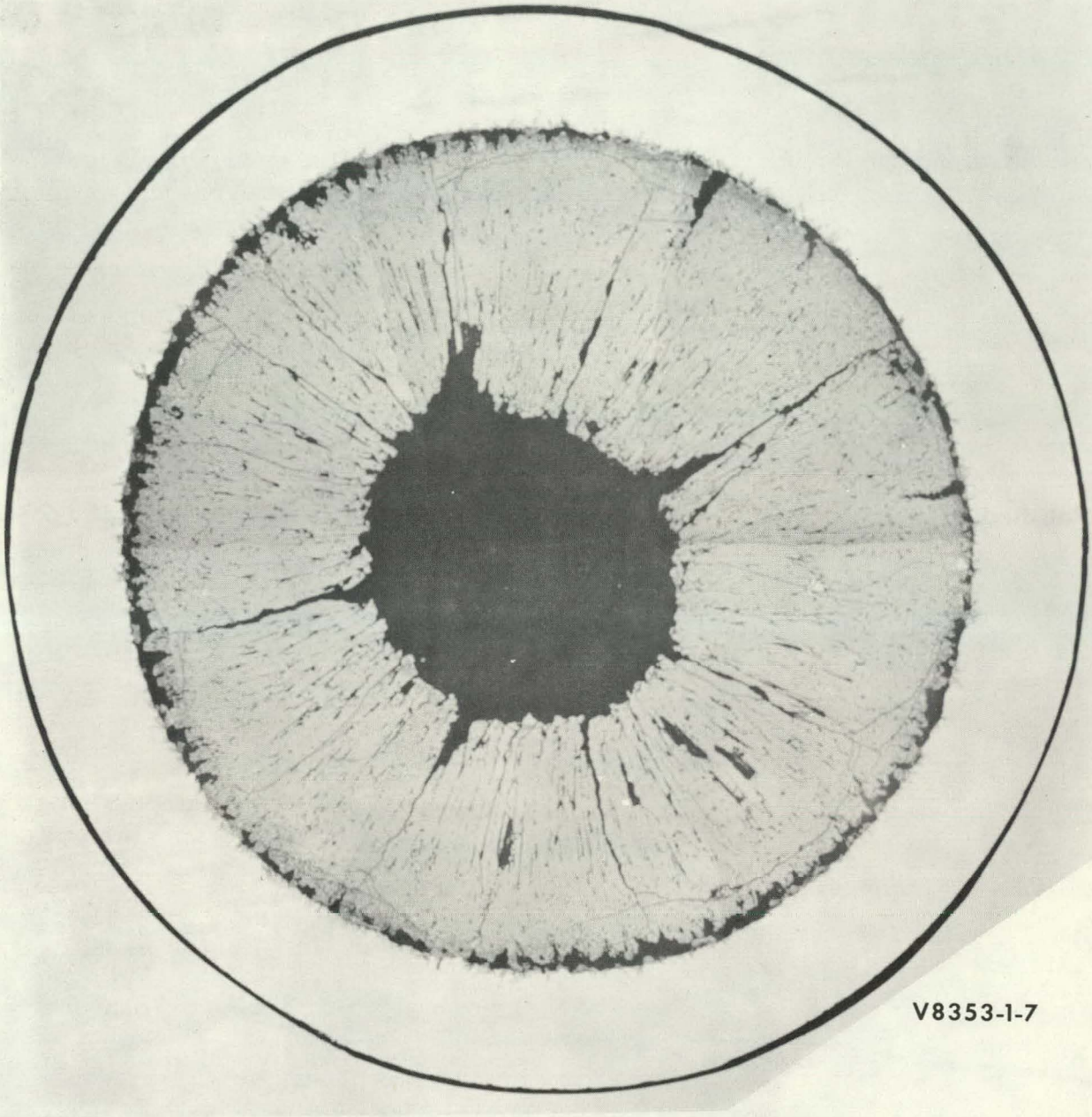

Figure 54. SPECIMEN VI-1-S. (69,100 MWD/T), TRANSVERSE CROSS SECTION THROUGH FUEL AND CLADDING

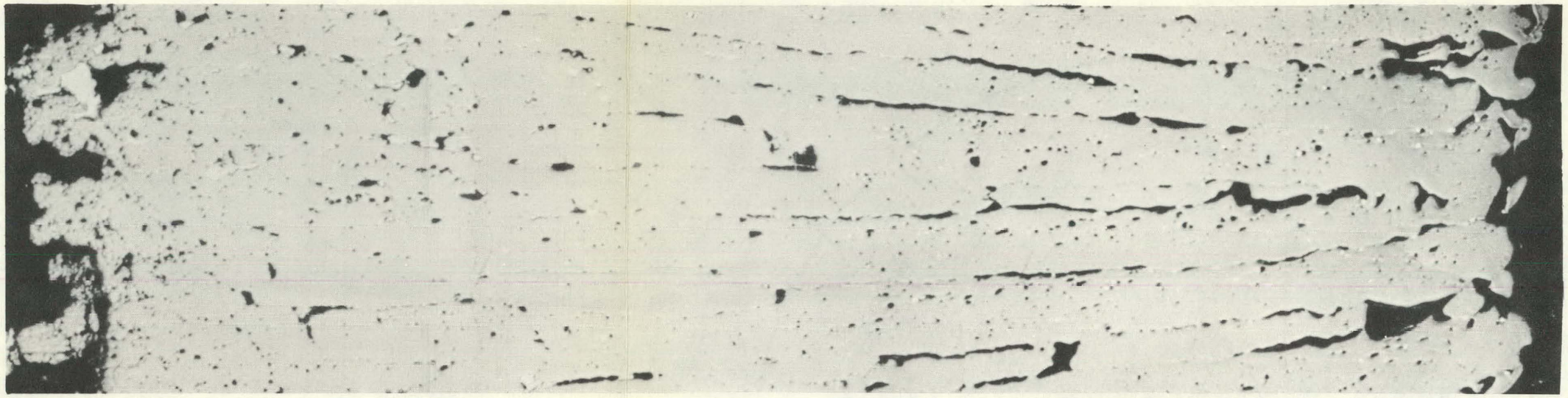

250X As Polished V8353-23-26

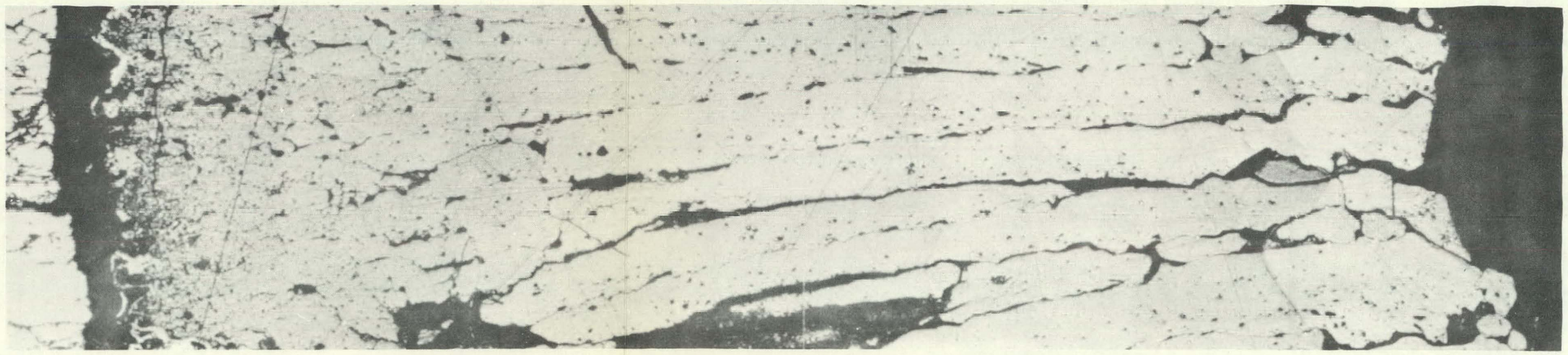

250X Etched V8352-15-18

Figure 55. SPECIMEN VI-1-S. (69,100 MWD/T, EDGE TO CENTER PHOTOGRAPHS OF FUEL

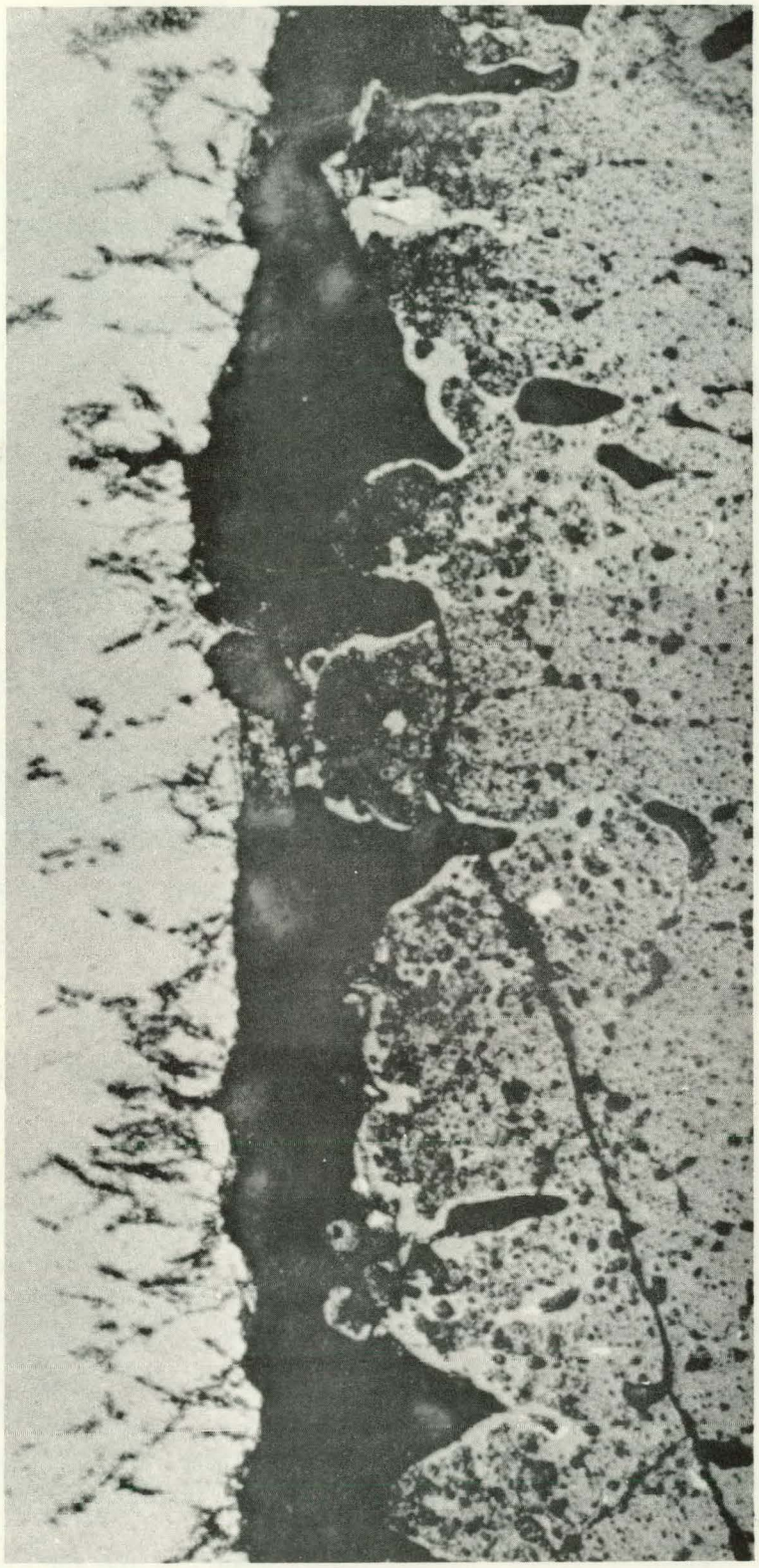

500X As Polished V8353-19-21

Figure 56. SPECIMEN VI-1 S. GREY PHASE ALONG EDGE OF FUEL

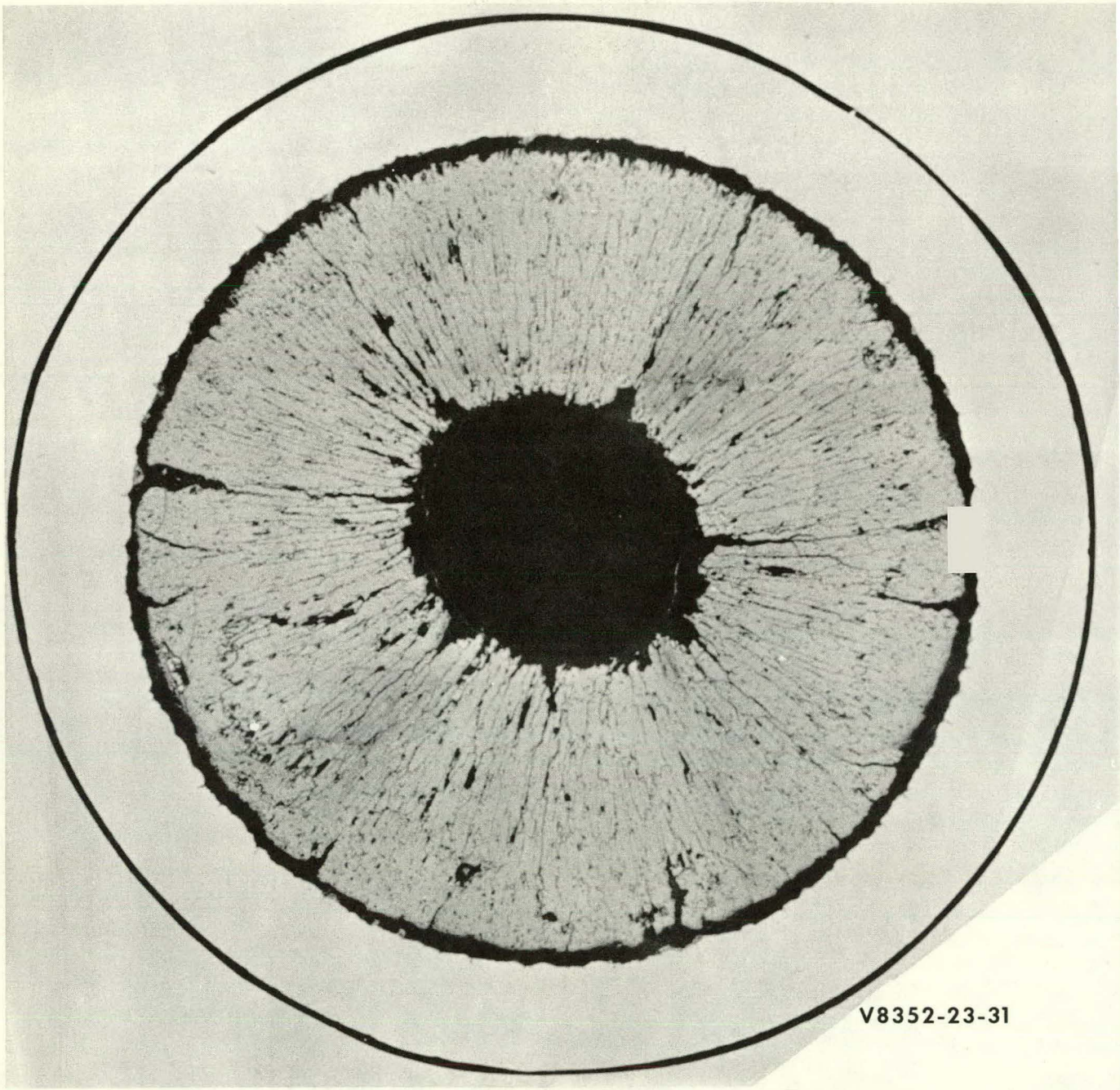

Figure 57. SPECIMEN V-4-S. (42,700 MWD/T), TRANSVERSE CROSS SECTION THROUGH FUEL AND CLADDING

250X As Polished V8352-19-22

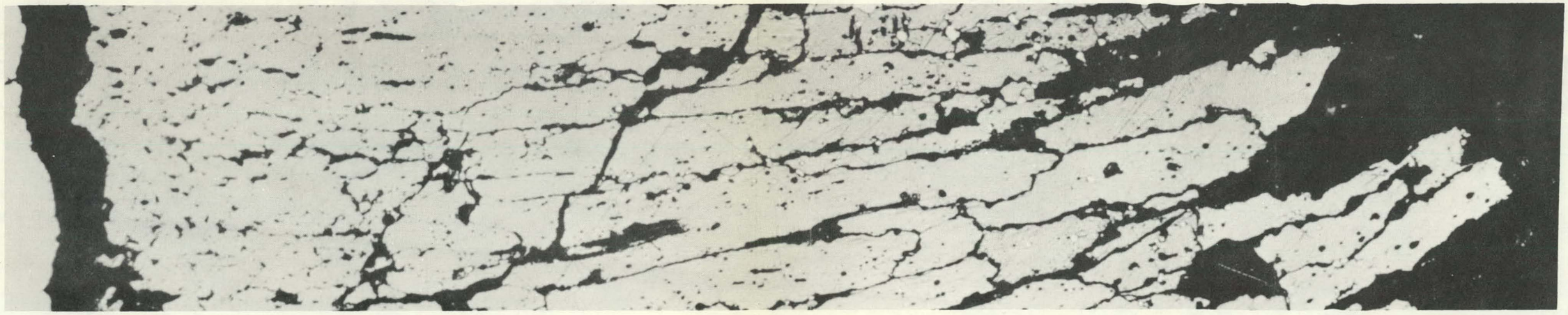

250X Etched V8353-15-18

Figure 58. SPECIMEN V-4-S. (42,700 MWD/T), EDGE TO CENTER PHOTOGRAPHS OF FUEL

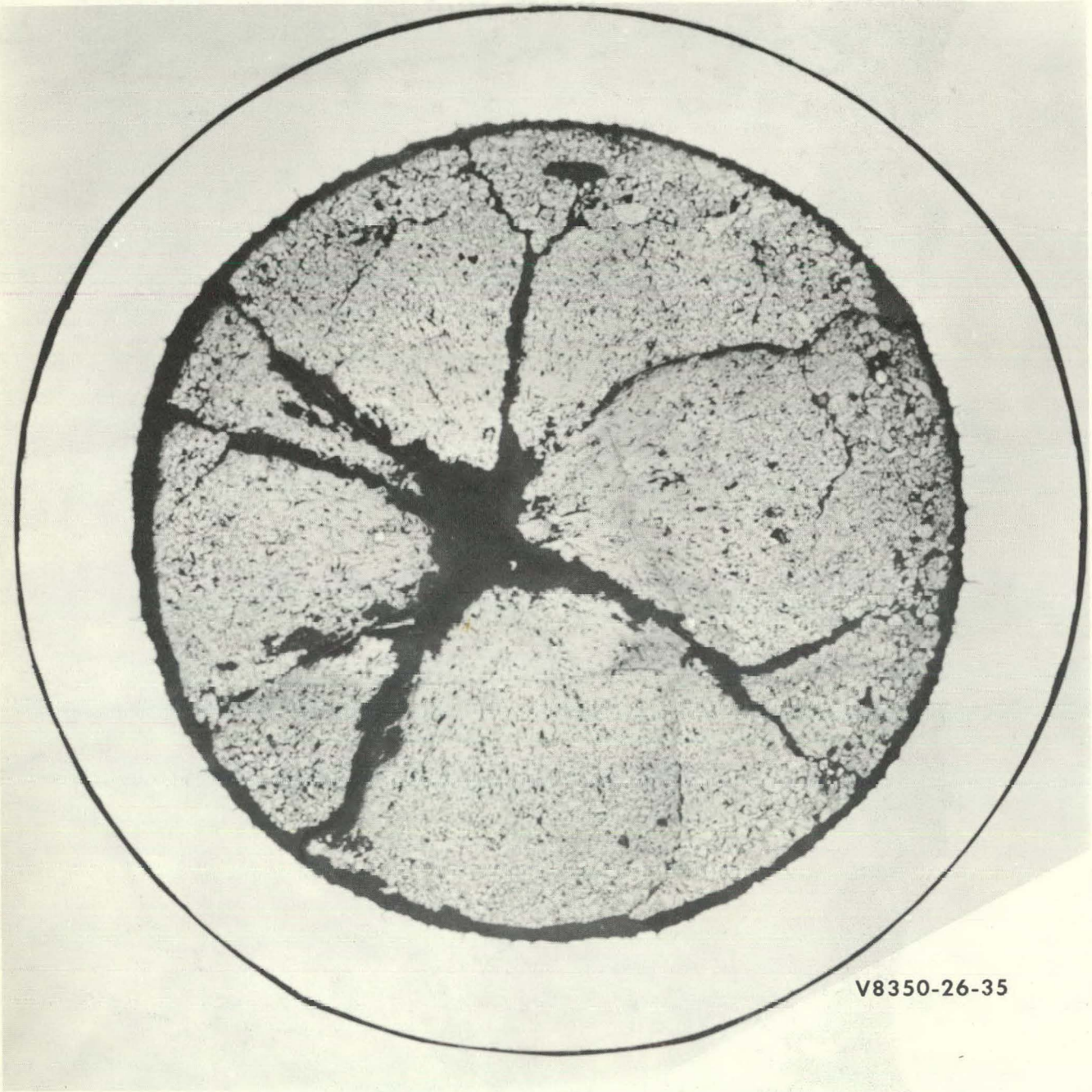

Figure 59. SPECIMEN IV-4-S. (9,000 MWD/T), TRANSVERSE CROSS SECTION THROUGH FUEL AND CLADDING

250X As Polished V8350-21-24

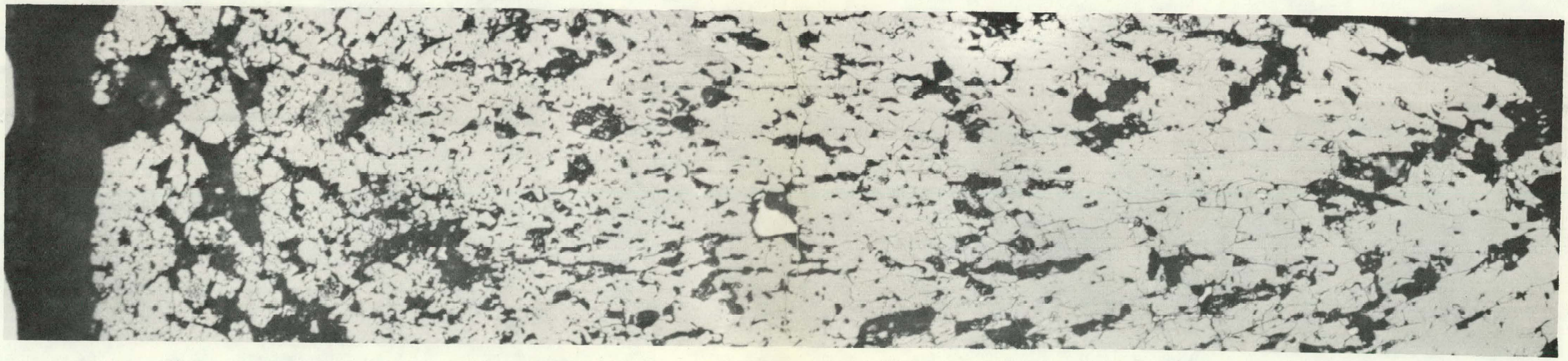

250X Etched V8350-37-41

Figure 60. SPECIMEN IV-4-S. (9,000 MWD/T) EDGE TO CENTER PHOTOGRAPHS OF FUEL

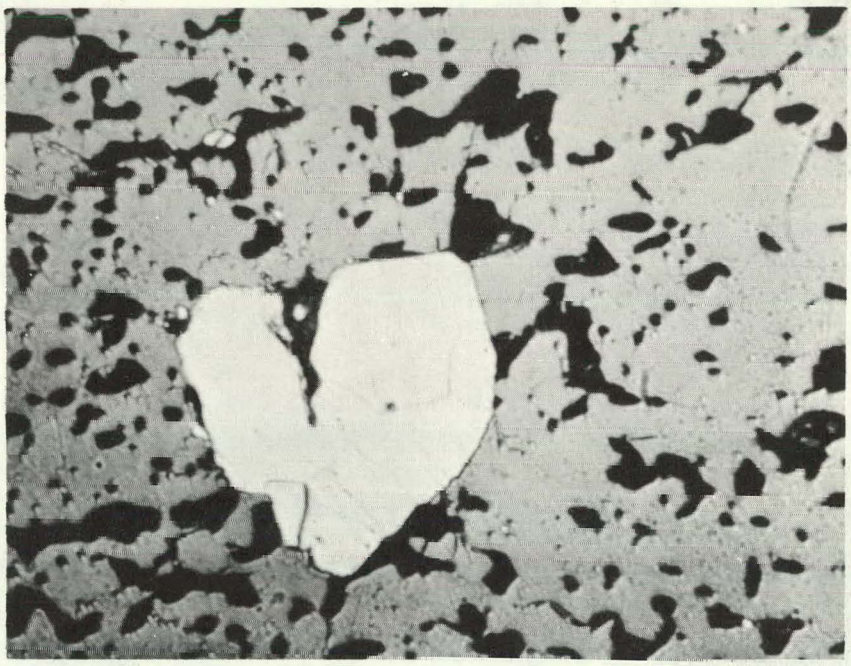

500X As Polished V8350-25

Figure 61. SPECIMEN IV-4-S. LARGE DEPOSIT OF SILVER PHASE IN FUEL

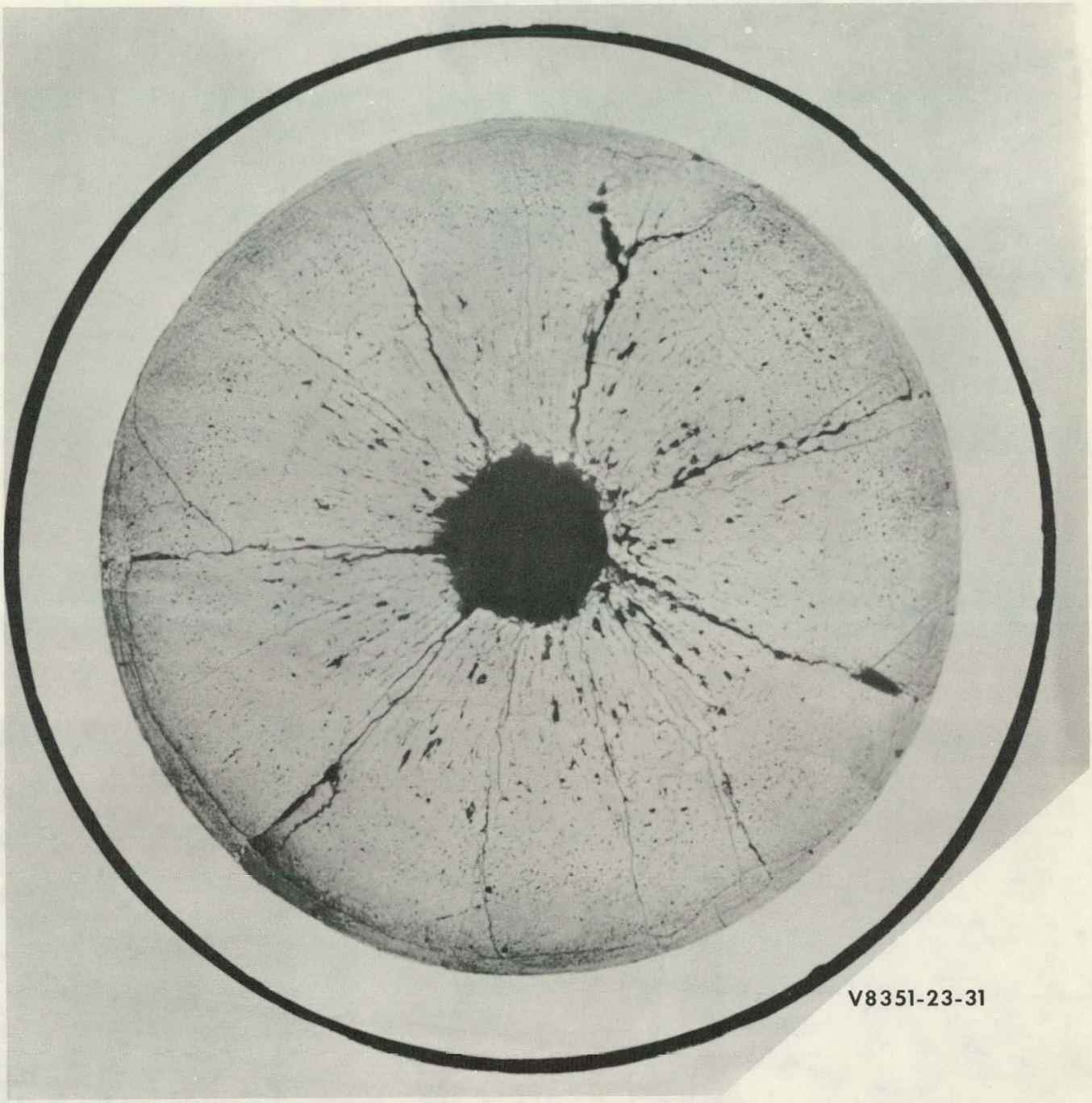

Figure 62. SPECIMEN V-2-P. (77,400 MWD/T), TRANSVERSE CROSS SECTION THROUGH FUEL AND CLADDING

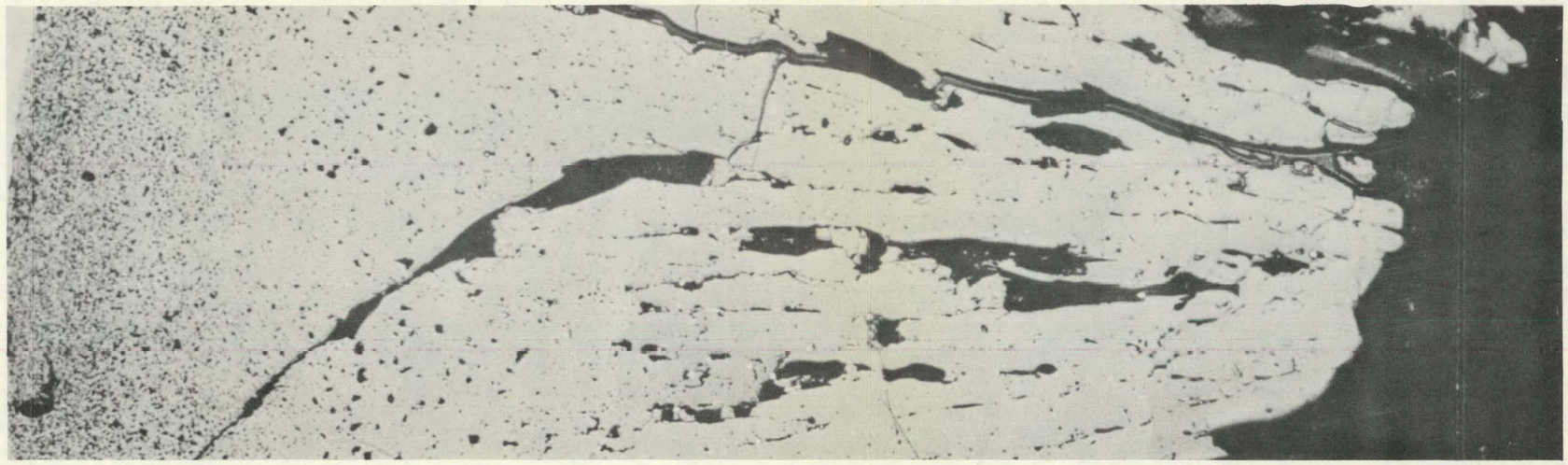

150X As Polished V8351-20-22

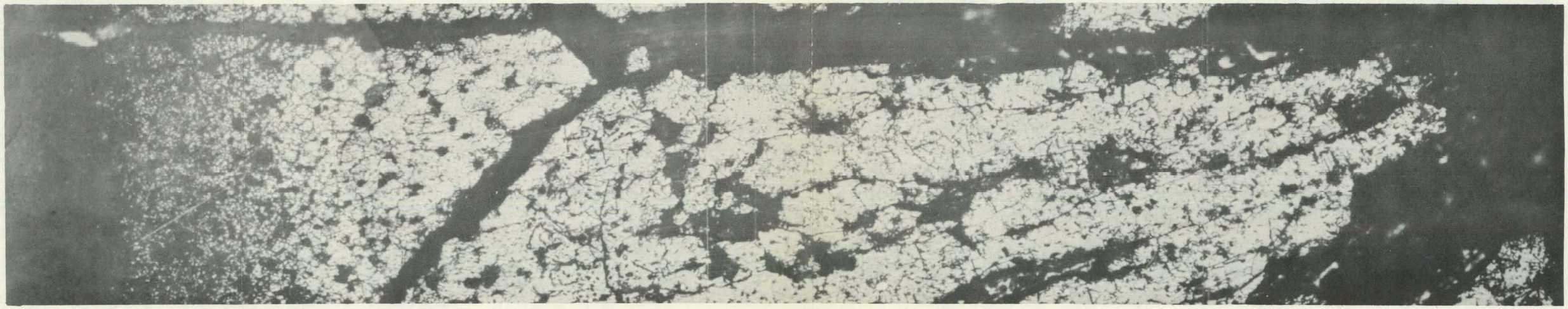

250X Etched V8351-15-18

Figure 63. SPECIMEN V-2-P. (77,400 MWD/T) EDGE TO CENTER PHOTOGRAPHS OF FUEL

750X Etched V 8351-19

Figure 64. SPECIMEN V-2-P, POLYGON SHAPED CRYSTALS WITHIN COLUMNAR STRUCTURE

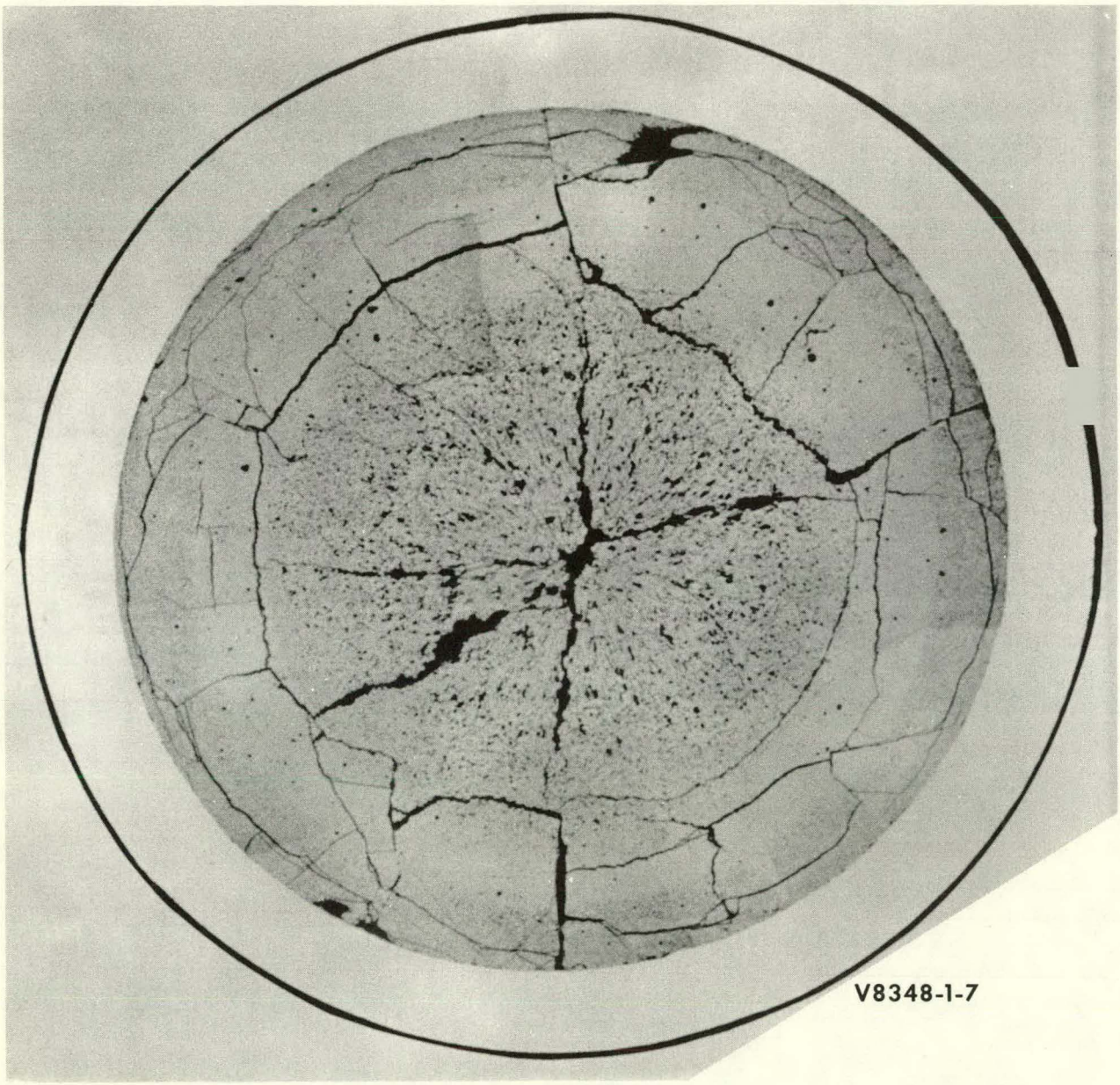

Figure 65. SPECIMEN V-3-P. (54,400 MWD/T), TRANSVERSE CROSS SECTION THROUGH FUEL AND CLADDING

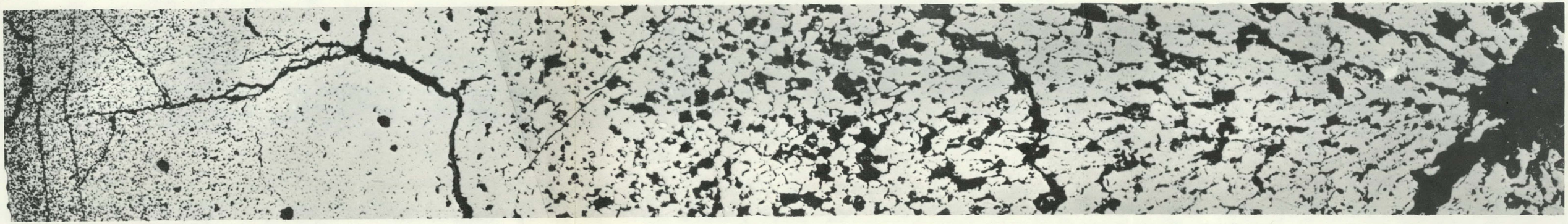

250X Etched V8348-21-26

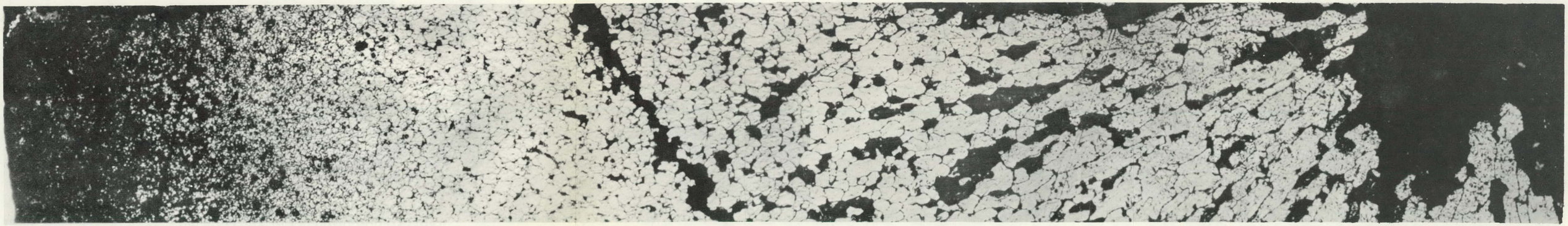

250X Etched V8348-15-20

Figure 66. SPECIMEN V-3-P. (54,400 MWD/T, EDGE TO CENTER PHOTOGRAPHS OF FUEL

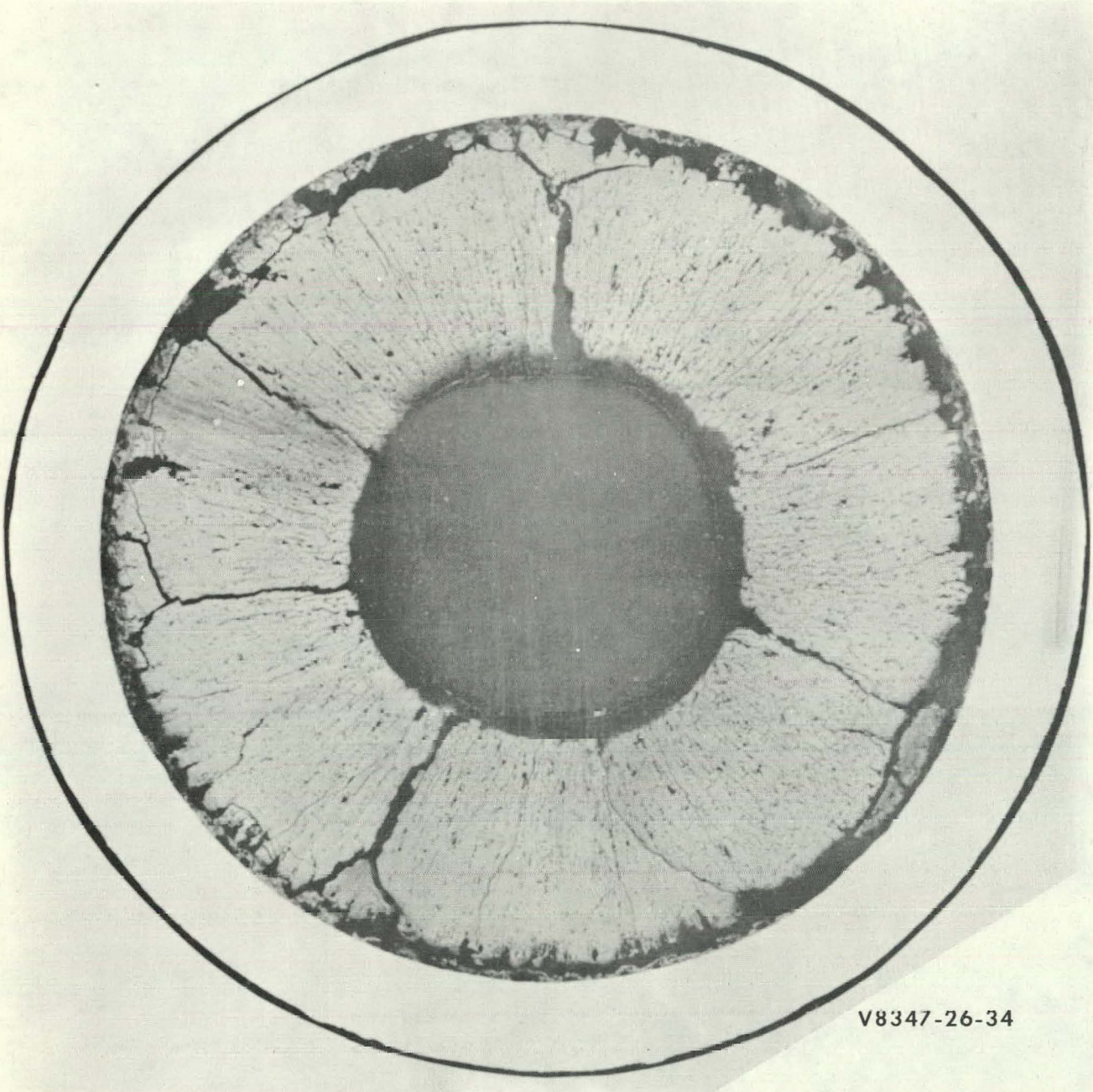

Figure 67. SPECIMEN IX-3-P. (34,500 MWD/T), TRANSVERSE CROSS SECTION THROUGH FUEL AND CLADDING

250X As Polished V8347-23-25

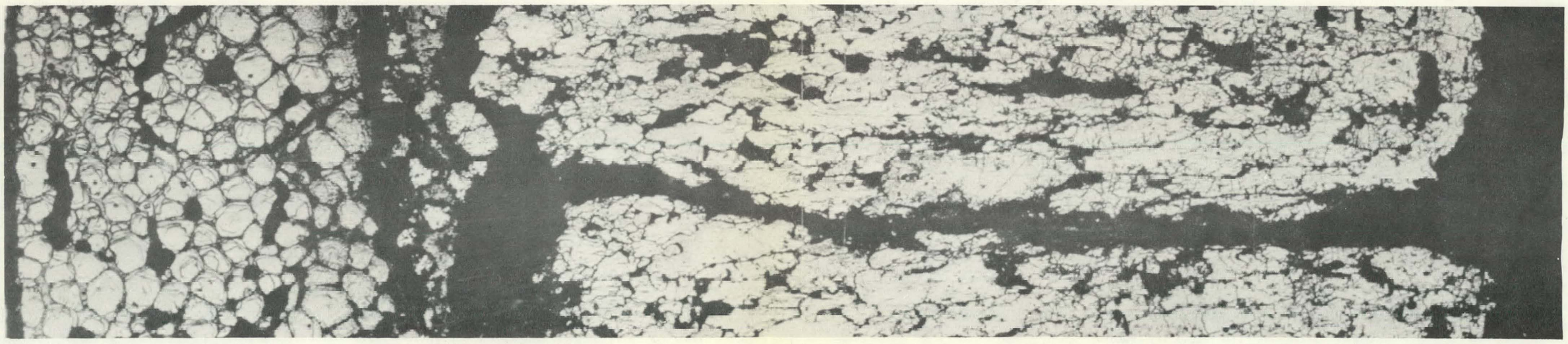

250X Etched V8347-16-19

Figure 68. SPECIMEN IX-3-P. (34,500 MWD/T) EDGE TO CENTER PHOTOGRAPHS OF FUEL

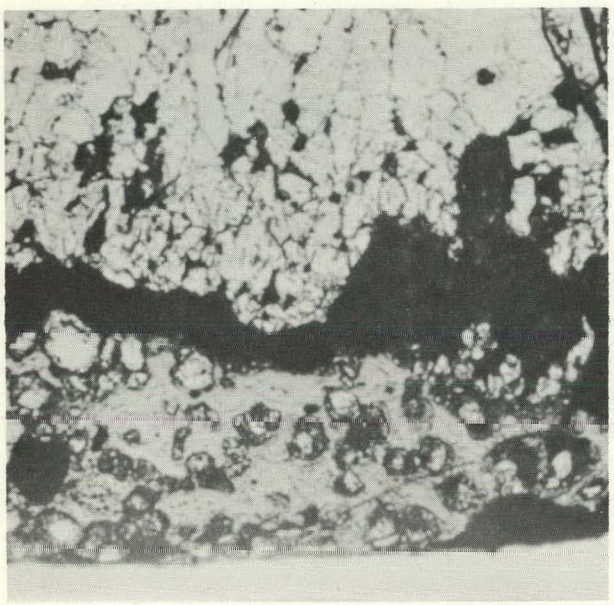

250X Etched V8347-20

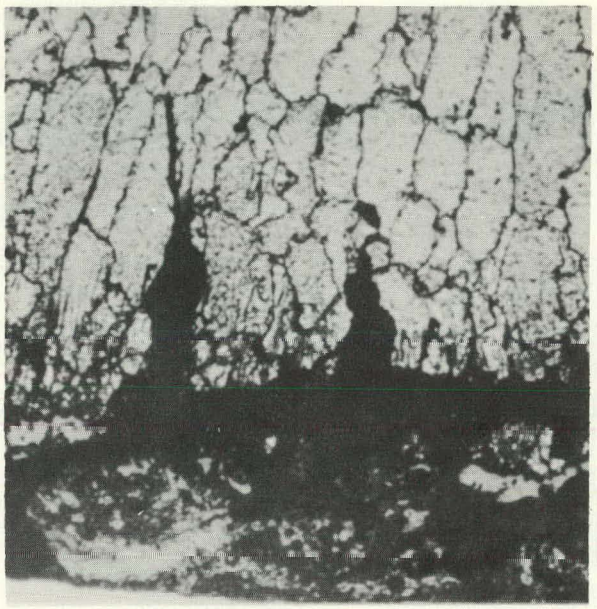

250X Etched V8347-21

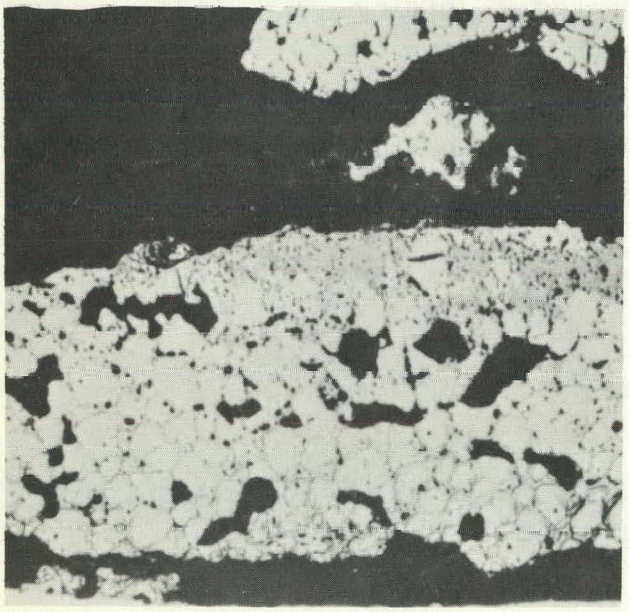

250X Etched V8347-8

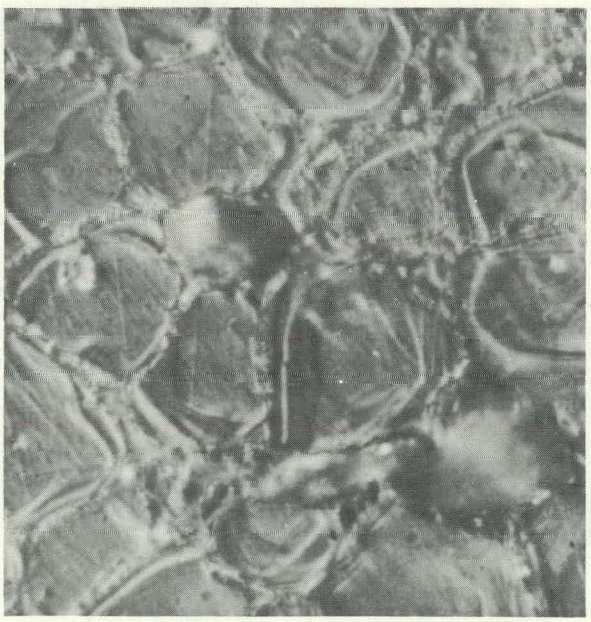

750X (Polarized Light) Etched V8347-22

Figure 69. SPECIMEN IX-3-P. GREY PHASE IN FUEL

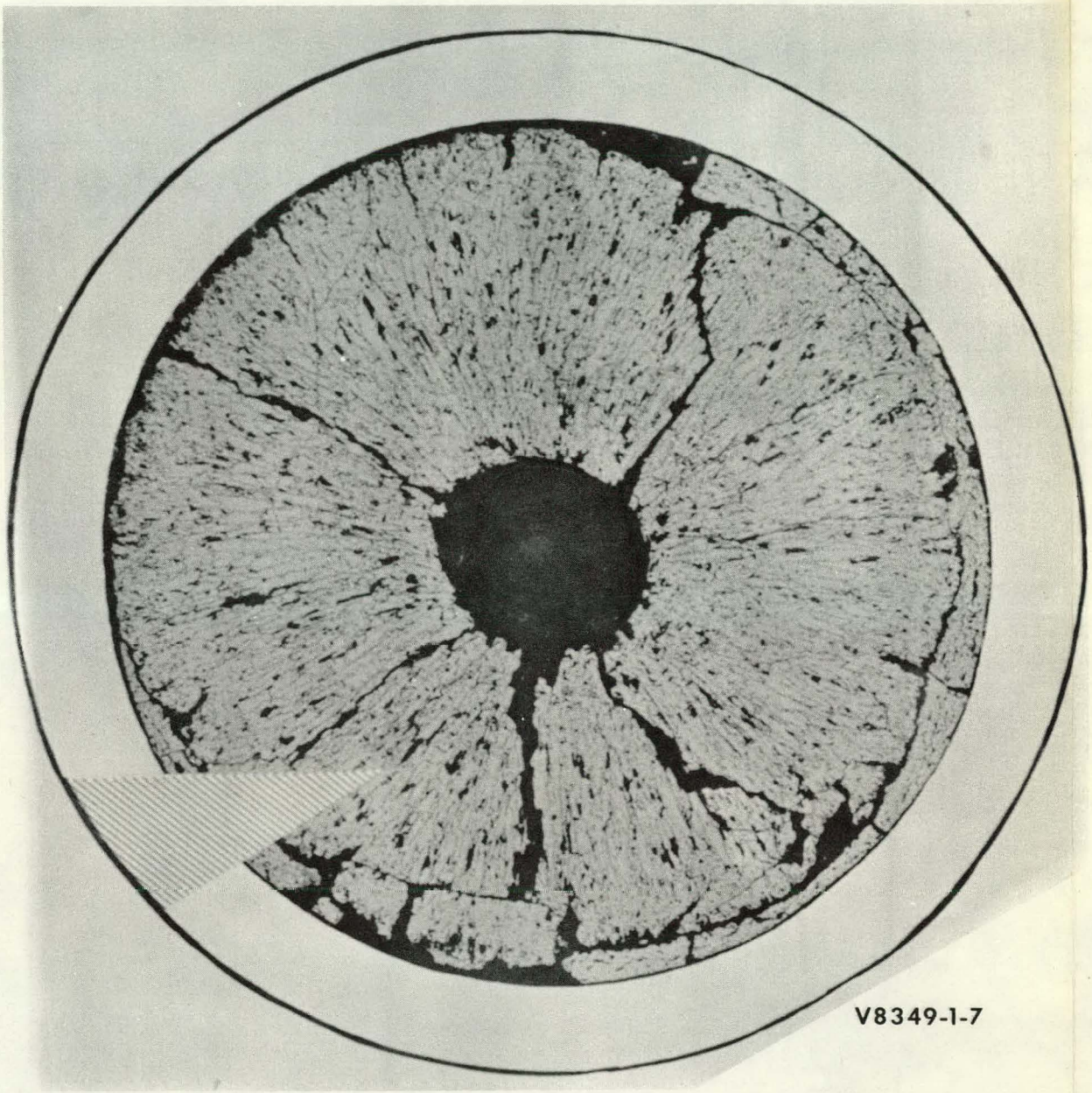

Figure 70. SPECIMEN IV-3-P. (10,900 MWD/T), TRANSVERSE CROSS SECTION THROUGH FUEL AND CLADDING

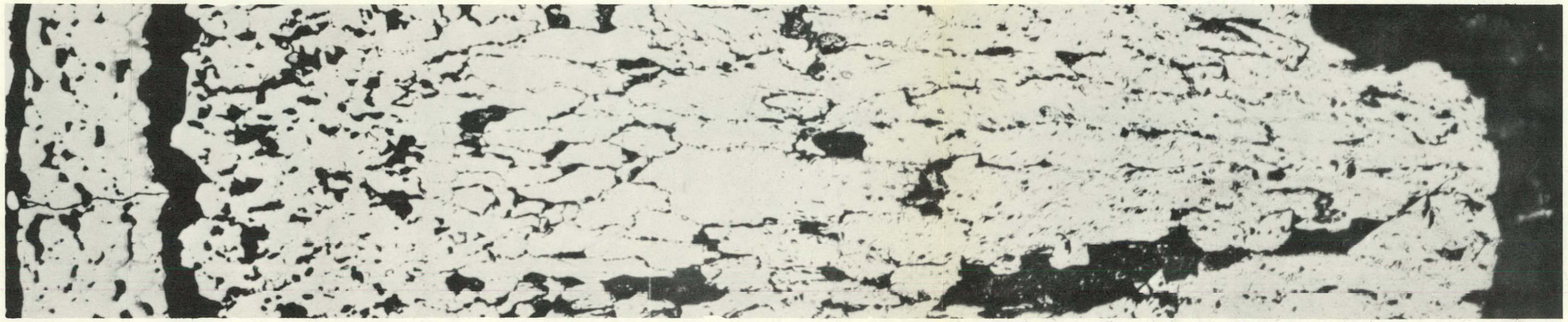

250X As Polished

250X Etched V8349-15-19

Figure 71. SPECIMEN IV-3-P. (10,900 MWD/T), EDGE TO CENTER PHOTOGRAPHS OF FUEL

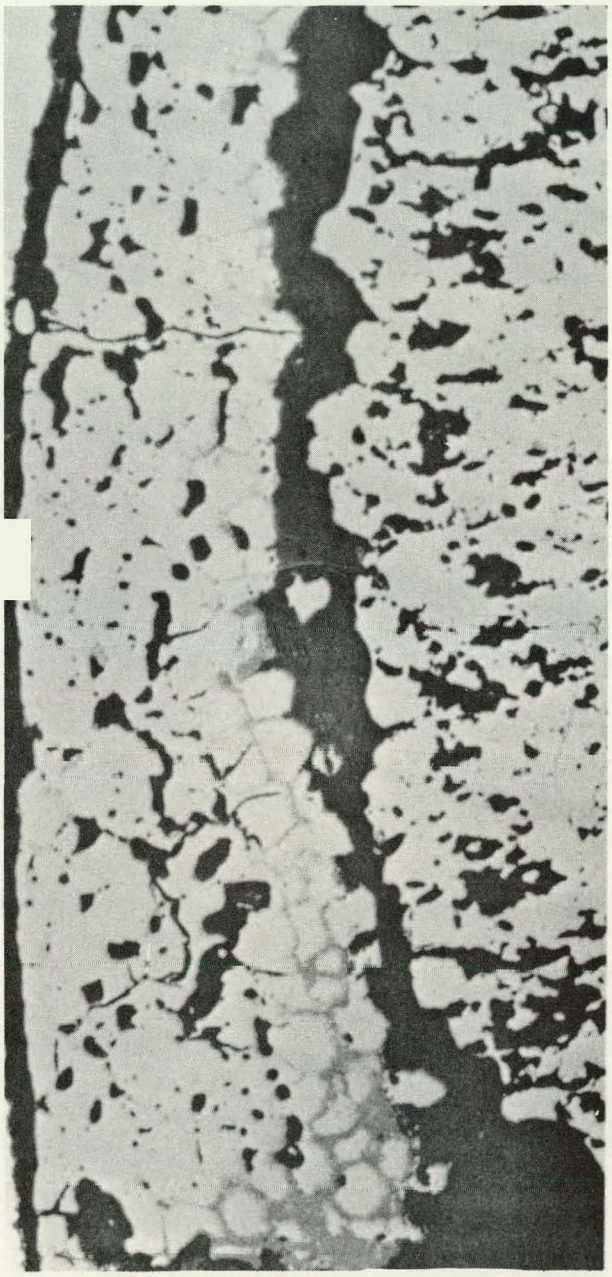

250X As Polished V 8349-21-25

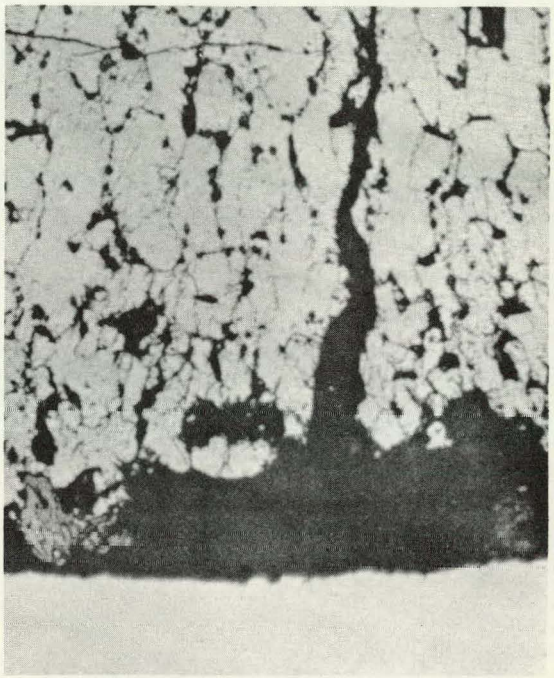

250X Etched V 8349-20

Figure 72. SPECIMEN IV-3-P. GREY PHASE IN FUEL

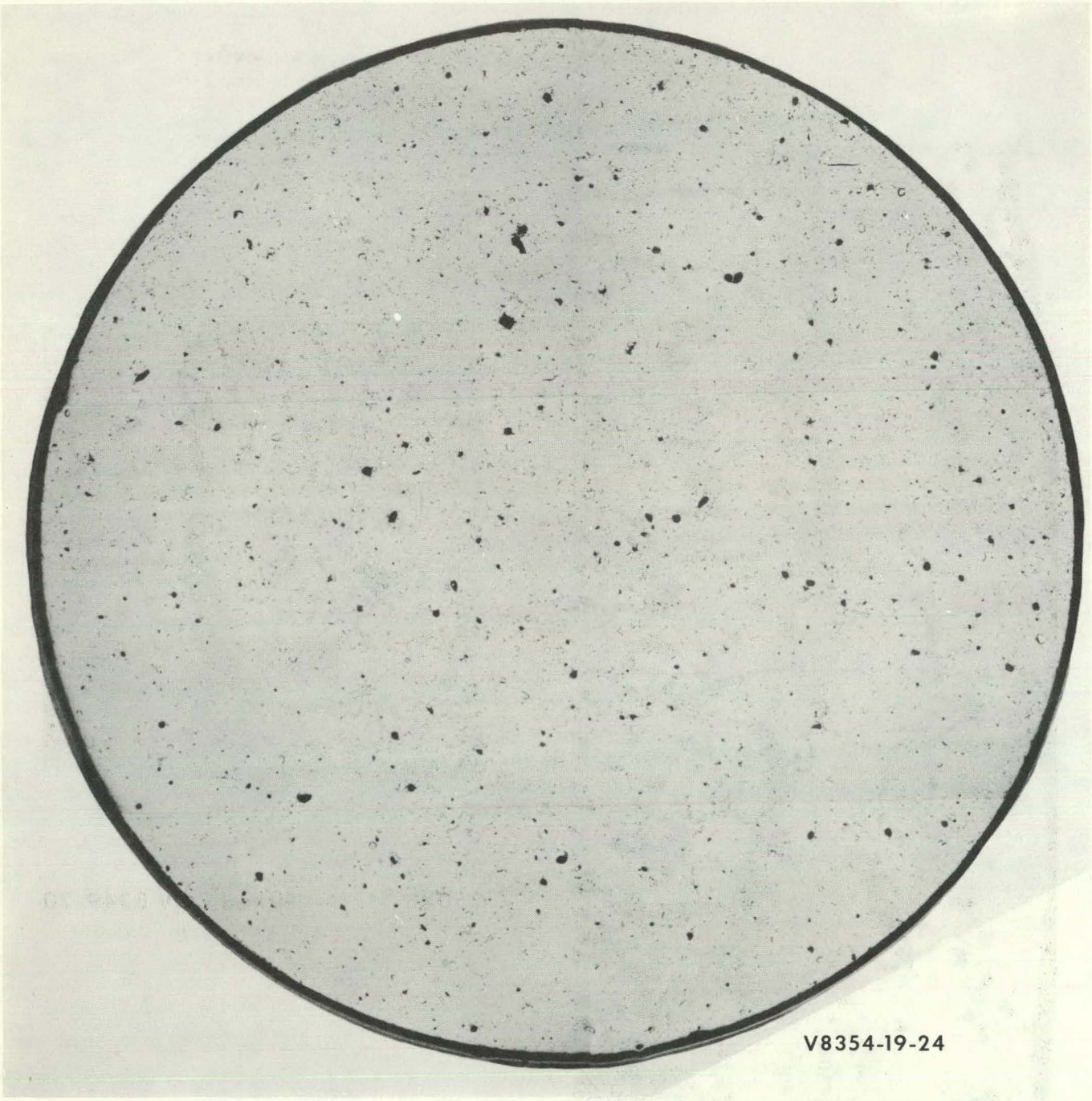

Figure 73. UNIRRADIATED PELLET, TRANSVERSE CROSS SECTION

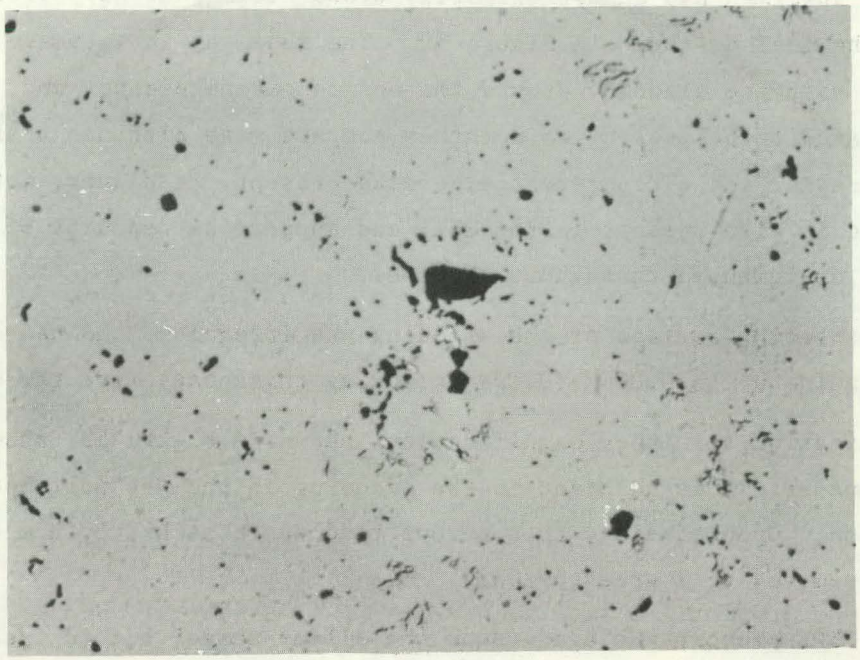

250X As Polished V8354-17

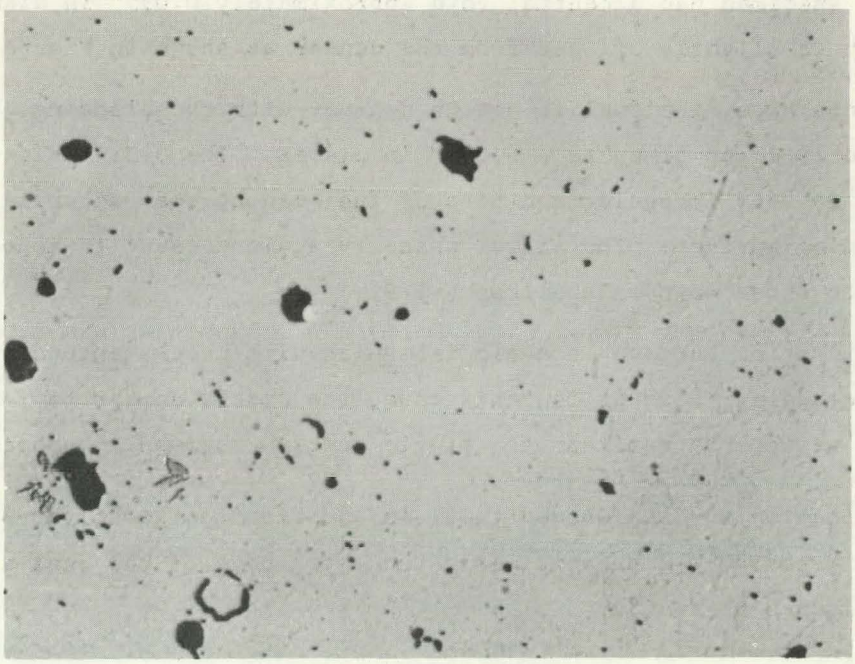

250X As Polished V8354-18

Figure 74. SILVER PHASE IN UNIRRADIATED PELLET

1. Specimen V-1-S (99,000 MWD/T, 1.52×10^6 Btu/hr-ft^2)

This specimen had an approximately 0.060" void centrally located in the fuel as shown in Figure 52. The fuel was in intimate contact with the cladding around the entire circumference, and appeared to be present as a rather compact mass although there are radial and circumferential cracks present. A silver, metallic phase is also present in the fuel and appears as deposits of varying size distributed throughout the fuel.

The interior surface of the cladding was irregular, and had cracks extending up to 0.004" (0.020" cladding thickness) into the cladding.

Examination at higher magnification, shown in Figure 53, showed a porous structure adjacent to the cladding in the "as polished" condition. Upon etching, this porous band was attached by the etchant and removed to a great extent.

The 250X photographs again show the silver phase, but in greater detail. It can be seen that while the silver phase is more or less uniformly distributed throughout the fuel, this material tends to collect in cracks and voids.

2. Specimen VI-1-S (69,100 MWD/T, 1.00×10^6 Btu/hr-ft^2)

This specimen had a central void approximately 0.055" in diameter which is slightly off set from the center as shown in Figure 54.

In this case, the fuel is not in contact with the cladding, but rather there is a gap of up to ~ 0.005" in places. The O.D. surface of the fuel is very irregular and bits of fuel can be seen adhering to the cladding surface. The silver phase is again present in deposits similar to those seen on specimen V-1-S.

The interior surface is again irregular with cracks extending into the cladding; however, in this case, the cracks appear to form a fine network rather than the single cracks observed in specimen V-1-S.

Examination at 250X showed that, in addition to the silver phase, a grey material was present along the outer edge of the fuel as shown in Figures 55 and 56.

The 250X "as polished" photographs did not show a distinct porous band in this case; however, the etched photographs show the columnar grains extending to within 0.010" from the cladding. Attempts to bring out the grain structure near the cladding were not successful.

3. Specimen V-4-S (42,700 MWD/T, 0.86×10^6 Btu/hr-ft^2)

This specimen had a 0.050" centrally located void. The transverse cross-section shown on Figure 57 shows a distinct gap between the fuel and the cladding. Fuel cracking in this specimen was confined to radial cracks only. The silver phase is again present but no trace of the grey phase was found. The interior surface of the cladding is again irregular with single, distinct cracks extending into the fuel.

Examination at 250X (Figure 58) confirmed the absence of any grey phase and showed the fuel to be almost entirely devoid of any porous material near the cladding. The grain structure appears to be equiaxed near the cladding; however, the etchant was not very effective in bringing out the grain structure.

4. Specimen IV-4-S (9,000 MWD/T, 0.53×10^6 Btu/hr-ft^2)

This specimen had a small central void, or what may be the beginning of a central void with small columnar grains surrounding it. The location of the void, as shown on Figure 59, is definitely "off center" in this case, and is displaced toward the edge with the largest gap. The cracking in the fuel is entirely radial in this case. The interior surface of the cladding is irregular with distinct cracks extending into the cladding.

The silver phase is again present; however, the deposits are larger than any previously observed.

At 250X magnification (Figure 60), the fuel appears to have sintered in the center of the specimens but is present as unsintered particles, or perhaps partially sintered agglomerates, near the cladding.

Examination of the largest of the silver deposits showed what appears to be a substructure in the deposit as shown on Figure 61.

5. Specimen V-2-P (77,400 MWD/T, 1.58 x 10^6 Btu/hr-ft^2)

This specimen had a centrally located, approximately 0.030" diameter, central void as shown on Figure 62. The fuel was in intimate contact with the cladding along the entire circumference. The transverse cross-section showed a distinct porosity band around the edge of the fuel, and both radial and circumferential cracks in the main body of the fuel.

The as-polished specimen, when examined at 250X (Figure 63) showed a porosity gradient ranging from many small pores near the cladding through larger and more widely dispersed voids toward the central void. The silver phase was present as small dispersed deposits. The silver material was generally located in voids and cracks with the majority of the deposits being spherical in shape. No trace of the grey phase was found. Etching of the sample removed most of the fuel along the O.D., but did bring out the equiaxed and columnar structure to a certain extent.

A possible fourth phase was observed in the sample as shown on Figure 64. Examination of the columnar grains at 750X revealed the presence of polygon shaped crystals within the larger columnar grains. The color of these crystals was similar to that of the main fuel matrix; however, the material had a distinct crystalline outline ranging from a 4 to 6-sided structure (in one plane).

This substructure was not observed in any other sample; however, considering the difficulties experienced in etching these samples, it may be that this is the only sample in which etching conditions were just right for bringing out this structure.

6. Specimen V-3-P (54,400 MWD/T, 1.28 x 10^6 Btu/hr-ft^2)

This sample did not have a clearly defined central void, but showed what is probably an incipient central void as shown on Figure 65. This sample also showed a ring of porous material around the edge of the fuel. In this case, however, the porous zone appears as a very sharply defined ring about 0.012" wide. Both radial and circumferential cracks were present and the fuel was in intimate contact with the cladding all around the circumference.

Examination at 250X again showed the silver phase to be present, but the grey phase was not found. Figure 66 shows the sample in the "as polished" condition with the silver phase in the cracks and voids.

Etching the sample removed almost all of the material in the porous zone, but did bring out the structure in the remainder of the fuel. This sample exhibited a range of grain sizes ranging from the original unirradiated size at the O.D., through an equiaxed structure, to columnar grains at the center.

7. Specimen IX-3-P (34,500 MWD/T, 1.21×10^6 Btu/hr-ft^2)

This specimen had a centrally located void approximately 0.070" in diameter. The fuel was not in contact with the cladding but apparently had, at some time, been in contact since fuel was observed adhered to the cladding around the entire circumference as shown on Figure 67. The cracking in the fuel is mostly radial in the main body of the fuel with circumferential cracks near the cladding. The grey material is clearly visible even in the as-polished condition at low magnification.

At 250X magnification, both the grey and silver phases were observed as shown on Figure 68.

Etching of the sample brought out the grain structure and showed a sharp change in grain size across the circumferential crack indicating that this crack was present during operation, and there was a sharp temperature discontinuity at the crack.

Various photographs of the grey phase were taken and are shown on Figure 69. They showed that this grey phase is present only in the fuel which is separated from the main body of fuel by a circumferential crack, and that this grey phase seems to collect in the grain boundaries. The etchant removes this grey material as shown by the photograph taken at 750X under polarized light.

8. Specimen IV-3-P (10,900 MWD/T, 0.69 x 10^6 Btu/hr-ft^2)

The central void in this specimen is approximately 0.035" in diameter, and was centrally located as shown on Figure 70 (the missing section in the composite photograph was caused by a shifting of the sample during photographing). The sample had radial and circumferential cracks similar to those seen on specimen IX-3-P. The grey phase is again visible in the low magnification photographs.

At 250X, both the grey and silver phases are again visible as shown on Figures 71 and 72. These figures again show the tendency for the grey material to collect in the grain boundaries in that portion of the fuel separated from the main body by a circumferential crack.

Etching of the sample brought out the grain structure and showed grain growth out to the cladding.

9. Unirradiated Pellet

Examination of the unirradiated pellet showed a uniform cross-section with voids of various sizes uniformly dispersed as shown on Figure 73.

No trace of the silver or grey phase were found at low magnification, however, at 250X two deposits were found as shown on Figure 74. These were the only deposits found on the entire exposed surface. Grey material was also observed but in this case, however, examination under polarized light revealed that the grey material was the hysol potting compound used to mount the sample.

The individual observations made on each metallographic sample can be summed up under several general headings and some conclusions can be made.

1. Central Void Formation

All of the samples showed either a definite central void, or the beginning of a central void. The outline of the central void was irregular with large columnar grains surrounding the void. This indicates that the mechanism for the formation of the central void was grain growth brought about by sintering and/or vaporization and redeposition rather than melting which would tend to produce a smooth glassy surface.

The voids were centrally located on most of the specimens. In the case of specimens VI-1-S and IV-4-S, the void is off center; however, these samples also have a fuel to clad gap so that the off center central void suggests that this gap was not completely closed when the fuel was at operating temperature.

2. Fuel Cracking

Most of the specimens showed some evidence of both radial and circumferential cracks. The radial cracks observed were exclusively intergranular and were most common in the portion of fuel exhibiting columnar grain growth. The circumferential cracks observed were of two different types. In one case, the cracks are narrow with little change in grain size from one side of the crack to the other. This type of crack is best illustrated on Figures 62 and 65. The second type of circumferential crack is shown on Figures 67 and 70, in which there is a definite difference in the amount of grain growth on the opposite sides of the crack. Thus, it appears that the first type of crack was either closed when the fuel was at temperature or these cracks were introduced during the sectioning operation. The second type appears to be more of a true circumferential crack, and this crack was apparently present when the fuel was at temperature.

In general, despite the cracks, the fuel appeared to be present as a compact mass with no evidence of loose fuel.

3. Fuel-to-Clad Gap

Both the pelleted and the swaged samples showed fuel to clad gaps ranging from intimate contact between the fuel and the cladding, through cases where there is partial contact, to cases where there is essentially no contact between the fuel and the cladding. The presence of a fuel to clad gap on the pelleted specimens is not surprising since these specimens were fabricated with a 6-8 mil diametrical gap[1]. In the case of the swaged specimens, the fuel was in intimate contact with the cladding before irradiation but apparently developed a gap during irradiation. In at least one case, there is evidence that this gap in a swaged specimen was present when the specimen was at temperature. Comparison of as-etched photographs of specimens V-1 (Figure 53)

and V-4 (Figure 56) shows that the fuel in specimen V-4 has experienced grain growth out to the O.D. of the fuel whereas the fuel in specimen V-1 shows little or no evidence of grain growth. Thus, the O.D. fuel temperature in specimen V-4 must have been higher than that of specimen V-1. A comparison of the heat flux for the two specimens shows that specimen V 4 had only about 1/2 the heat flux of specimen V-1 so that the only way in which specimen V-4 could have a higher temperature at the O.D. of the fuel would be to have a fuel to clad gap during operation.

4. Fuel Porosity

Several of the samples examined showed a very porous structure near the cladding similar to that observed by Barney and Wemple[10] in irradiated UO_2. This porous band around the O.D. of the fuel was observed only in those specimens in which the fuel was in intimate contact with the cladding. This porous band appears to be confined to that portion of the fuel that has not experienced grain growth; however, it is not present in the unirradiated material. Hence, this porous band can be characterized as a condition that is brought about by irradiation and removed or obscured when grain growth occurs. The most logical explanation is that this porosity ring is caused by immobile fission gas bubbles. As long as the fuel temperature is below that which will cause grain growth the fission gas collects in small bubbles and remains immobile. In those areas where grain growth is occurring, a shifting of the porosity takes place and the small bubbles have a chance to agglomerate and move, along with the pre-irradiation porosity, to the central void. This agglomeration and movement can be seen quite clearly in the "as polished" photographs in Figures 58 and 71. The fact that this fuel is highly enriched in fissionable material and hence quite "black" serves to accentuate this condition due to the higher burnup in the fuel near the O.D.

The apparent preferential attack of the etchant on the material in this porous ring is, if the above analysis is correct, probably due to the larger amount of exposed surface and the smaller grain size, rather than any compositional variation in the fuel.

5. Silver Phase in the Fuel

With the evidence at hand, it is impossible to identify the composition of the silver phase found in the fuel. It is possible, however, to characterize the behavior of this material as follows:

i. It is found in both irradiated and unirradiated fuel. However, the amount observed in the unirradiated pellet was quite small in comparison to the amount found in the irradiated fuel.

ii. The amount of silver material present does not vary with either heat flux or burnup. The size of the individual deposits does seem to be related to the density of the fuel with the largest deposits being found in a swaged specimen (IV-4-S) which did not have a central void.

iii. The material has a certain amount of mobility and appears to be deposited by a vaporization-condensation mechanism. The material is found almost exclusively in voids and cracks.

iv. Large deposits of this material appear to have a substructure within the deposit as shown on Figure 61.

6. Grey Phase in the Fuel

As with the silver phase, there is insufficient evidence at present to permit even a tentative identification of this phase, but its behavior can also be characterized somewhat.

i. In contrast to the silver phase, this material is not found throughout the fuel and is not found in all specimens. It is found only in the "cooler" parts of the fuel and is associated with a condition that would have caused a sharp temperature discontinuity in the fuel, i.e., on the cladding side of a wide circumferential crack or at places where the fuel might have been in contact with the cladding.

ii. The grey phase is found mostly in grain boundaries and is more rapidly attacked by a H_2SO_4-H_2O_2 etchant than the fuel.

V. FUTURE WORK

Examination of this fuel is continuing at present and will be reported in a later document. Among the areas of investigation will be:

1. Metallographic examination and microhardness testing of the cladding.
2. Fuel sampling at discrete radial positions to determine U/Pu ratio and burnup as a function of radial distance.
3. Further examination and tests to attempt to identify the silver and grey phases.

VI. SUMMARY AND CONCLUSIONS

The performance of the swaged and pelleted fuel was comparable, and the fuel performed well up to approximately 100,000 MWD/T. No evidence of gross longitudinal fuel movement was found. The size of the central void observed can, except for the localized "chamber" type voids, be explained by radial movement of the fuel.

Measurement of the percentage fission gas release showed values ranging from 10% to 65%, with averages of 36% and 47% for the pelleted and swaged specimens respectively, and no apparent correlation between fission gas release and heat flux. The percentage fission gas release was higher in most cases than would be expected in UO_2 fuel irradiated under similar conditions.

There is evidence of fission gas bubbles within the fuel grains as indicated by a spongy structure in the fuel similar to that observed in the case of UO_2 irradiated under high performance conditions.

The use of gas plenum was effective as a means to contain the fission gas, and allowed the fuel to go to high burnup without rupture of the specimens although two specimens did achieve moderate burnups without a gas plenum.

TABLE IX

SUMMARY OF METALLOGRAPHIC OBSERVATIONS

Specimen	Fig. No.	Burnup (MWD/T)	Average Heat Flux ($Btu/hr-ft^2$)	Pre-Irrad. Density (% of theo.)	Approx.Dia. of Central Void(inches)	Fuel Cracking	Structure	Other Phases and Constituents	Fuel-to-Clad Ga
V-1-S	52 53	99,000	1.27×10^6	~ 75	0.060	Mainly radial with some circumferential	Small grains at O.D., long columnar grains extending out from central void. Porous band along O.D. of fuel. Little or no grain growth at O.D.	Silver phase present throughout fuel.	Fuel in contact with cladding.
VI-1-S	54 55 56	69,100	0.89×10^6	~ 75	0.055	Mainly radial with some circumferential	Equiaxed grains at O.D. Long columnar grains extending out from central void. Some grain growth at O.D.	Silver phase present throughout fuel. Grey phase present along O.D. of fuel.	Fuel-to-clad gap with particles of fuel adhering to cladding.
V-4-S	57 58	42,700	0.55×10^6	~ 75	0.050	Radial	Equiaxed grains at O.D. Columnar grains extending out from central void. Grain growth at O.D.	Silver phase present throughout fuel.	Fuel-to-clad gap
IV-4-S	59 60 61	9,000	0.37×10^6	~ 75	Small irregular shape	Radial	Unsintered or partially sintered fuel at O.D. Small columnar grains at central void.	Large deposits of silver phase throughout fuel.	Fuel-to-clad gap
V-2-P	62 63 64	77,400	1.30×10^6	95.8	0.030	Mainly radial with some circumferential	Small grains at O.D. Long columnar grains extending out from central void. Porous band along O.D. of fuel. Little or no grain growth at O.D.	Silver phase present throughout fuel. Polygon shaped crystals within columnar grains.	Fuel in contact with cladding
V-3-P	65 66	54,400	0.92×10^6	94.5	Very small irregular shape	Mainly circumferential, some radial	Small grains at O.D., equiaxed grains in mid-radius region, short columnar grains around central void.	Silver phase present throughout fuel.	Fuel in contact with cladding
IX-3-P	67 68 69	34,500	0.84×10^6	83.7	0.070	Mainly radial with some wide circumferential cracks near O.D.	Equiaxed grains at O.D., long columnar grains extending out from central void. Grain growth at O.D.	Silver phase present throughout fuel. Grey phase present along O.D.	Fuel-to-clad gap
IV-3-P	70 71 72	10,900	0.55×10^6	89.0	0.035	Radial and wide circumferential cracks	Equiaxed grains at O.D. Long columnar grains extending out from central void. Grain growth at O.D.	Silver phase present throughout fuel. Grey phase present along O.D.	Fuel-to-clad gap
Unirradiated Pellet	73 74	-	-	93.7	-	None	Uniform cross-section	Two small deposits of silver phase.	

In the case of irradiated fuel which had established intimate fuel-clad contact, grain size varies radially from that characteristic of the unirradiated material near the periphery, through an intermediate region of larger equiaxed grains, to relatively long columnar grains extending into the central void. This is the familiar pattern observed with UO_2. A different grain size distribution was found for pelleted and swaged fuel having a fuel-clad gap.

Evidence was found that at least one swaged specimen, although fabricated with no fuel-to-clad gap, developed a gap during irradiation which remained open when the specimen was at power.

There are at least three different phases present in the fuel: the main fuel matrix, a localized grey phase, and a silvery phase which is dispersed throughout the fuel matrix.

The inner surface of the swaged cladding was very irregular and had cracks which penetrated into the cladding to a depth of as much as 4 mils.

The use of insulator pellets at the ends of the active fuel zone was effective as a means to protect the specimen end caps, and to prevent movement of the fuel into the gas plenum.

VII. ACKNOWLEDGMENTS

The author would like to express appreciation to C. L. Stanger for his work in the Radioactive Materials Laboratory, and to W. V. Ketron for the preparation and photography of the metallographic samples. The efforts of R. G. Gest and M. E. Urata in the fission gas analysis, and the interest and advice of F. J. Leitz and H. W. Alter are also gratefully acknowledged.

VIII. REFERENCES

1. Cleveland, Jesse M., et al, Fast Oxide Breeder Project I, Fuel Fabrication GEAP-3486, (August 15, 1960)
2. Cochran, J. S., Preliminary Evaluation of Two Plutonium-Uranium Oxide Irradiation Capsules, GEAP-3834 (to be issued)

3. Horst, K. M., Memo Report, Summary on the Thermal Analysis of FOB Capsules I-X, (April 27, 1961)

4. Letter K. M. Horst to F. J. Leitz, "Evaluation of the Fuel Exposure in the FOB Capsules from Temperature Measurements", (July 20, 1960)

5. Gerhart, J. M., Post-Irradiation Examination of Allis-Chalmers (NSPR) Capsules I, II, & III, GEAP-3694, (February, 1961)

6. Eichenberg, J. D., et al, Effects of Irradiation on Bulk UO_2, WAPD-183, (October, 1957)

7. Katcoff, S., Nucleonics, 18, 201-208 (1960)

8. Robertson, J. A. L., et al, "Irradiation Behavior of UO_2 Fuel Elements", Nuclear Metallurgy, Vol VI (1950)

9. Brandt, F. A., et al, Irradiation Results, N.S. Savannah Core II Prototype Fuel Assemblies, GEAP-3559, (November 1960)

10. Barney, W. K., and Wemple, B. D., Metallography of Irradiated UO_2-Containing Fuel Element, KAPL-1836, (January 15, 1958)